# COLLECTED PAPERS on Nanophotoics

## Vol. 22

## August 2006 – July 2007

Prof. Motoichi OHTSU

# MEMBERS

**(From April 1, 2007)**

## *[I] THE UNIVERSITY OF TOKYO**

### Professor

Motoichi OHTSU[(a-d)] (Dr. Eng.)

### Graduate Student (Doctor Candidate)

Shunsuke YAMAZAKI
Kokoro KITAMURA

### Graduate Students (Master Course)

Hyungsu JEONG
Shunsuke TANAKA
Takumi YAMAMOTO
Hiroki SUGIYAMA
Towa TAKAHASHI

### Undergraduate Students

Jun OMASA
Shoken Eckhart KANEKO

### Secretary

Sachiyo KOJIMA

a) Also a team leader, "Nanophotonics team," SORST (Solution Oriented Research for Science and Technology), JST (Japan Science and Technology Agency)
b) Also a director, "Nanophotonics Total Expansion: Industry-University Cooperation and Human Resource Development", METI (Ministry of Economy, Trade and Industry) and NEDO (New Energy and Industrial Technology Development Organization)
c) Also a director, "Innovative Nanophotonics Components Development" project, METI (Ministry of Economy, Trade and Industry) and NEDO (New Energy and Industrial Technology Development Organization)
d) Also a director, NPO-Research Institute of Nanophotonics

(*)
Department of Electronics Engineering, School of Engineering,
The University of Tokyo
(Room 215, Bldg. Eng. 9)
2-11-16 Yayoi, Bunkyo-ku, Tokyo 113-8656, Japan
Phone: +81-3-5841-1189
FAX: +81-3-5841-1140
E-mail: ohtsu@ee.t.u-tokyo.ac.jp
URL(1):http://uuu.t.u-tokyo.ac.jp
URL(2):http://www.nanophotonics.info/

東京大学大学院 工学系研究科 電子工学専攻
〒113-8656　東京都文京区弥生 2-11-16　工学部 9 号館 215 号室
電話: 03-5841-1189, ファックス: 03-5841-1140
E-mail: ohtsu@ee.t.u-tokyo.ac.jp
URL(1): http://uuu.t.u-tokyo.ac.jp
URL(2):http://www.nanophotonics.info/

## *[II] NANOPHOTONICS TEAM‡*


**Researcher**

Takashi YATSUI (Dr. Eng.)

**Manager**

Akiyoshi ORIDE

**Secretary**

Toshiko TERADA

(‡)
Nanophotonics Team, SORST (Solution Oriented Research for Science and Technology), JST (Japan Science and Technology Agency)

The University of Tokyo
(Room 213, Bldg. Eng.-9)
2-11-16 Yayoi, Bunkyo-ku, Tokyo 113-8656, Japan
Phone: +81-3-5842-2231
FAX: +81-3-3813-3325

（独）科学技術振興機構 戦略的創造研究推進事業「発展・継続」研究
ナノフォトニクスチーム
〒113-8656 東京都文京区弥生 2-11-16 工学部 9 号館 213 号室
電話: 03-5842-2231, ファックス: 03-3813-3325

## *[III] Nanophotonics Total Expansion: Industry-University Cooperation and Human Resource Development†*

### Visiting Project Associate Professor

Makoto NARUSE[(e)] (Dr. Eng.)

### Project Research Associate

Naoya TATE (Dr. Eng.)
Kazuhiro NISHIBAYASHI (Dr. Sci.)
Wataru NOMURA (Dr. Eng.)

### Managers

Kazuhiko TAMAKI
Masako TAMURA

### Secretary

Kumiko NOZAWA

### Visiting Scientists

Hiroyasu FUJIWARA[(f)]
Tatsushi HAMAGUCHI[(g)]
Shin SAITO[(h)] (Dr. Eng.)
Kazuya HIRATA[(i)]
Yasuhiro OSHIMA [(j)]
Tetsuji MORI[(k)]

(e) Permanent affiliation: National Institute of Information and Communication Technology
(f) Permanent affiliation: Hamamatsu Photonics. K.K.
(g) Permanent affiliation: Nichia Corp.
(h) Permanent affiliation: Tohoku University
(i) Permanent affiliation: Sigma Koki Co., Ltd.
(j) Permanent affiliation: Nisshinbo Industries, Inc.
(k) Permanent affiliation: Ricoh Company, Ltd.

(†)

Department of Electronics Engineering, School of Engineering,
The University of Tokyo
(Room 219, Bldg. Eng.-9)
2-11-16 Yayoi, Bunkyo-ku, Tokyo 113-8656, Japan
Phone: +81-3-5841-1670
FAX: +81-3-5841-1140
E-mail: info@ nanophotonics.t.u-tokyo.ac.jp
URL: http://uuu.t.u-tokyo.ac.jp

東京大学大学院 工学系研究科 電子工学専攻
〒113-8656 東京都文京区弥生 2-11-16 工学部 9 号館 219 号室
電話：+81-3-5841-1670, ファックス: +81-3-5841-1140
E-mail: info@ nanophotonics.t.u-tokyo.ac.jp
URL: http://uuu.t.u-tokyo.ac.jp

## *[IV] Innovative Nanophotonics Components Development Project*[*]


**Project Associate Professor**

Tadashi KAWAZOE (Dr. Sci.)

**Research Assistants**

Hisayo ITO
Masako NISHIDA
Katsuhito TAKAHASHI

(*)
Department of Electronics Engineering, School of Engineering,
The University of Tokyo
(Room 720, Bldg. Eng.-9)
2-11-16 Yayoi, Bunkyo-ku, Tokyo 113-8656, Japan
Phone: +81-3-5841-1670
FAX: +81-3-5841-1140
URL: http://uuu.t.u-tokyo.ac.jp

東京大学大学院 工学系研究科 電子工学専攻
〒113-8656 東京都文京区弥生 2-11-16 工学部 9 号館 720 号室
電話: 03-5841-1670, ファックス: 03-5841-1140
URL: http://uuu.t.u-tokyo.ac.jp

## *[V] RESEARCH INSTITUTE OF NANOPHOTONICS**

**Director**

Motoichi OHTSU

(*)
Research Institute of Nanophotonics,
Nonprofit Organization
1-20-10 Sekiguchi, Bunkyo-ku, Tokyo 112-0014, Japan
Phone: +81-3-5225-6432. Fax: +81-3-5225-6435
E-mail: ohtsu-rinps@nanophotonics.t.u-tokyo.ac.jp
URL: http://www.nanophotonics.info/

特定非営利法人 ナノフォトニクス工学推進機構
〒112-0014 東京都文京区関口 1-20-10
電話: 03-5225-6432, ファックス: 03-5225-6435
E-mail: ohtsu-rinps@nanophotonics.t.u-tokyo.ac.jp
URL: http://www.nanophotonics.info/

# LIST OF PAPERS

**[(pp.XX-XX);** pages in this issue of the COLLECTED PAPERS**]**

## [I] ORIGINAL PAPERS

[1] T. Kawazoe, K. Kobayashi, and M. Ohtsu, "Initial Growth Process of a Zn Nanodot Fabricated using Nonadiabatic Near-field Optical CVD," Journal of Photopolymer Science and Technology, Vol. 20, No. 1, June 2007, pp. 129-131

**(pp.1-3)**

[2] M. Naruse, H. Hori, K. Kobayashi, and M. Ohtsu, "Tamper resistance in optical excitation transfer based on optical near-field interactions," Optics Letters, Vol. 32, Issue 12, June 2007, pp. 1761-1763

**(pp.5-7)**

[3] T. Yatsui, S. Sangu, T. Kawazoe, M. Ohtsu, S. J. An, J. Yoo, and G.-C. Yi, "Nanophotonic switch using ZnO nanorod double-quantum-well structures," Applied Physics Letters, Vol. 90, Issue 22, May 2007, pp.223110 1-3
[selected for the June 11, 2007 issue of the Virtual Journal of Nanoscale Science & Technology]
[selected for the July, 2007 issue of the Virtual Journal of Ultrafast Science (Vol. 6, Issue 7)]

**(pp.9-11)**

[4] T. Yatsui, J. Lim, T. Nakamata, K. Kitamura, M. Ohtsu, and G.-C. Yi, "Low-temperature (~270 °C) growth of vertically aligned ZnO nanorods using photoinduced metal organic vapour phase epitaxy," Nanotechnology, Vol. 18, Issue 6, February 2007, pp 065606 1-4

**(pp.13-16)**

[5] Y. Inao, S. Nakasato, R. Kuroda, and M. Ohtsu, "Near-field lithography as prototype nano-fabrication tool," Microelectronic Engineering, Vol. 84, January 2007, pp. 705-710

**(pp.17-22)**

[6] H. Yonemitsu, T. Kawazoe, K. Kobayashi, and M. Ohtsu, "Nonadiabatic photochemical reaction and application to photolithography," Journal of Photoluminescence, Vol.122-123, January 2007, pp.230-233

**(pp.23-26)**

[7] Y. Saito, S. Mononobe, M. Ohtsu, and H. Honma, “Electroless Nickel Plating under Continuous Ultrasonic Irradiation to Fabricate a Near-Field Probe Whose Metal Coat Decreases in Thickness toward the Tip,” Optical Review, Vol.13, No.4, July/August 2006, pp. 225-227

**(pp.27-29)**

[8] K. Kitamura, T. Yatsui, and M. Ohtsu, “Near-Field Evaluation of a Quantum Size Effect in Self-Aligned GaN Whiskers Fabricated Using Photochemical Etching,” Optical Review, Vol. 13, No. 4, July/August 2006, pp. 222-224

**(pp.31-33)**

[9] T. Yatsui, M. Ohtsu, S. J. An, J. Yoo, and G.-C. Yi, “Evaluating the Quantum Confinement Effect of Isolated ZnO Nanorod Single-Quantum-Well Structures Using Near-Field Ultraviolet Photoluminescence Spectroscopy,” Optical Review, Vol. 13, No. 4, July/August 2006, pp. 218-221

**(pp.35-38)**

## [II] PRESENTATIONS IN INTERNATIONAL CONFERENCES

[1] M. Ohtsu, "Nanophotonics," Abstracts of The 6th Asia-Pacific Conference on Near-Field Optics, National Natural Science Foundation of China, June 13-17, 2007, Yellow mountain, China , p. 1
**[Invited presentation]**

**(p.39)**

[2] T. Kawazoe, S. Tanaka, and M. Ohtsu, "Single-Photon Excitation Energy Transfer between Quantum Dots via an Optical Near-Field Interaction," of The 6th Asia-Pacific Conference on Near-Field Optics, National Natural Science Foundation of China, June 13-17, 2007, Yellow mountain, China , p. 85

**(p.41)**

[3] T. Yatsui, G.-C. Yi, and M. Ohtsu, "Progress in developing nanophotonic integrated circuits," The 1-st International Conference on Industrial Applications of Lasers 2007 (INDLAS 2007), National Institute for Laser,May 23-25, 2007, Bran, Romania,
**[Invited presentation]**

**(p.43)**

[4] T. Kawazoe, K. Nishibayashi, K. Akahane, N. Yamamoto, and M. Ohtsu, "Observation of the Dark States of Near-field Coupled InAs Quantum Dots Using Optical Near-field Microscopy," Technical digest of the Conference on Lasers and Electro-Optics/Quantum Electronics and Laser Science Conference, Optical Society of America, May 6-11, 2007, Baltimore, USA (paper number JThD62)

**(pp.45-46)**

[5] T. Yatsui, S. Sangu, T. Kawazoe, M. Ohtsu, J. Yoo, S. J. An, and G.-C. Yi, "Nanophotonic switch using one-dimensional ZnO double-quantum-well structures," Technical digest of the Conference on Lasers and Electro-Optics/Quantum Electronics and Laser Science Conference, Optical Society of America, May 6-11, 2007, Baltimore, USA (paper number CME6)

**(pp.47-48)**

[6] M. Naruse T. Yatsui, J. H. Kim, and M. Ohtsu, "Hierarchy in Optical Near-Fields by Nano-Scale Shape Engineering and its Application to Traceable Memory," Technical digest of the Conference on Lasers and Electro-Optics/Quantum Electronics and Laser Science Conference, Optical Society of America, May 6-11, 2007, Baltimore, USA (paper number CThV3)

**(pp.49-50)**

[7] T. Kawazoe, T. Yatsui, and M. Ohtsu, "Nanophotonic devices using excitation energy transfers," First European Topical Meeting on Nanophotonics and metamaterials," Abstracts of Nanometa 2007, European Physical Society, January 9, 2007, Seefeld, Tirol, Austria, (Paper number TUE1o.1)
**[Invited presentation]**

**(p.51)**

[8] T. Yatsui, S. Sangu, T. Kawazoe, M. Ohtsu, J. Yoo, S. J. An, and G.-C. Yi, "Direct Observation of the Optical Near-field Energy Transfer Among the Resonant Energy States Between ZnO Nanorod Double-quantum-well Structures," Abstracts of MRS fall meeting 2007, Materials Research Society, November 27-December 1, 2006, Boston, USA (paper number Q19.3)

**(p.53)**

[9] K. Kitamura, T. Yatsui, M. Ohtsu, T. Nakamata, J. Lim, and G.-C. Yi, "Low-temperature (~270°C) Growth of Vertically Aligned ZnO Nanorods Using Photo-assisted Metal Organic Vapor Phase Epitaxy," Abstracts of MRS fall meeting 2007, Materials Research Society, November 27-December 1, 2006, Boston, USA (paper number K2.6)

**(p.55)**

[10] S. Mononobe and M. Ohtsu, "Effect of additive chloride ion on submicron size-dependence of electroless nickel plating," Digest of Papers in Microprocesses and Nanotechnology 2006 (2006 International Microprocesses and Nanotechnology Conference) , The Japan Society of Applied Physics, October 25-27, 2006, Kamakura, Japan (paper number 26C-7-45)

**(pp.57-58)**

[11] Y. Inao, S. Nakasato, R. Kuroda, and M. Ohtsu, "Near-Field Lithography as prototype nano-fabrication tool," Proceeding in Micro-and Nano-Engineering, Consejo Superior de Investigaciones Cienrificas (CSIC), September 17-20, 2006, Barcelona, Spain (paper number p2C-6)

**(pp.59-60)**

[12] T. Kawazoe, K. Akahane, N. Yamamoto, K. Nishibayashi, and M. Ohtsu, "Nanophotonic Devices using InAs Quantum Dots," Abstract in 9th International Conference on Near-field Optics, Nanophotonics & Related Techniques, Plasmo-nano-devices, September 10-15, 2006, Lausanne, Switzerland (paper number ThP-28) p.290

**(p.61)**

[13] T. Kawazoe, and M. Ohtsu, "Nanophotonics using Optical Near-field," Abstract in 9th International Conference on Near-field Optics, Nanophotonics & Related Techniques, Plasmo-nano-devices, September 10-15, 2006, Lausanne, Switzerland (paper number Th5-1) p.245
**[Invited presentation]**

**(p.63)**

[14] T. Kawazoe, K. Kobayashi, and M. Ohtsu, "Deposition of 5nm-diameter Zn-nanodot using near field optical CVD with optically inactive $Zn(acac)_2$," Abstract in 9th International Conference on Near-field Optics, Nanophotonics & Related Techniques, Plasmo-nano-devices, September 10–15, 2006, Lausanne, Switzerland (paper number Tu4-4) p.118

**(p.65)**

[15] T. Yatsui, M. Naruse, and M. Ohtsu, "Plasmonic circuits for nanophotonic devices," Proc. of SPIE Optics & Photonics 2006, SPIE, Vol. 6323, August 13–17, 2006, San Diego, CA, USA (paper number 6323-25) pp. 63230O-1–63230O-9
**[Invited presentation]**

**(pp.67-75)**

## [III] REVIEW PAPERS

**[1]** T. Yatsui, S. Sangu, and M. Ohtsu, "Progress in nanophotonic devices driven by optical near field," Oyo Buturi, Vol.76, No.2, February 2007, pp.160-163
【八井 崇、三宮 俊、大津元一、「近接場相互作用により駆動するナノフォトニックデバイスの進展」、『応用物理』、第 76 巻、第 2 号、2007 年２月、pp. 160-163】

**(pp.77-80)**

**[2]** M. Ohtsu, "Establishing novel science and technology merging light and matter," Kagaku, Vol.62, No.1, January 2007, pp.18-19
【大津元一、「光と物質の融合した科学技術を完成させたい」（ー私のチャレンジしたい化学の未解決問題ー新春特集・化学の夢・未来）、化学、第 62 巻、第 1 号、2007 年 1 月、pp. 18-19】

**(pp.81-82)**

**[3]** T. Yatsui, W. Nomura, and M. Ohtsu, "Nanodot couplers provide efficient near-field energy transfer," SPIE Newsroom, October 2006, (DOI: 10.1117/2.1200610.0427) http://newsroom.spie.org/x4926.xml

**(pp.83-84)**

**[4]** M. Ohtsu, "Innovation named nanophotonics----Past and future of novel concepts realizing qualitative innovation to optical technology," Kagaku, Vol.76, No.10, October 2006, pp.984-990
【大津元一、「ナノフォトニクスという変革ー光技術に質的変革をもたらした新概念の歩みと将来」、『科学』岩波書店、第 76 巻、第 10 号、2006 年 10 月、pp. 984-990】

**(pp.85-92)**

**[5]** M. Ohtsu, "Engaged in reviewing the national fund for science and technology," Japanese Scientific Monthly, Vol.59, No.10, October 2006, pp.37-38
【大津元一、「工学系の科研費審査に携わって」、『学術月報』、第 59 巻、第 10 号、2006 年 10 月、pp. 37-38】

**(pp.93-94)**

## [IV] PUBLISHED BOOKS

**[1]** M. Ohtsu, “Nanooptics, “, Chapter 15 in *Handbook of Lasers and Optics*, edited by F. Träger, Springer Verlag, Berlin, 2007, pp.1079-1090

**(pp.95-106)**

**[2]** M. Ohtsu(ed.), *Development of Nanophotonics,* , Yoneda Publising, Chiba, April 2007 (178 pages)

【大津元一（監修）、「ナノフォトニクスの展開」、米田出版、千葉、2007 年 4 月 (178 ページ)】

**(pp.107-112)**

## [V] LECTURES

**[1]** M. Ohtsu, *Nanophotonics*: *Qualitative Innovation in Optical Science and Technology*, Nanotechnology Seminar Series, the Center for NanoTechnology, the University of Washington, Seattle, WA, USA. May 15, 2007

## [VI] AWARDS

**[1]** M. Ohtsu, *Outstanding Achievement Award*, The Institute of Electronics, Information and Communication Engineers, May 25, 2007
【大津元一、「社団法人電子情報通信学会 業績賞」、（社）電子情報通信学会、2007 年 5 月 25 日】

**[2]** M. Ohtsu, *Fellow Award*, Japan Society of Applied Physics,August 3, 2007
【大津元一、「フェロー称号」、（社）応用物理学会、2007 年 8 月 3 日】

# [I] ORIGINAL PAPERS

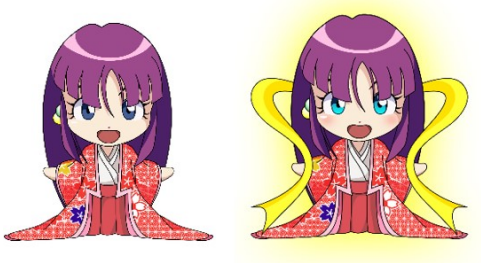

Communication

Journal of Photopolymer Science and Technology
Volume 20, Number 1 (2007) 129–131 ©2007TAPJ

# Initial Growth Process of a Zn Nanodot Fabricated using Nonadiabatic Near-field Optical CVD

**Tadashi Kawazoe*,***, Kiyoshi Kobayashi***, Motoichi Ohtsu*,*****

** Japan Science and Technology Agency,*
*2-11-16 Yayoi, Bunkyo-ku, Tokyo 113-8656, Japan.*
***Department of Electronics Engineering, The University of Tokyo*
*2-11-16 Yayoi, Bunkyo-ku, Tokyo 113-8656, Japan.*
**** Department of Physics, Tokyo Institute of Technology,*
*Meguro-ku, Tokyo 152-8551, Japan.*

**Keywords : photodissociation, chemical vapor deposition, optical near field**

## 1. Introduction

In order to realize high spatial resolution, high precision in controlling size and position, a nanofabrication technique is required. In the self-organized growth method [1], its spatial precision is not sufficiently high to meet this requirement. To improve the precision, an e-beam [2], scanning tunneling microscope (STM) [3], and surface modification [4] are used for site-control of the substrate. However, it has a disadvantage in that it limits the materials that can be deposited because it cannot deal with insulators. By the conventional optical chemical vapor deposition (CVD), vapors of metal organic molecules are dissociated by otochemical reaction with the far-field light; er, it is difficult to fabricate nanometric ma... due to the diffraction limit of light.

Spatial localized nature of the optical near field is suitable for nano-fabrications. So far, we have found in the near-field optical chemical vapor deposition (NFO-CVD) that the metal organic molecules are photodissociated by a nonresonant optical near field with photon energy lower than the dissociation energy of the molecule[5]. We have explained that this unique photodissociation comes from the nonadiabatic photochemical process based on the exciton-phonon polariton model which we have developed [6]. According to this model, the photodissociation is induced by a visible light even for the optically inactive molecule. In this paper, we introduce the fabrication of Zn nanodots using zinc-bis(acetylacetonate) ($Zn(acac)_2$) and the Its initial growth process. Although $Zn(acac)_2$ is optically inactive, we observed the deposition of Zn-nanodots on the substrate just below the apex of the fiber probe using NFO-CVD. Finally, we obtained Zn nanodot of 5-nm in diameter by the optimizations of the deposit conditions.

## 2. Experimental

Figure 1 shows the experimental setup for NFO-CVD. In the experiment, $Zn(acac)_2$ was used as the source of the reacting molecular gas. An $Ar^+$ laser ($\lambda = 457$ nm) was used as the light source. The fiber probe used for NFO-CVD was a high-throughput single-tapered fiber probe, which was fabricated by pulling and etching a pure silica core fiber. The cone angle of the fabricated fiber

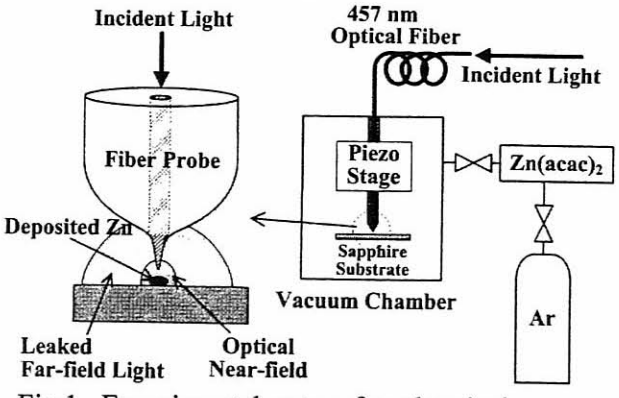


Fig.1. Experimental setup for chemical vapor deposition using an optical near field.

Received April 9, 2007
Accepted May 25, 2007

probe was 30 degrees and its apex diameter was 30 nm. During deposition, the pressure of $Zn(acac)_2$ was 70 mTorr in the CVD chamber. Ultra-high purity argon (Ar) was used as a buffer gas. In the nonadiabatic NFO-CVD, the deposition effect of the far-field light leaking is negligible [6]. Thus a fiber probe without the usual metal coating, *i.e.*, a bare fiber probe could be used for the deposition, and the optical near-field was strongly generated at the apex of the fiber probe. The separation between the fiber probe and the sapphire substrate was controlled to within several nanometers by using a shear-force technique. The laser output power from the fiber probe was measured with a photo-diode placed behind the sapphire substrate. It should be noted that the deposition of Zn on the fiber probe and the resultant decrease in the efficiency of optical near-field generation are negligible because the deposition time is sufficiently short, as has been pointed out [6].

## 3. Results and discussion

Figure 2 shows the shear-force topographical image of the sapphire substrate after NFO-CVD. The observed laser power and the irradiation time were 1 mW and 15 s, respectively. The diameter and height of the Zn dot were 70 nm and 24 nm, respectively. $Zn(acac)_2$ is not usually used for conventional optical CVD due to its low optical activity. However, in case of NFO-CVD, the optical near field can activate the molecule and photodissociated Zn atom is adsorbed under the fiber probe. In NFO-CVD, its deposition rate was almost the same as that of deposition in which diethylzinc (DEZn) gas was used, although for the conventional optical CVD, we carried out that

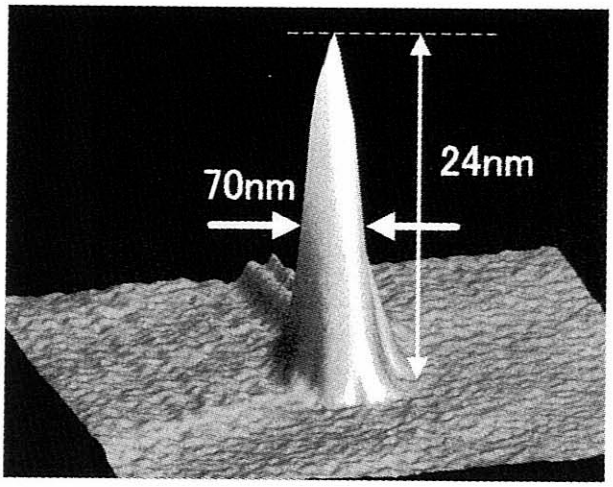


Fig.2. Shear-force topographical images after NFO-CVD using $Zn(acac)_2$ at wavelengths of $\lambda$ = 457nm.

DEZn has a deposition rate of more than 1000 times higher that of $Zn(acac)_2$. We consider that the physical origin of the photodissociation of $Zn(acac)_2$ is also the nonadiabatic photochemical process by ONF [6].

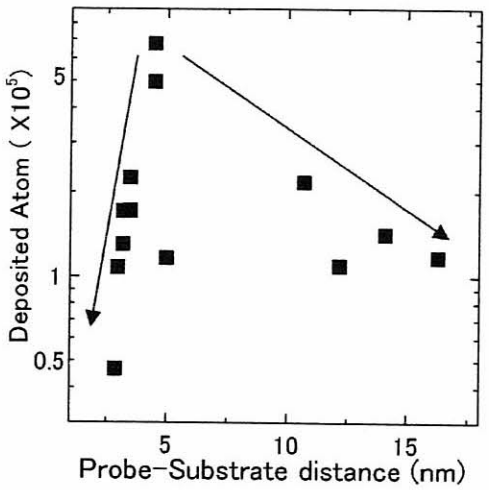


Fig.3. The probe-substrate separation dependence of deposition rate.

It is necessary to improve size-controllability of deposited dots, in order to deposit a Zn nanodot smaller than 10 nm in diameter for the fabrication of a ZnO quantum dot [7]. So, we investigated the

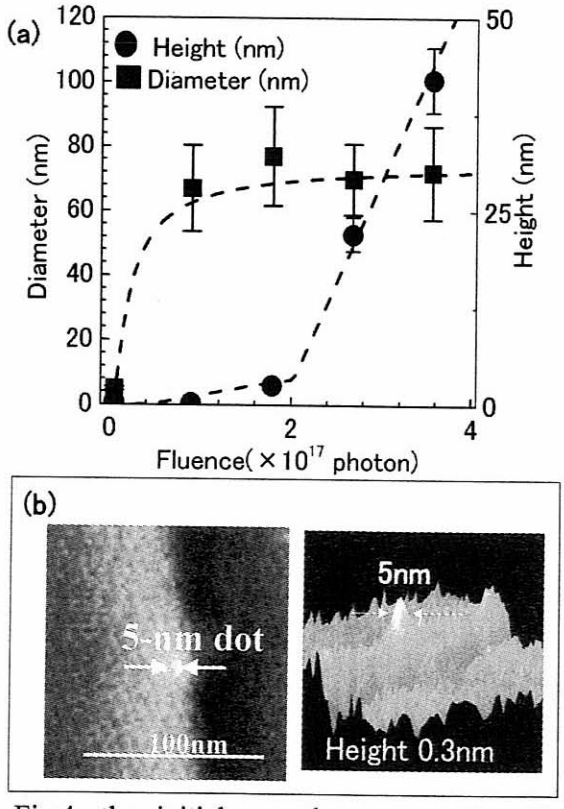


Fig.4. the initial growth process of a Zn nanodot.

deposition rate depending on the probe-substrate separation was investigated, as shown in Fig. 3. The observed laser power and the irradiation time were 160 μW and 60 s, respectively. When the separation was narrower than 5nm, the deposition rate decreased with the decrease in the separation. This deceleration of deposition rate comes from the insufficient supply of $Zn(acac)_2$ molecule. This is because the separation between the substrate and the fiber probe is too narrow to supply $Zn(acac)_2$ for the separation of less than 5-nm. When the separation was broader than 10nm, the deposition rate decreased with the increase in the separation. In this deposit condition, since photodissociated Zn-atoms diffuse away, the deposition rate may decelerate. As a result, we selected the probe-substrate separation of 5nm during the deposition.

Figure 4 (a) shows the initial growth process of a Zn nanodot. The observed laser power was 65 μW. The diameter of the nanodot rapidly increased to the diameter of the probe. On the other hand, its height slowly increased until the diameter broadened to the diameter of the probe. When the fluence is $5\times10^{15}$ photons, the diameter of Zn nanodot was 5nm, as shown in Fig. 4(b). Its height was 0.3 nm which correspond to the monolayer of Zn. So, we have considered the epitaxial growth even in the NFO-CVD. This deposited Zn nanodot by NFO-CVD was the minutest structure that we have fabricated.

## References

1. D. Leonard, M. Krishnamurthy, C. M. Reaves, S. P. Denbaars, and P. M. Petroff, Appl. Phys. Lett., **63**(1993) 3203.
2. T. Tsutsui, K. Kawasaki, M. Mochizuki, and T. Matsubara, Microelectron. Eng., **47** (1999) 135.
3. S. Kohmoto, H. Nakamura, T. Ishikawa, and K. Asakawa, Appl. Phys. Lett., **75** (1999) 3488.
4. E. Kuramochi, J. Temmyo, T. Tamamura, and H. Kamada, Appl. Phys. Lett., **71** (1997) 1655.
5. T. Kawazoe, Y. Yamamoto, and M. Ohtsu, Appl. Phys. Lett., **79** (2001) 1184.
6. T. Kawazoe, K. Kobayashi, S. Takubo, and M. Ohtsu, J. Chem. Phys., **122** (2005) 024715.
7. T. Yatsui, M. Ueda, Y. Yamamoto, T. Kawazoe, M. Kourogi, M. Ohtsu, Appl. Phys. Lett. **81** (2002) 3651.

# Tamper resistance in optical excitation transfer based on optical near-field interactions

**Makoto Naruse,[1,2,*] Hirokazu Hori,[3] Kiyoshi Kobayashi,[4] and Motoichi Ohtsu[2]**

[1]*National Institute of Information and Communications Technology, 4-2-1 Nukui-kita, Koganei, Tokyo 184-8795, Japan*

[2]*The University of Tokyo, 2-11-16 Yayoi, Bunkyo-ku, Tokyo 113-8656, Japan*

[3]*University of Yamanashi, 4-3-11 Takeda, Kofu, Yamanashi 400-8511, Japan*

[4]*Tokyo Institute of Technology, 2-12-1 Ookayama, Meguro-ku, Tokyo 152-8551, Japan*

[*]*Corresponding author: naruse@nict.go.jp*

Received February 5, 2007; accepted April 26, 2007;
posted May 4, 2007 (Doc. ID 79765); published June 13, 2007

We present tamper resistance in optical excitation transfer via optical near-field interactions based on the energy dissipation process occurring locally in nanometric devices such as quantum dots. A theoretical comparison with electrical systems is also shown, focusing on the required environmental conditions. Numerical simulations based on virtual photon models demonstrate high tamper resistance. © 2007 Optical Society of America

*OCIS codes:* 260.2110, 270.0270, 070.6020.

Recent advances in optical near-fields have allowed the design of optical devices and systems at densities beyond those conventionally limited by the diffraction of light. Basic fundamental processes, such as optical excitation transfer via optical near-fields between quantum dots (QDs) [1] or metal nanoparticles [2], have been studied in detail. With the goal of achieving room-temperature operation, materials such as ZnO nanocrystallites [3,4] and InAlAs QDs [5] have also been studied and have demonstrated promising results. In addition to breaking through the diffraction limit of light, such local interactions of optical near-fields also have important functional aspects, such as in security application, particularly tamper resistance against attacks. One of the most critical security issues in present electronic devices is so-called side-channel attacks, by which information is tampered with either invasively or noninvasively; this may be achieved, for instance, merely by monitoring their power consumption [6].

In this Letter, we show that devices based on optical excitation transfer via near-field interactions are physically more tamper resistant than their conventional electronic counterparts. We note that the flow of information in nanoscale devices cannot be completed unless they are appropriately coupled with their environment [7], which could possibly be the weakest link in terms of their tamper resistance. We present a theoretical approach to investigate the tamper resistance of optical excitation transfer, including a comparison with electrical devices, for example, a single charge tunneling device [8], and we describe numerical calculations based on a virtual photon model [9].

Here, we define tampering of information as involving simple signal transfer processes, since our primary focus is on their fundamental physical properties. We begin with the interaction Hamiltonian between an electron and an electric field, which is given by

$$\hat{H}_{\mathrm{int}} = -\int \hat{\psi}^{\dagger}(\vec{r})\vec{\mu}\hat{\psi}(\vec{r}) \cdot \hat{\vec{D}}(\vec{r})\mathrm{d}\vec{r}, \tag{1}$$

where $\vec{\mu}$ is a dipole moment, $\hat{\psi}^{\dagger}(\vec{r})$ and $\hat{\psi}(\vec{r})$ are, respectively, creation and annihilation operators of an electron at $\vec{r}$, and $\hat{\vec{D}}(\vec{r})$ is the operator of electric flux density. In usual light–matter interactions, the operator $\hat{\vec{D}}(\vec{r})$ is a constant since the electric field of propagating light is considered to be constant on the nanometer scale. Therefore, as is well known, we can derive optical selection rules by calculating a transfer matrix of an electrical dipole. As a consequence, in the case of cubic quantum dots for instance, transition to states containing an even quantum number are prohibited. In the case of optical near-field interactions, on the other hand, due to the steep electric field of optical near-fields in the vicinity of nanoscale material, an optical transition that violates conventional optical selection rules is allowed. Detailed theory can be found in [1].

Using near-field interactions, optical excitations in nanostructures, such as quantum dots, can be transferred to neighboring ones [1,2,5]. For instance, assume two cubic quantum dots whose side lengths $L$ are $a$ and $\sqrt{2}a$, which we call $\mathrm{QD_A}$ and $\mathrm{QD_B}$, respectively, as shown in Fig. 1(a). Suppose that the energy eigenvalues for the quantized exciton energy level specified by quantum numbers $(n_x,n_y,n_z)$ in a QD with side length $L$ are given by

$$E_{(n_x,n_y,n_z)} = E_B + \frac{\hbar^2\pi^2}{2ML^2}(n_x^2 + n_y^2 + n_z^2), \tag{2}$$

where $E_B$ is the energy of the bulk exciton and $M$ is the effective mass of the exciton. According to Eq. (2), there exists a resonance between the level of quantum number (1,1,1) for $\mathrm{QD_A}$ and that of quantum number (2,1,1) for $\mathrm{QD_B}$. There is an optical near-field

0146-9592/07/121761-3/$15.00 

interaction, which is denoted by $U$, due to the steep electric field in the vicinity of $QD_A$. Therefore, excitons in $QD_A$ can move to the (2,1,1)-level in $QD_B$. Note that such a transfer is prohibited in propagating light since the (2,1,1)-level in $QD_B$ contains an even number. In $QD_B$, the exciton sees a sublevel energy relaxation, denoted by $\Gamma$, which is faster than the near-field interaction, and so the exciton goes to the (1,1,1)-level of $QD_B$. We should also note that the sublevel relaxation determines the unidirectional exciton transfer from $QD_A$ to $QD_B$.

To compare the tamper resistance capability, here we introduce an electronic system based on single charge tunneling, where a tunnel junction with capacitance $C$ and tunneling resistance $R_T$ is coupled to a voltage source $V$ via the external impedance $Z(\omega)$, as shown in Fig. 1(b). To achieve single charge tunneling, besides the condition that the electrostatic energy $E_C=e^2/2C$ of a single excess electron be greater than the thermal energy $k_BT$, the environment must have appropriate conditions, as discussed in detail in [8]. For instance, by an inductance $L$ in the external impedance, the fluctuation of the charge is given by

$$\langle \delta Q^2 \rangle = \frac{e^2}{4\rho} \coth\left(\frac{\beta\hbar\varpi_s}{2}\right), \tag{3}$$

where $\rho=E_C/\hbar\varpi_S$, $\varpi_S=(LC)^{-1/2}$, and $\beta=1/k_BT$. Therefore charge fluctuations cannot be small even at zero temperature unless $\rho \gg 1$. This means that a high-impedance environment is necessary, which makes tampering technically easy, for instance by adding another impedance circuit.

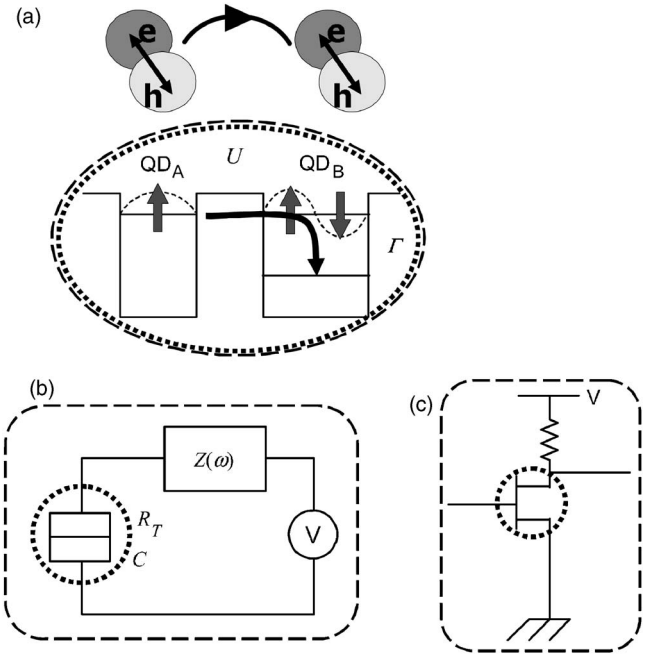


Fig. 1. Model of tamper resistance in devices based on (a) optical excitation transfer, (b) single charge tunneling, and (c) transistor. Dotted curves show the scale of a key device, and dashed curves show the scale of the environment required for the system to work. In (a), an exciton can move from $QD_A$ to $QD_B$ via optical near-field interactions and sublevel relaxation.

Here, we define two scales to illustrate tamper resistance: (I) the scale associated with the key device size, and (II) the scale associated with the environment required for operating the system, which are, respectively, indicated by the dotted and dashed lines in Fig. 1. In the case of Fig. 1(b), scale I is the scale of a tunneling device, whereas scale II covers all of the components. It turns out that the low tamper resistance of such wired devices is because scale II is typically the macroscale, even though scale I is the nanometer scale.

As another example, the system in Fig. 1(c) contains a field effect transistor (FET), which is the key device that we associate with scale I. Since an FET needs connections to ground and power supply to function, the flow of information is determined by the energy dissipation occurring outside of scale I. Therefore, again we can define scale II so that it covers all of the components. Therefore, scales I and II, as well as the tamper resistance, have the same properties as in the previous case.

In contrast, in the case of the optical excitation transfer shown in Fig. 1(a), the two quantum dots and their surrounding environment are governed by scale I; it is also important to note that scale II is the same as scale I. More specifically, the transfer of an exciton from $QD_A$ to $QD_B$ is completed due to the nonradiative relaxation process occurring at $QD_B$, which is usually difficult to tamper with. Theoretically, the sublevel relaxation constant is given by

$$\Gamma = 2\pi|g(\omega)|^2 D(\omega), \tag{4}$$

where $\hbar g(\omega)$ is the exciton–phonon coupling energy at frequency $\omega$, $\hbar$ is the Planck constant divided by $2\pi$, and $D(\omega)$ is the phonon density of states. Therefore, tampering with the relaxation process requires somehow "stealing" the exciton–phonon coupling, which would be extremely difficult technically.

We should also note that the energy dissipation occurring in the optical excitation transfer, derived theoretically as $E_{(2,1,1)}-E_{(1,1,1)}$ in $QD_B$ based on Eq. (2), should be larger than the exciton–phonon coupling energy of $\hbar\Gamma$, otherwise the two levels in $QD_B$ cannot be resolved. This is similar to the fact that the condition $\rho \gg 1$ is necessary in the electron tunneling example, which means that the mode energy $\hbar\varpi_s$ is smaller than the required charging energy $E_C$. By regarding $\hbar\Gamma$ as a kind of mode energy in the optical excitation transfer, the difference between the optical excitation transfer and a conventional wired device is the physical scale at which this mode energy is realized: nanoscale for the optical excitation transfer, and macroscale for electric circuits.

Another possible method of attack is to use a probe, that is, an invasive attack, to tamper with the exciton flow. This is modeled by the system shown in Fig. 2(a), where the original two quantum dots are depicted by A and B, and the attacker is represented by C. By using a virtual photon model [9], the solid curves shown in Figs. 2(b) and 2(c) show the calculated evolution of the population of the lower level of

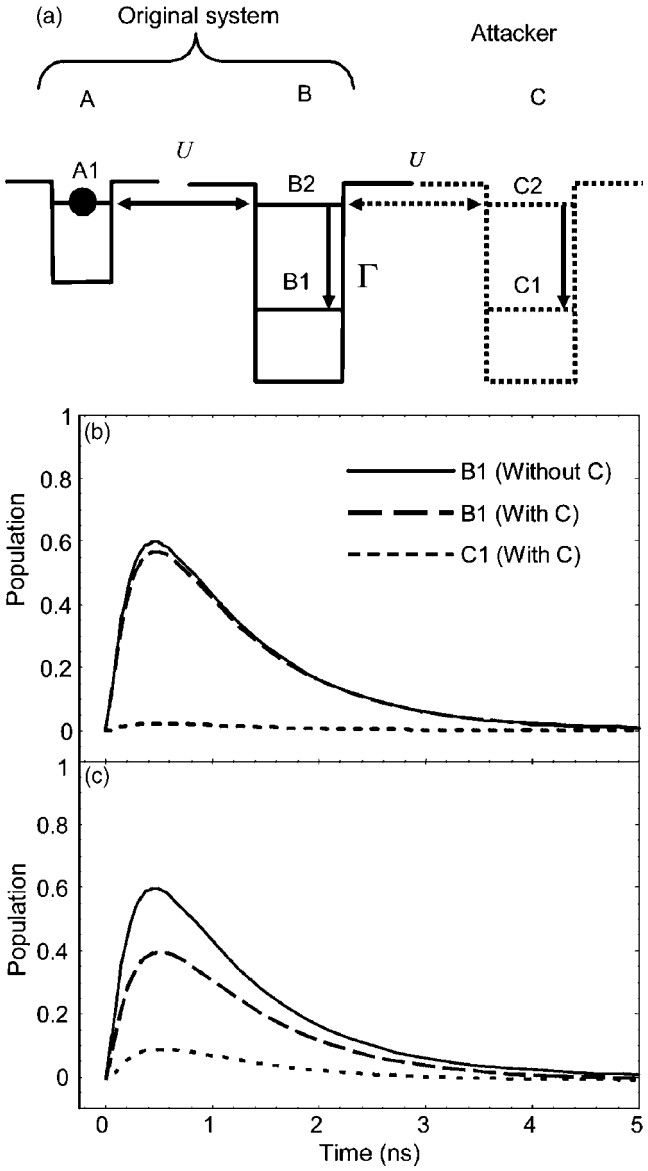


Fig. 2. Tamper resistance in optical excitation transfer system. (a) Physical model based on virtual photon model. (b), (c) Evolution of population of B1-level without QD C (solid curve), B1-level with QD C (dashed curve), and C1-level (dotted curve).

B (=B1) in the absence of the attacker dot C. The interdot interaction is assumed to be 100 ps ($U^{-1}$), and the sublevel relaxation at B is assumed to be 5 ps ($\Gamma^{-1}$), as typical parameters. Now, in the presence of C, the dashed curve and the dotted curve in Fig. 2(b), respectively, show the evolution of the lower levels of B (B1) and C (C1). It is clear that there is little population in C1, meaning that tampering is difficult, since the sublevel relaxation at B is faster than the interaction between B2 and C2. Now, suppose that the interaction between B2 and C2 could be made faster (for example, 50 ps); then, the attacker could have a higher population, as shown by the dotted curve in Fig. 2(c). However, at the same time, the population of B1 (dashed curve) is degraded accordingly, meaning that the attack is detectable from the performance degradation of the original system.

In summary, we have analyzed the tamper resistance of optical excitation transfer via optical near-field interactions by noticing the energy dissipation process or the relation to the environment for signal transfer. The tamper resistance is associated with the physical scale required for the environment, which is the nanoscale and the macroscale for optical excitation transfer and conventional electrical circuits, respectively. Numerical simulations are also presented that support the difficulty of tampering with the excitation transfer process.

## References

1. M. Ohtsu, K. Kobayashi, T. Kawazoe, S. Sangu, and T. Yatsui, IEEE J. Sel. Top. Quantum Electron. **8**, 839 (2002).
2. S. A. Maier, P. G. Kik, H. A. Atwater, S. Meltzer, E. Harel, B. E. Koel, and A. A. G. Requicha, Nat. Mater. **2**, 229 (2003).
3. M. H. Huang, S. Mao, H. Feick, H. Yan, Y. Wu, H. Kind, E. Weber, R. Russo, and P. Yang, Science **292**, 1897 (2001).
4. T. Yatsui, M. Ohtsu, S. J. An, J. Yoo, and G.-C. Yi, Appl. Phys. Lett. **87**, 033101 (2005).
5. T. Kawazoe, K. Kobayashi, K. Akahane, M. Naruse, N. Yamamoto, and M. Ohtsu, Appl. Phys. B **84**, 243 (2006).
6. For example, http://www.cryptography.com/resources/whitepapers/DPATechInfo.pdf.
7. H. Hori, in *Optical and Electronic Process of Nano-Matters*, M. Ohtsu, ed. (Kluwer Academic, 2001), p. 1.
8. G.-L. Ingold and Y. V. Nazarov, in *Single Charge Tunneling*, H. Grabert and M. H. Devoret, eds. (Plenum, 1992), p. 21.
9. K. Kobayashi and M. Ohtsu, J. Microsc. **194**, 249 (1999).

# Nanophotonic switch using ZnO nanorod double-quantum-well structures

Takashi Yatsui[a)]
*SORST, Japan Science and Technology Agency, Bunkyo-ku, Tokyo 113-8656, Japan*

Suguru Sangu
*Advanced Technology R&D Center, Ricoh Co. Ltd., Yokohama, Kanagawa 224-0035, Japan*

Tadashi Kawazoe and Motoichi Ohtsu[b)]
*School of Engineering, The University of Tokyo, Bunkyo-ku, Tokyo 113-8656, Japan*

Sung Jin An, Jinkyoung Yoo, and Gyu-Chul Yi
*National CRI Center for Semiconductor Nanorods, Pohang University of Science and Technology (POSTECH), San 31 Hyoja-dong, Pohang, Gyeongbuk 790-784, Korea and Department of Materials Science and Engineering, Pohang University of Science and Technology (POSTECH), San 31 Hyoja-dong, Pohang, Gyeongbuk 790-784, Korea*

(Received 12 March 2007; accepted 5 May 2007; published online 30 May 2007)

The authors report on time-resolved near-field spectroscopy of ZnO/ZnMgO nanorod double-quantum-well structures (DQWs) for a nanometer-scale photonic device. They observed nutation of the population between the resonantly coupled exciton states of DQWs. Furthermore, they demonstrated switching dynamics by controlling the exciton excitation in the dipole-inactive state via an optical near field. The results of time-resolved near-field spectroscopy of isolated DQWs described here are a promising step toward designing a nanometer-scale photonic switch and related devices. © *2007 American Institute of Physics*. [DOI: 10.1063/1.2743949]

Systems of optically coupled quantum dots (QDs) should be applicable to quantum information processing.[1,2] Additional functional devices (i.e., nanophotonic devices[3–6]) can be realized by controlling the exciton excitation in QDs. ZnO is a promising material for room-temperature operation, owing to its large exciton binding energy[7–9] and recent achievements in the fabrication of nanorod heterostructures.[10,11] This study used time-resolved near-field spectroscopy to demonstrate the switching dynamics that result from controlling the optical near-field energy transfer in ZnO nanorod double-quantum-well structures (DQWs). We observed nutation of the population between the resonantly coupled exciton states of DQWs, where the coupling strength of the near-field interaction decreased exponentially as the separation increased.

To evaluate the energy transfer, three samples were prepared [Fig. 1(a)]: (1) single-quantum-well structures (SQWs) with a well-layer thickness of $L_w$=2.0 nm (SQWs), (2) DQWs with $L_w$=3.5 nm with 6 nm separation (1-DQWs), and (3) three pairs of DQWs with $L_w$=2.0 nm with different separations (3, 6, and 10 nm), where each DQW was separated by 30 nm (3-DQWs). These thicknesses were determined by the transmission electron microscopy (TEM) measurement. ZnO/ZnMgO quantum-well structures (QWs) were fabricated on the ends of ZnO nanorods with a mean diameter of 80 nm using catalyst-free metal organic vapor phase epitaxy.[10] The average concentration of Mg in the ZnMgO layers used in this study was determined to be 20 at. %.

The far-field photoluminescence (PL) spectra were obtained using a He–Cd laser (λ=325 nm) before detection using near-field spectroscopy. The near-field photoluminescence (NFPL) spectra were obtained using a He–Cd laser (λ=325 nm), collected with a fiber probe with an aperture diameter of 30 nm, and detected using a cooled charge-coupled device through a monochromator. Blueshifted PL peaks were observed at 3.499($I_S$), 3.429($I_{1D}$), and 3.467 ($I_{3D}$) eV in the far- and near-field PL spectra [Fig. 2(a)]. We believe that these peaks originated from the respective ZnO QWs because their energies are comparable to the predicted ZnO well-layer thicknesses of 1.7($I_S$), 3.4($I_{1D}$), and 2.2 ($I_{3D}$) nm, respectively, calculated using the finite square-well potential of the quantum confinement effect in ZnO SQWs.[10] To confirm the near-field energy transfer between QWs, we compared the time-resolved near-field PL ($TR_{NFPL}$) signals at the $I_S$, $I_{1D}$, and $I_{3D}$ peaks. For the time-resolved near-field spectroscopy, the signal was collected with a fiber probe with an aperture diameter of 30 nm and detected using a microchannel plate through a bandpass filter with 1 nm spectral width. Figure 2(b) shows the typical $TR_{NFPL}$ of SQWs ($TR_S$), 1-DQWs ($TR_{1D}$), and 3-DQWs ($TR_{3D}$), respectively, using the 4.025 eV (λ=308 nm) light with a pulse of 10 ps duration to excite the barrier layers of ZnO QWs.

We calculate the exciton dynamics using quantum mechanical density-matrix formalism,[12,13]

$$\dot{\rho} = -\frac{i}{\hbar}[H,\rho] + \sum_n \frac{\gamma_n}{2}(2A_n\rho A_n^\dagger - A_n^\dagger A_n\rho - \rho A_n^\dagger A_n) \qquad (1)$$

($\rho$: density operator, $H$: Hamiltonian in the considered system, $A_n^\dagger$ and $A_n$: creation and annihilation operators for an exciton energy level labeled $n$, and $\gamma_n$: photon or phonon relaxation constant). The exciton population is calculated using matrix elements for all exciton states in the system considered. First, we apply the calculation to a three-level system of SQWs [inset of Fig. 2(c)], where the continuum state $\hbar\Omega_C$ is initially excited using a 10 ps laser pulse. Then, the initial exciton population in ZnO QWs is created in $\hbar\Omega_{1S}$, where an incoherent Gaussian excitation term with a tempo-

a)Electronic mail: yatsui@ohtsu.jst.go.jp
b)Also at SORST, Japan Science and Technology Agency, 2-11-16 Yayoi, Bunkyo-ku, Tokyo 113-8656, Japan.

 

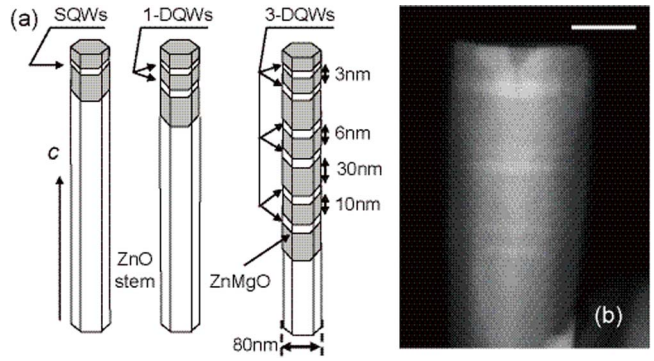


FIG. 1. ZnO/ZnMgO nanorod quantum-well structures. c: *c* axis of the ZnO stem. (a) Schematics of ZnO/ZnMgO SQWs, DQWs (1-DQWs), and triple pairs of DQWs (3-DQWs). (b) *Z*-contrast TEM image of 3-DQWs clearly shows the compositional variation, with the bright layers representing the ZnO well layers. Scale bar: 50 nm.

ral width of $2\sigma_{1S}$ is added in Eq. (1) because nonradiative relaxation paths via exciton-phonon coupling make a dephased input signal, statistically. Finally, an exciton carrier relaxes due to the electron-hole recombination with relaxation constant $\gamma_{1S}$. Figure 2(c) shows a numerical result and experimental data. Here, we used $2\sigma_{1S}=100$ ps, and $\gamma_{1S}$ was evaluated as 460 ps.

A similar calculation was applied for DQWs. We used two three-level systems, coupled via an optical near field with a coupling strength of $U_{12}$ [inset of Fig. 2(d)]. Figure 2(d) shows the numerical results for the exciton population in $QWs_1$ and the experimental data. Here $2\sigma_{1D}$ and $2\sigma_{2D}$ were set at 200 ps, which is twice the value for SQWs, because the relaxation paths extend the barrier energy state in the two quantum well (QW). $\gamma_{1D}$ and $\gamma_{2D}$ are evaluated as 200 ps. We believe that the faster relaxation for DQWs compared with SQWs reflects the lifetime of the coupled states mediated by the optical near-field. Furthermore, the characteristic behavior that results from near-field coupling appears as the oscillatory decay in Fig. 2(d). This indicates that the time scale of the near-field coupling is shorter than the decoherence time, and that coherent coupled states, such as symmetric and antisymmetric states,[14] determine the system dynamics. Furthermore, nutation never appears unless unbalanced initial exciton populations are prepared for $\hbar\Omega_{1D}$ and $\hbar\Omega_{2D}$. In the far-field excitation, only the symmetric state is excited because the antisymmetric state is dipole inactive. By contrast, in the near-field excitation, both the symmetric and antisymmetric states are excited due to the presence of a near-field probe. Since the symmetric and antisymmetric states have different eigenenergies, the interference of these states generates a detectable beat signal. The unbalanced excitation rate is given by $A_1/A_2=10$ here. From the period of nutation, the strength of the near-field coupling is estimated to be $U_{12}=7.7$ ns$^{-1}$ (=4.9 $\mu$eV).

We evaluated nutation frequencies using Fourier analysis. In Fig. 3(a), the power spectral density of SQWs ($PS_S$) does not exhibit any peaks, indicating a monotonic decrease. By contrast, the power spectral density of 1-DQWs ($PS_{1D}$) had a strong peak at a frequency of 2.6 ns$^{-1}$. Furthermore, that of 3-DQWs ($PS_{3D}$) had three peaks at 1.9, 4.7, and 7.1 ns$^{-1}$. Since, the degree of the coupling strength, which is proportional to the frequency of the nutation, increases as the separation decreases, the three peaks correspond to the signals from DQWs with separations of 10, 6, and 3 nm, respectively. Since the coupling strength $\hbar U$ (eV) is given by $\hbar\pi f$ ($f$: nutation frequency), $\hbar U$ are estimated as 4.0, 9.9, and 14.2 $\mu$eV for DQWs with respective separations of 10, 6, and 3 nm. Furthermore, the peak intensity for the DQWs with 3 nm separation is much lower than for those with 10 nm separation, which might be caused by decoherence of the exciton state due to penetration of the electronic carrier. Considering the carrier penetration depth, the strong peak of DQWs with 10 nm separation originates from the near-field coupling alone. The solid line in Fig. 3(b) shows the separation dependence of the peak frequency. The exponentially

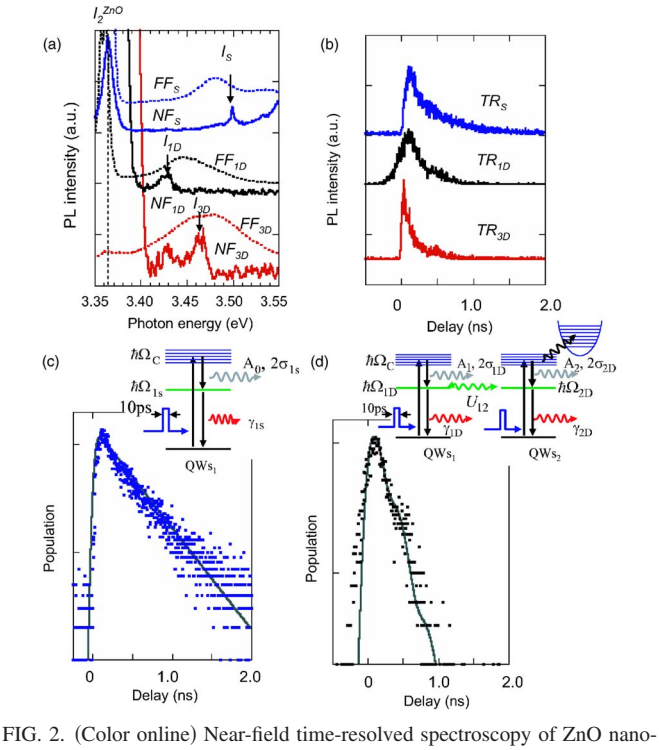


FIG. 2. (Color online) Near-field time-resolved spectroscopy of ZnO nanorod DQWs at 15 K. (a) $NF_S$, $NF_{1D}$, and $NF_{3D}$: near-field PL spectra. $FF_S$, $FF_{1D}$, and $FF_{3D}$: far-field PL spectra of ZnO SQWs (Lw=2.0 nm), 1-DQWs (Lw=3.5 nm, 6 nm separation), and 3-DQWs (Lw=2.0 nm and 3, 6, and 10 nm separation). (b) $TR_S$, $TR_{1D}$, and $TR_{3D}$ show $TR_{NFPL}$ signal obtained at $I_S$, $I_{1D}$, and $I_{3D}$. Theoretical results on the transient exciton population dynamics (solid curves) and experimental PL data (filled squares) of (c) SQWs [same as curve $TR_S$ in (b)] and (d) 1-DQWs [same as curve $TR_{1D}$ in (b)]. The insets schematically depict the respective system configurations. $\hbar\Omega_C$: barrier energy state with a central energy.

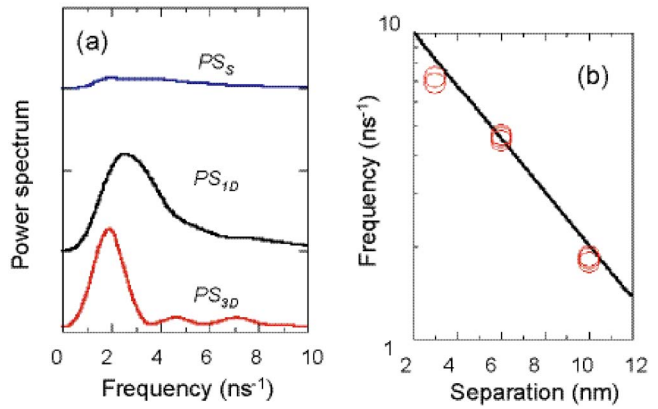


FIG. 3. (Color online) Evaluation of the nutation frequencies between the QWs. (a) $PS_S$, $PS_{1D}$, and $PS_{3D}$ show the power spectra of $TR_S$, $TR_{1D}$, and $TD_{3D}$, respectively. (b) Separation $D$ dependence of frequency of the nutation.

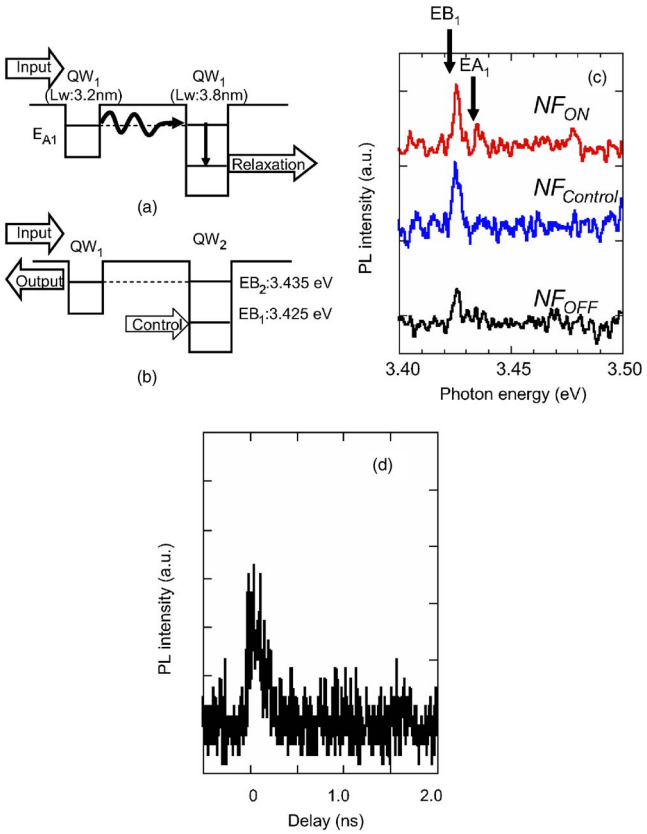


FIG. 4. (Color online) Switching operation by controlling the exciton excitation. Schematic of the nanophotonic switch of (a) "off" state and (b) "on" state. (c) $NF_{on}$, $NF_{control}$, and $NF_{off}$ show NFPL signal obtained with the illumination of input laser along, control laser alone, and input and control laser, respectively. (d) Near-field time-resolved PL signal with on state.

decaying dependence represented by this line supports the origin of the peaks in the power spectra from the localized near-field interaction between the QWs.

Next, we performed the switching operation. Figures 4(a) and 4(b) explain the "off" and "on" states of the proposed nanophotonic switch, consisting of two coupled QWs. $QW_1$ and $QW_2$ are used as the input/output and control ports of the switch, respectively. Assuming $L_w$=3.2 and 3.8 nm, the ground exciton state in $QW_1$ and the first excited state in $QW_2$ resonate. In the off operation [Fig. 4(a)], all the exciton energy in $QW_1$ is transferred to the excited state in the neighboring $QW_2$ and relaxes rapidly to the ground state. Consequently, no output signals are generated from $QW_1$. In the on operation [Fig. 4(b)], the escape route to $QW_2$ is blocked by the excitation of $QW_2$, owing to state filling in $QW_2$ on applying the control signal; therefore, an output signal is generated from $QW_1$.

Figure 4(c) shows the NFPL for the three pairs of DQWs with $L_w$=3.2 and 3.8 nm with different separations (3, 6, and 10 nm). Curve $NF_{off}$ was obtained with continuous input light illumination from a He–Cd laser (3.814 eV). No emission was observed from the exciton ground state of $QW_1$ ($EA_1$) or the excited state of $QW_2$ ($EB_2$) at a photon energy of 3.435 eV, indicating that the excited energy in $QW_1$ was transferred to the excited state of $QW_2$. Furthermore, the excited state of $QW_2$ is a dipole-forbidden level. Curve $NF_{control}$ shows the NFPL signal obtained with control light excitation of 3.425 eV with a 10 ps pulse. Emission from the ground state of $QW_2$ at a photon energy of 3.425 eV was observed. Both input and control light excitations resulted in an output signal with an emission peak at 3.435 eV, in addition to the emission peak at 3.425 eV (curve $NF_{on}$), which corresponds to the ground state of $QW_2$. Since the excited state of $QW_2$ is a dipole-forbidden level, the observed 3.435 eV emission indicates that the energy transfer from the ground state of $QW_1$ to the excited state of $QW_2$ was blocked by the excitation of the ground state of $QW_2$.

Finally, the dynamic properties of the nanophotonic switching were evaluated by using the time correlation single photon counting method. We observed $TR_{NFPL}$ signals using a fiber probe with an aperture diameter of 30 nm at 3.435 eV with both input and control laser excitations [see Fig. 4(d)]. The decay time constant was found to be 483 ps. The output signal increased synchronously, within 100 ps, with the control pulse. Since the rise time is considered equal to one-quarter of the nutation period $\tau$,[15] the value agrees with those obtained for DQWs with the same well width in the range from $\tau/4=36$ ps (3 nm separation) to $\tau/4=125$ ps (10 nm separation).

We observed the nutation between DQWs and demonstrated the switching dynamics by controlling the exciton excitation in the QWs. For room-temperature operation, since the spectral width reaches thermal energy (26 meV), a higher Mg concentration in the barrier layers and narrower $L_w$ are required so that the spectral peaks of the first excited state ($E_2$) and ground state ($E_1$) do not overlap. This can be achieved by using two QWs with $L_w$=1.5 nm ($QW_1$) and 2 nm ($QW_2$) with a Mg concentration of 50%, where the energy difference between $E_2$ and $E_1$ in $QW_2$ is 50 meV.[16]

The work at POSTECH was supported by the National Creative Research Initiative Project, Korea and AOARD 04-49 (Quotation No. FA5209-040T0254).

[1]M. Bayer, P. Hawrylak, K. Hinzer, S. Fafard, M. Korkusinski, Z. R. Wasilewski, O. Stern, and A. Forchel, Science **291**, 451 (2001).
[2]E. A. Stinaff, M. Scheibner, A. S. Bracker, I. V. Ponomarev, V. L. Korenev, M. E. Ware, M. F. Doty, T. L. Reinecke, and D. Gammon, Science **311**, 636 (2002).
[3]M. Ohtsu, K. Kobayashi, T. Kawazoe, S. Sangu, and T. Yatsui, IEEE J. Sel. Top. Quantum Electron. **8**, 839 (2002).
[4]T. Kawazoe, K. Kobayashi, S. Sangu, and M. Ohtsu, Appl. Phys. Lett. **82**, 2957 (2003).
[5]T. Kawazoe, K. Kobayashi, K. Akahane, M. Naruse, N. Yamamoto, and M. Ohtsu, Appl. Phys. B: Lasers Opt. **84**, 243 (2006).
[6]M. Naruse, T. Miyazaki, F. Kubota, T. Kawazoe, K. Kobayashi, S. Sangu, and M. Ohtsu, Opt. Lett. **30**, 201 (2005).
[7]A. Ohtomo, K. Tamura, M. Kawasaki, T. Makino, Y. Segawa, Z. K. Tang, K. L. Wong, Y. Matsumoto, and H. Koinuma, Appl. Phys. Lett. **77**, 2204 (2000).
[8]M. H. Huang, S. Mao, H. Feick, H. Yan, Y. Wu, H. Kind, E. Weber, R. Russo, and P. Yang, Science **292**, 1897 (2001).
[9]H. D. Sun, T. Makino, Y. Segawa, M. Kawasaki, A. Ohtomo, K. Tamura, and H. Koinuma, J. Appl. Phys. **91**, 1993 (2002).
[10]W. I. Park, G.-C. Yi, M. Y. Kim, and S. J. Pennycook, Adv. Mater. (Weinheim, Ger.) **15**, 526 (2003).
[11]W. I. Park, S. J. An, J. Long, G.-C. Yi, S. Hong, T. Joo, and M. Y. Kim, J. Phys. Chem. B **108**, 15457 (2004).
[12]B. Coffey and R. Friedberg, Phys. Rev. A **17**, 1033 (1978).
[13]K. Kobayashi, S. Sangu, T. Kawazoe, and M. Ohtsu, J. Lumin. **112**, 117 (2005).
[14]S. Sangu, K. Kobayashi, A. Shojiguchi, and M. Ohtsu, Phys. Rev. B **69**, 115334 (2004).
[15]S. Sangu, K. Kobayashi, T. Kawazoe, A. Shojiguchi, and M. Ohtsu, Trans. Mater. Res. Soc. Jpn. **28**, 1035 (2003).
[16]W. I. Park, G.-C. Yi, and M. Jang, Appl. Phys. Lett. **79**, 2022 (2001).

INSTITUTE OF PHYSICS PUBLISHING NANOTECHNOLOGY
Nanotechnology **18** (2007) 065606 (4pp) doi:10.1088/0957-4484/18/6/065606

# Low-temperature (∼270 °C) growth of vertically aligned ZnO nanorods using photoinduced metal organic vapour phase epitaxy

**T Yatsui[1], J Lim[2], T Nakamata[3], K Kitamura[3], M Ohtsu[1,3] and G-C Yi[4]**

[1] SORST, Japan Science and Technology Agency, Machida, Tokyo 194-0004, Japan
[2] Interdisciplinary Graduate School of Science and Engineering, Tokyo Institute of Technology, Yokohama, Kanagawa 226-8502, Japan
[3] School of Engineering, The University of Tokyo, Bunkyo-ku, Tokyo 113-8656, Japan
[4] National CRI Center for Semiconductor Nanorods and Department of Materials Science and Engineering, Pohang University of Science and Technology (POSTECH), San 31 Hyoja-dong, Pohang, Gyeongbuk 790-784, Korea

E-mail: yatsui@ohtsu.jst.go.jp

Received 5 October 2006, in final form 2 December 2006
Published 10 January 2007
Online at stacks.iop.org/Nano/18/065606

**Abstract**
We successfully produced a drastic decrease in the required growth temperature of single-crystalline ZnO nanorods, and enabled successful growth of vertically aligned ZnO nanorods on a Si(100) substrate using photoinduced metal organic vapour phase epitaxy (MOVPE). We introduced 325 nm light during the MOVPE growth, and achieved vertical growth of single-crystalline ZnO nanorods with a hexagonal crystal structure on Si(100) at a growth temperature of 270 °C. The successful low-temperature growth of ZnO nanorods on the Si(100) substrate described here is a promising step toward designing nanoscale photonic and electronic devices required by future systems.

## 1. Introduction

Future optical transmission systems will require nanometre-scale photonic devices (nanophotonic devices [1]) composed of quantum dots to increase data transmission rates and capacity. ZnO nanocrystallites are potentially ideal components for realizing room-temperature operation of nanophotonic devices because of their high exciton-binding energy [2–4] and great oscillator strength [5]. One representative device studied by researchers is a nanophotonic switch using CuCl quantum cubes [6], in which the switching dynamics are controlled by a dipole-forbidden optical energy transfer among resonant energy levels in nanometre-scale quantum dots via an optical near field. Use of ZnO nanocrystallites, with their great potential depth, could facilitate construction of this device by avoiding carrier penetration. A high atomic concentration of Mg is required to produce a ZnO quantum structure using a ZnMgO buffer layer [2]. To meet this requirement, the growth temperature must be lowered to avoid Mg interdiffusion. Recently, researchers fabricated ZnO/ZnMgO nanorod heterostructures using a metal organic vapour phase epitaxy (MOVPE) system; growth temperatures ranged from 400 to 500 °C, and the system produced a successful quantum confinement effect even from single-quantum-well structures (SQWs) [7, 8].

Both ZnO films and nanostructures have been prepared as substrates for ZnO growth with high-quality crystallinity, typically on sapphire substrates, because this produces a good lattice match with ZnO [7–11]. Nevertheless, the use of Si substrates enables the deposition of nanomaterials on large and inexpensive substrates, offering possible mass production of nanomaterials. More importantly, since ZnO nanorod field-effect transistors have large mobility [12], the preparation of ZnO nanorods on Si appears to be a breakthrough

 

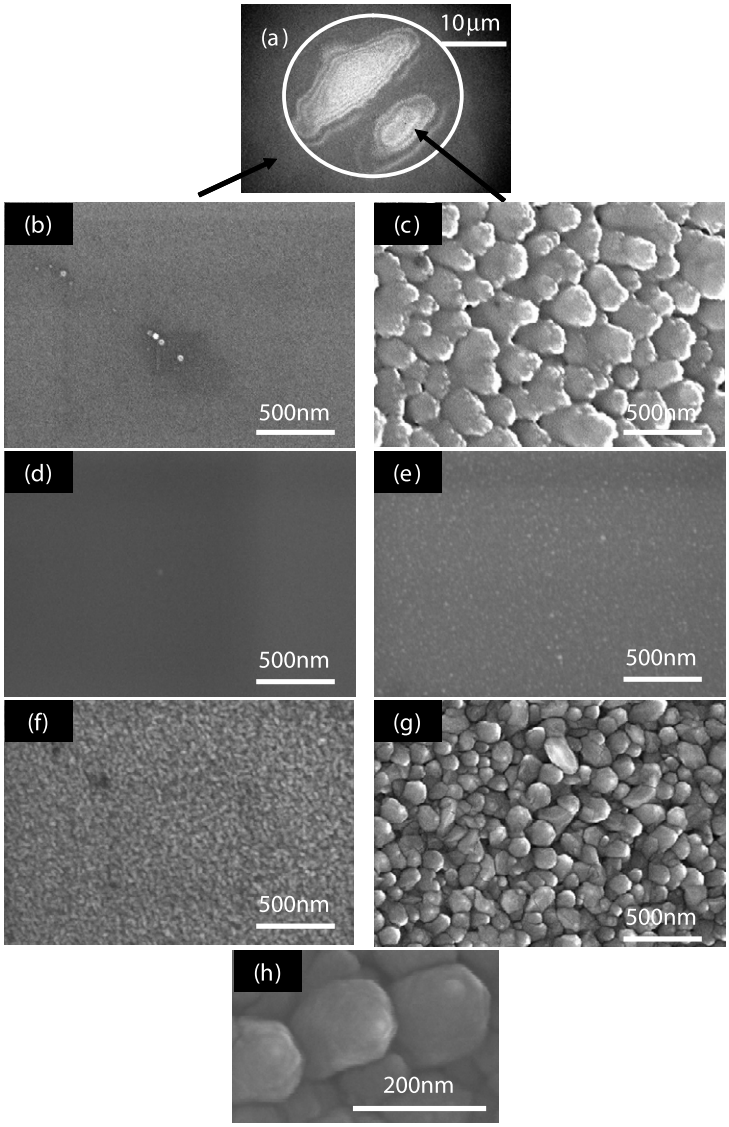


**Figure 1.** (a) SEM image of ZnO films deposited at room temperature. Magnified SEM images at ((b) and (c)) room temperature, ((d) and (e)) 150 °C, and ((f)–(h)) 270 °C, respectively. ((b), (d), and (f)): outside the spot; ((c), (e), (g), and (h)): inside the spot. (h) Magnified SEM image of (g).

for nanomaterial integration in Si-based electronic devices. Despite the importance of nanomaterial growth on Si substrates, vertically well-aligned one-dimensional ZnO nanostructure growth of Si has only been reported on Si(111) substrates [13], which have a hexagonal surface structure. Since Si-based electronic devices use Si(100) substrates with a cubic surface structure, producing a high-quality one-dimensional ZnO nanostructure on a Si(100) substrate using a low growth temperature should offer improved function for devices. In this study, we used photoinduced MOVPE to obtain high-quality crystallinity of ZnO nanorods on a Si(100) substrate using a low growth temperature.

## 2. Experimental technique

ZnO nanorods were grown on Si(100) substrates using a photoinduced MOVPE system. The substrate was dipped in sulfuric acid and hydrogen peroxide solution to remove any organic or metallic impurities, and the native oxide on top was removed using hydrofluoric acid. Diethyl zinc ($Et_2Zn$) and oxygen were used as reactants, and they had flow rates ranging from 20 to 100 sccm and 0.5 to 5 sccm, respectively. During nanorod growth, we used a He–Cd laser light ($\lambda = 325$ nm, 300 $\mu$W) as a light source to assist the MOVPE growth. The photon energy is lower than that of the absorption edge of gas-phase $Et_2Zn$ and higher than that of the absorption edge of adsorption-phase $Et_2Zn$, indicating that the conditions are nonresonant for gas-phase $Et_2Zn$ and resonant for adsorption-phase $Et_2Zn$ [14]. The growth time was 30 min.

We used scanning electron microscopy (SEM) to examine the growth temperature dependence of the surface morphology of films deposited on Si(100). As shown in figures 1(a)–(c), irradiation with a He–Cd laser light (inside the white ellipse) at room temperature covered the Si(100) substrate with several

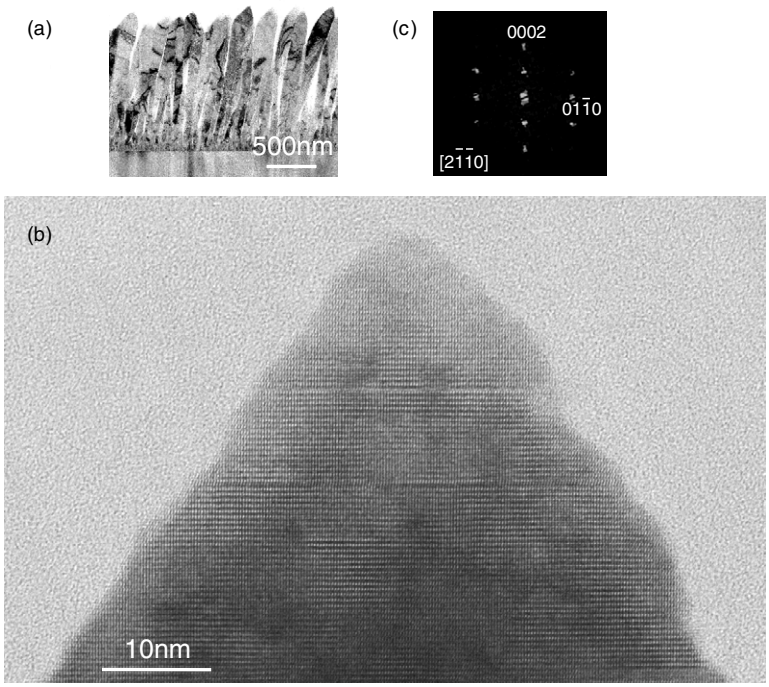


**Figure 2.** (a) Low-magnification and (b) high-resolution TEM images of ZnO nanorods grown at 270 °C. (c) The corresponding SAD pattern.

hundred nanometre-scale grains. The grain size (several 10 nm) was drastically reduced at a growth temperature of 150 °C (see figure 1(e)). However, when the growth temperature increased to 270 °C, hexagon-shaped nanorods with diameters ranging from 50 to 150 nm appeared where the He–Cd laser had irradiated (see figures 1(g) and (h)). The reduced amount of deposition grown at 150 °C resulted from desorption of the adsorption layer of diethyl zinc ($Et_2Zn$) on the substrate [15]. The increased amount of deposition grown at 270 °C resulted from the thermal decomposition of $Et_2Zn$. These postulates are supported by the fact that grains of several 10 nm were deposited outside the beam spot (figure 1(f)).

## 3. Results and discussion

Transmission electron microscopy (TEM) was employed for further investigation of structural characteristics. A low-magnification TEM image (figure 2(a)) reveled vertical growth in the nanorod structure on the Si(100) substrate. Furthermore, a high-resolution TEM image of the nanorod tip (figure 2(b)) and the corresponding selection area diffraction (SAD) pattern (figure 2(c)) revealed that the lattice spacing (0.26 and 0.28 nm) matched the (0002) and $(01\bar{1}0)$ wurtzite planes of ZnO, respectively. TEM images of all the nanorods investigated in this study revealed that ZnO nanorods grew along the [0001] direction. Although the native oxide was removed before deposition, since the deposition was carried out in ambient oxygen, the ZnO nanorods were grown on an oxidized Si substrate. The results indicate that vertically aligned ZnO nanorods with hexagonal structures can be obtained on various substrate types, even glass substrates. Detailed discussions on substrate dependence will be given elsewhere.

We checked the photoluminescence (PL) spectra to evaluate the optical properties of the deposited films. PL spectroscopy was employed for nanorod optical characterization. A 325 nm line from a continuous-wave He–Cd laser was used as the excitation source. Although deposited films grown at both room temperature and 150 °C did not exhibit any peaks in PL spectra at between 5 and 300 K, the deposited hexagon-shaped nanorods grown at 270 °C revealed a strong room-temperature PL emission peak at 3.283 eV (see figure 3(a)). This peak approaches a previously reported peak of 3.29 eV ($\lambda = 380$ nm) [16], corresponding to spontaneous emission from the free exciton in high-quality ZnO nanocrystallites. The full width at half-maximum of the PL spectrum was about 105 meV, which is comparable with the 90 meV of high-quality ZnO nanorods grown using MOVPE at 400 °C [16]. The low-temperature (5 K) PL spectra exhibited a strong PL emission peak, $I_2$, at 3.365 eV (see figure 3(b)), corresponding to the emission from the neutral-donor bound exciton in ZnO. As shown in figure 3(b), the intensity of peak $I_2$ decreased drastically as the temperature increased, and the peak almost disappeared at temperatures above 160 K, while peak $I_{ex}$ grew relative to $I_2$. This behaviour resulted from the decomposition of bound excitons to free excitons due to increased thermal energy, and supports the argument described above that $I_{ex}$ corresponds to a free exciton peak and that $I_2$ is the well-known neutral-donor bound exciton peak emitted from ZnO nanorod stems. Compared to previous reports, the additional peaks observed at 3.319, 3.244, and 3.174 eV were presumably caused by phonon replicas of free excitons [17, 18]. These results demonstrate that metallic Zn films and *c*-axis oriented ZnO nanorods were grown at room temperature and 270 °C, respectively.

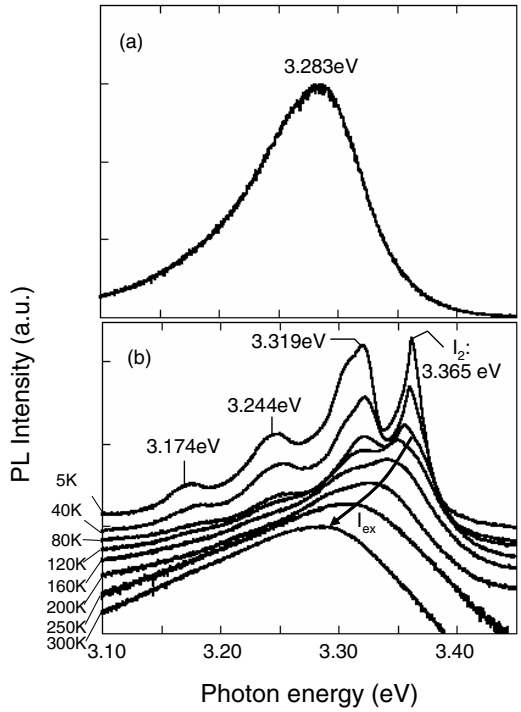


**Figure 3.** (a) Room-temperature (300 K) PL spectrum of a ZnO nanorod grown at 270 °C. (b) Temperature dependence of the PL spectra of a ZnO nanorod grown at 270 °C.

The structural changes in the deposited films described above indicate that UV irradiation allows crystal growth at lower substrate temperatures. That is, UV photon energy assists the reaction during the vapour phase, surface reactions (such as adsorption, desorption, and acceleration of surface migration), and carrier excitation effect. Although the low-temperature (250 °C) growth of ZnO nanorods with high-quality crystallinity has been reported without UV illumination [19], no vertically well-aligned growth at low temperature (270 °C) has been reported on any substrate. The successful growth of ZnO nanorods at low temperature originated from the selective deposition of adsorption-phase $Et_2Zn$. As reported previously [20], we have shown that the photodissociation of adsorption-phase $Et_2Zn$ is selectively generated at the tip of the sharpened fibre probe, where the strong optical near-field is generated. Such a strong field localization may cause a perturbation of the free-molecule potential surface in the adsorbed phase, which would result in a redshift in the absorption spectrum of $Et_2Zn$ and accelerate the deposition rate. Similar selective deposition can be achieved with the sharpened tip of ZnO nanorods.

## 4. Conclusion

In conclusion, the use of photoinduced MOVPE allowed reduced growth temperatures for single-crystalline ZnO nanorods and the fabrication of vertically aligned ZnO nanorod structures on a Si(100) substrate. Electron microscopy revealed that these nanorods possessed high-quality crystallinity and we confirmed their excellent photoluminescence characteristics. Furthermore, since the deposition technique using a photochemical reaction resulted in size- and position-controlled lateral integration [21, 22], this deposition method should produce nanometre-sized lateral integration of nanorods.

## Acknowledgments

The work at POSTECH was supported by the National Creative Research Initiative Project, Korea and AOARD 05-84 (Quotation No. FA5209-05-T0369), United States.

## References

[1] Ohtsu M, Kobayashi K, Kawazoe T, Sangu S and Yatsui T 2002 *IEEE J. Sel. Top. Quantum Electron.* **8** 839
[2] Ohtomo A, Tamura K, Kawasaki M, Makino T, Segawa Y, Tang Z K, Wong G K L, Matsumoto Y and Koinuma H 2000 *Appl. Phys. Lett.* **77** 2204
[3] Huang M H, Mao S, Feick H, Yan H, Wu Y, Kind H, Weber E, Russo R and Yang P 2001 *Science* **292** 1897
[4] Sun H D, Makino T, Segawa Y, Kawasaki M, Ohtomo A, Tamura K and Koinuma H 2002 *J. Appl. Phys.* **91** 1993
[5] Reynolds D C, Look D C, Jogai B, Litton C W, Cantwell G and Harsch W C 1999 *Phys. Rev.* B **60** 2340
[6] Kawazoe T, Kobayashi K, Sangu S and Ohtsu M 2003 *Appl. Phys. Lett.* **82** 2957
[7] Park W I, Yi G-C, Kim M Y and Pennycook S J 2003 *Adv. Mater.* **15** 526
[8] Park W I, An S J, Yang J L, Yi G-C, Hong S, Joo T and Kim M Y 2004 *J. Phys. Chem.* B **108** 15457
[9] Bagnall D M, Chen Y F, Zhu Z, Yao T, Shen M Y and Goto T 1998 *Appl. Phys. Lett.* **73** 1038
[10] Zhu P, Tang Z K, Wong G K L, Kawasaki M, Ohtomo A, Koinuma H and Segawa Y 1997 *Solid State Commun.* **103** 459
[11] Park W I, Yi G-C and Jang H M 2001 *Appl. Phys. Lett.* **79** 2022
[12] Park W I, Kim J S, Yi G-C, Bae M H and Lee H-J 2004 *Appl. Phys. Lett.* **85** 5052
[13] Park W I, Yi G-C, Kim M Y and Pennycook S J 2002 *Adv. Mater.* **14** 1841
[14] Krchnavek R R, Gilgen H H, Chen J C, Shaw P S, Licata T J and Osgood R M Jr 1987 *J. Vac. Sci. Technol.* B **5** 20
[15] Kuniya Y, Deguchi Y and Ichida M 1991 *Appl. Org. Chem.* **5** 337
[16] Park W I, Kim D H, Jung S-W and Yi G-C 2002 *Appl. Phys. Lett.* **80** 4232
[17] Bagnall D M, Chen Y F, Shen M Y, Zhu Z, Goto T and Yao T 1998 *J. Cryst. Growth* **184/185** 605
[18] Park W I and Yi G-C 2001 *J. Electron. Mater.* **30** 32
[19] Xu C, Rho K, Chun J and Kim D-E 2005 *Appl. Phys. Lett.* **87** 253104
[20] Yatsui T, Kawazoe T, Ueda M, Yamamoto Y, Kourogi M and Ohtsu M 2002 *Appl. Phys. Lett.* **81** 3651
[21] Yatsui T, Nomura W and Ohtsu M 2005 *Nano Lett.* **5** 2548
[22] Yatsui T, Takubo S, Lim J, Nomura W, Kourogi M and Ohtsu M 2003 *Appl. Phys. Lett.* **83** 1716

Available online at www.sciencedirect.com
ScienceDirect
Microelectronic Engineering 84 (2007) 705–710
MICROELECTRONIC ENGINEERING
www.elsevier.com/locate/mee

# Near-field lithography as prototype nano-fabrication tool

Yasuhisa Inao [a,*], Shinji Nakasato [a], Ryo Kuroda [a], Motoichi Ohtsu [b]

[a] Canon Research Center, Canon Inc., 30-2, Shimomaruko 3-Chome, Ohta-ku, Tokyo 146–8501, Japan
[b] Department of Electronics Engineering, University of Tokyo, Bunkyo-ku, Tokyo 113–8656, Japan

Available online 27 January 2007

**Abstract**

We demonstrate a prototype of the near-field lithography system, which is a potential tool for low cost nano-fabrication. Resist patterns with 50 nm features are fabricated on the entire surface of a 4-in. silicon wafer by step and repeat exposure using a light source operating at 365 nm. Furthermore, we realize ultra-clean environment by facilitating a dual clean system. Finally, we fabricate dot and hole arrays, which are indispensable patterns for novel nano-devices, demonstrating the applicability of our system to various applications.


*Keywords:* Near-field; Lithography; Clean environment; Nano-optical elements; Step and repeat exposure

## 1. Introduction

Recently, ArF immersion lithography and extreme ultra violet lithography for 32 nm node and below have been intensively studied. The prices of these lithography tools have been constantly soaring by generation, because they require extremely sophisticated technologies. Although many nano-devices and their applications have also been intensively researched, a high cost lithography tool is not convenient for these activities from the standpoint of cost of ownership (CoO). A nano-fabrication tool, which has high enough resolution and is manageable at low-cost, will accelerate these activities to find practical applications of novel nano-devices.

## 2. Concepts of the system

In this paper, we report the development of the near-field lithography (NFL) tool with very high resolution at low cost. This feature would pave the way for developing a wide range of applications. In the course of the development of our system, we have taken into account the following three points as our basic concepts:

(a) In order to manage both nano-scaled high resolution and simple system architecture for low-cost operation, we employ near-field lithography principle.
(b) To achieve the full wafer scale fabrication, we incorporate the step and repeat exposure scheme within our NFL tool.
(c) Ultra-clean environment, also an important factor for high throughput fabrication, is accomplished without using special clean room facilities.

## 3. Structure and operation of the system

### 3.1. Taking the full advantage of the optical near fields

Optical near fields are known for years. It allows us to obtain high resolution with a spot size smaller than that of the propagating light, which is limited by the diffraction. The application of the optical near fields to the lithography enables us to fabricate fine resist patterns smaller than the wavelength used for the exposure [1–4]. As the resolution is not determined by the wavelength, the near-field lithography

* Corresponding author. Tel.: +81 3 5732 2575.
*E-mail address:* inao.yasuhisa@canon.co.jp (Y. Inao).

0167-9317/$ - see front matter © 2007 Elsevier B.V. All rights reserved.
doi:10.1016/j.mee.2007.01.043

does not demand a shorter wavelength light source for high resolution.

The optical near fields are localized around a tiny object or an aperture smaller than the wavelength. Therefore, the near-field lithography requires close contact between the mask and the photoresist. This is achieved by incorporating a membrane mask system, as schematically illustrated in Fig. 1. In this system, by applying the pressure to vessel, the mask deforms about 50 μm to the direction normal to the mask and fits to the wafer over an area of $5 \times 5\ mm^2$. Note that, due to the large mask area and small amount of the deformation, the bending radius is of the order of 10 cm. The resulting placement error depends upon the position of the pattern and is ~0.01% with respect to the mask dimensions. Therefore, this can be corrected when the mask is designed. Furthermore, we do not need a precise control over the focus, differing from the conventional projection lithography system. This greatly reduces the number of components within our NFL system, leading to the low system cost.

Fig. 2 shows a membrane structure of our photomask. A 500 nm thick SiN layer that is transparent to the illuminating light is deposited on a silicon substrate. A 50 nm thick absorber layer, typically made of chromium, is then formed by sputtering. We form an absorber pattern by using the electron beam lithography and the subsequent dry-etching process. Finally, we remove the silicon substrate by the wet-etching process, leaving only the silicon nitride membrane. The fabricated mask has a $10 \times 10\ mm^2$ elastic membrane area on a 4-in. wafer.

Fig. 3 shows the whole prototype lithography system, which shares $\sim 2 \times 3\ m^2$ by its footprint. A mercury lamp, which is our light source, is located outside the enclosure. The UV light is delivered into the system by a fiber bundle and illuminates the photomask from the top without using any special optics. The total power at the fiber end is approximately 1.5 W. Prior to the patterning process $z$-position of the mask is coarsely aligned (precise control is not required as described above). Then, we align the wafer by using the $x$–$y$ stages. The proximity contact is achieved by applying pressure of around 5 kPa to a pressure vessel. Note that the amount of deformation imposed on the mask is very small as we initially align the mask just 50 μm above the photoresist layer. Then

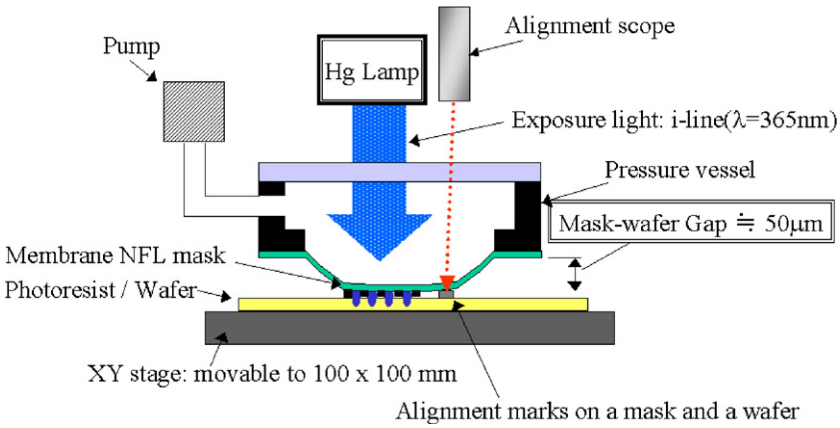


Fig. 1. Schematic illustration of prototype of near-field lithography.

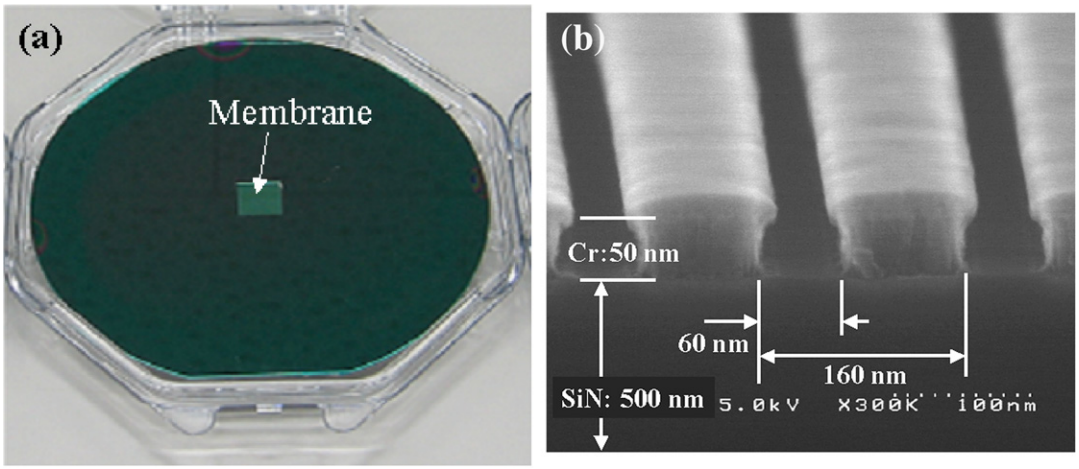


Fig. 2. (a) Photomask for near-field lithography and (b) chromium mask absorber pattern on a SiN membrane.

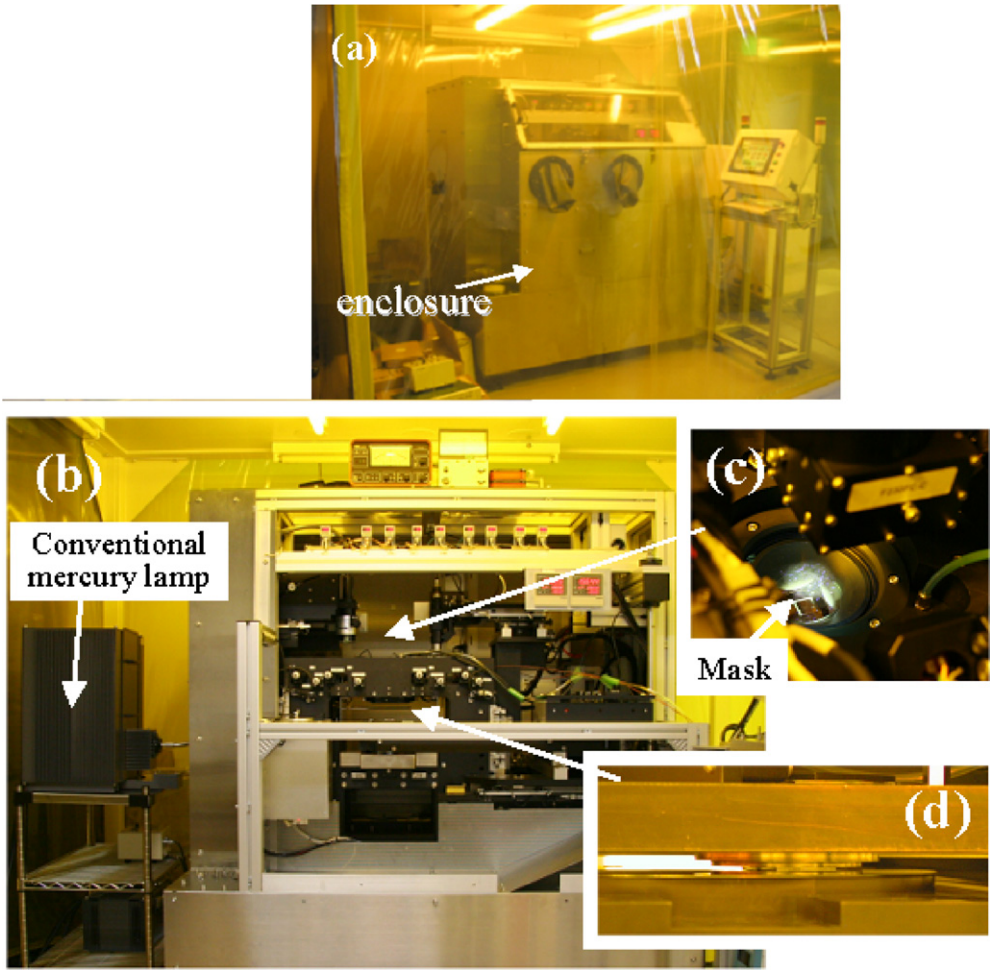


Fig. 3. Photograph of (a) whole system of our prototype, (b) inside of the enclosure and the light source, (c) photomask held under the pressure vessel illuminated by fiber bundle and (d) contact between photomask and wafer by applying pressure and deforming photomask.

the light is illuminated to the photoresist and the optical near field distribution is translated to the photoresist.

The fabricated pattern on the photoresist is shown in Fig. 4. The structural dimensions are 160 nm pitch and 50 nm wide, and which are smaller than the wavelength

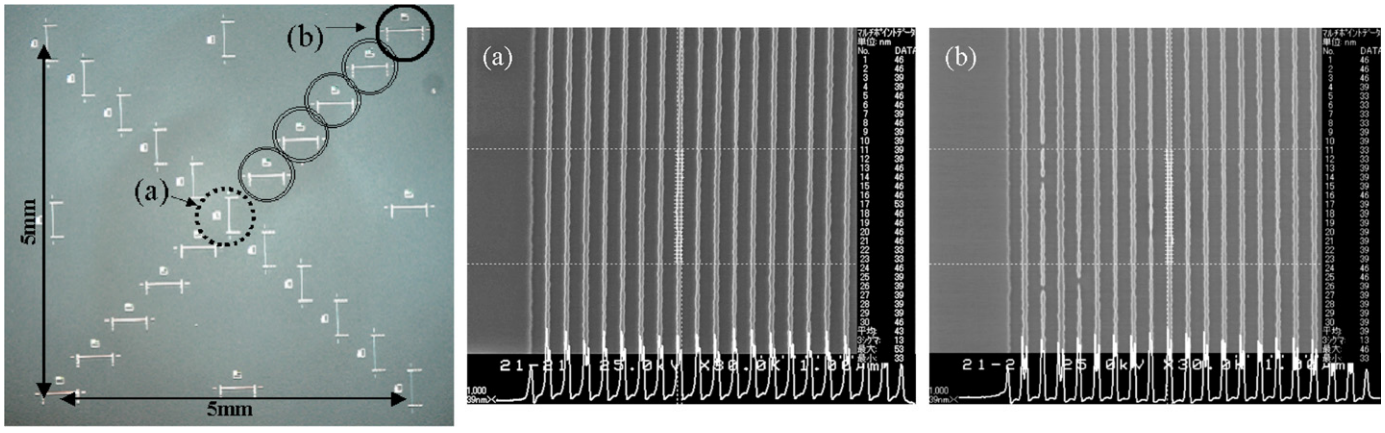


Fig. 4. Uniform pattern in an area of $5 \times 5$ mm$^2$, (a) SEM image of pattern located at the center of exposure area, (b) SEM image of pattern located at the edge of exposure area.

of the light that we used ($\lambda = 365$ nm). In this example, we employed the tri-layer resist stack, which consists of the photosensitive layer of 30 nm thick, the middle-etching mask layer of 20 nm thick and the bottom layer of 100 nm thick [2]. In our test mask, 25 sets of the patterns with similar line and space are distributed within an area of $5 \times 5\,\mathrm{mm}^2$ exposed by the light source. We checked the uniformity of the physical contact and the exposure by inspecting each pattern marked by the circles, as shown in Fig. 4. The average $3\sigma$ of the line width is approximately 20 nm, which we attribute to the accuracy of our chromium mask. Therefore, this value can be made further small by using an amorphous silicon photomask absorber [3]. We also note that it is important to improve the resist materials to improve the line edge roughness. From this result, we confirmed that our prototype near-field lithography system allows us to obtain extremely high resolution beyond the conventional wavelength limit while the system is retained to be simple and compact.

### 3.2. Whole wafer exposure: Step and repeat exposure and multi-window mask

We describe the operation of our prototype in Fig. 5. An NFL photomask is placed at the region marked by the circle while the alignment scope and the illumination optics are set on the top. By applying the pressure to the vessel, the photomask is brought into contact with the photoresist. Then, the alignment scope moves on to the wafer and the position of both the photomask relative to the wafer is checked first. Then, the illumination optics comes in and the exposure is carried out. We use a mechanical shutter for dosage control. After the mask is detached from the wafer, the wafer is moved to the next position. These series of action constitute our step and repeat process. The result of the step and repeat exposure is shown in Fig. 6. The patterns are formed on the entire surface of the 4-in. silicon wafer. In order to improve the throughput of the system further, a 4-in. mask with multiple membranes arranged in a matrix form can be used.

### 3.3. Ultra-clean environment by Dual-clean system

Our prototype system is set inside the conventional clean booth placed in normal room environment. The system is enclosed and clean air through ULPA filters is circulated inside the enclosure. A photomask and a wafer are kept in local clean environment as shown in Fig. 7.

We measured the particle counts depending on their sizes, in three different region of the system by using two

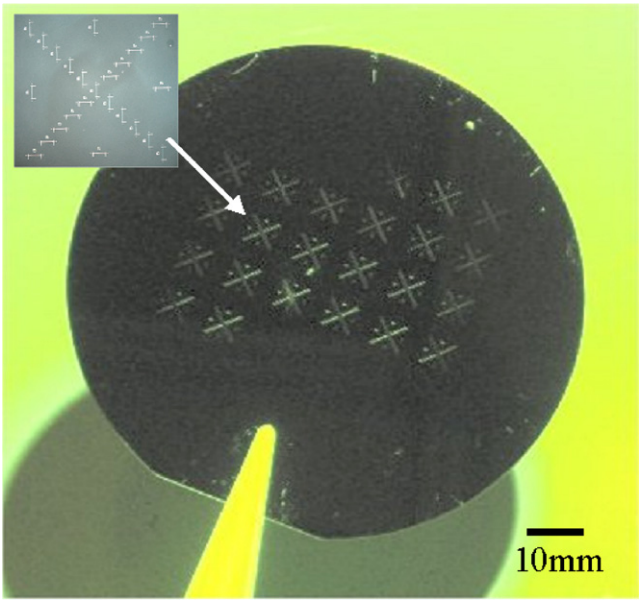


Fig. 6. Photoresist patterns on the entire surface of 4-in. silicon wafer using step and repeat exposure.

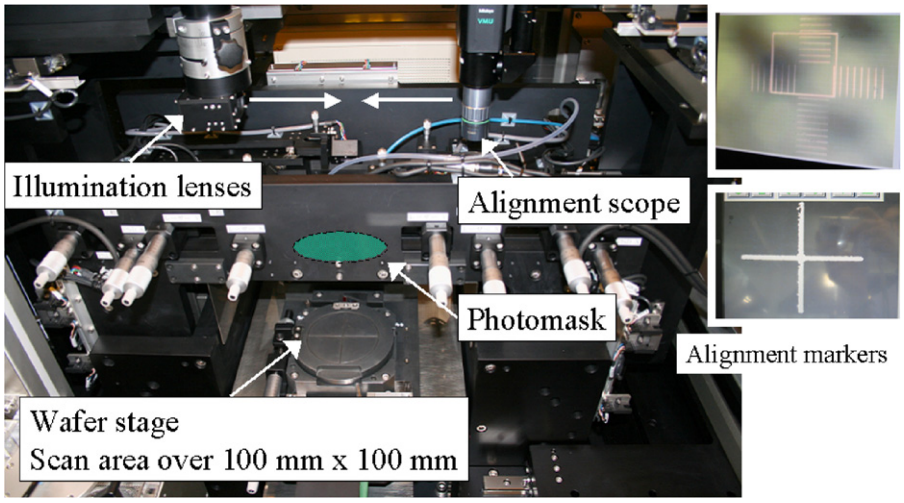


Fig. 5. Layout of components inside the prototype and alignment marks observed by the alignment scope.

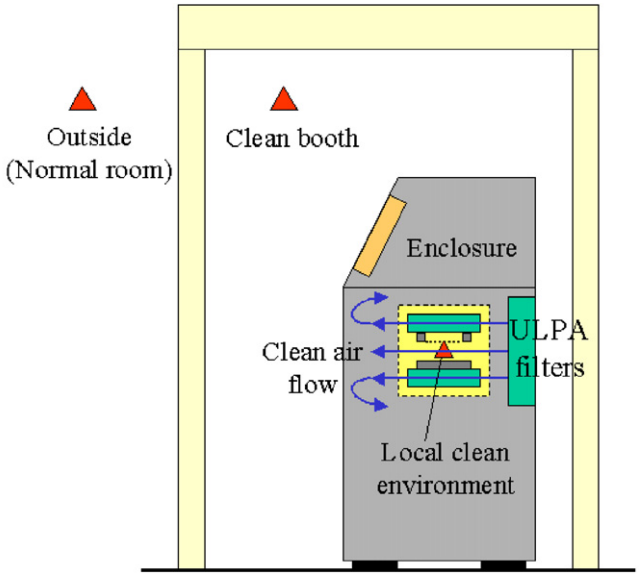


Fig. 7. Schematic illustration of structure of dual-clean system. The clean level was measured at the three points indicated by triangle marks.

Table 1
Particle counts depending on their sizes, in three different region of our system

| Particle size | Outside (particles/CF)[b] | In clean booth (particles/CF)[b] | Inside enclosure (particles/CF)[a] | | |
|---|---|---|---|---|---|
| | | | 0 min | 3 min | 7 min |
| 0.5μm | 25126 | 67 | 0 | 0 | 0 |
| 0.3μm | 357601 | 771 | 2646 | 0 | 0 |
| 0.2μm | – | – | 20466 | 216 | 0 |
| 0.1μm | – | – | 101979 | 1161 | 0 |
| 0.08μm | – | – | 25245 | 459 | 0 |

[a] Counted by KC-22B(RION CO., LTD).
[b] Counted by 243A(HIAC ROYCO).

different commercial particle counters (model: KC-22B [RION CO., LTD], 243A[HIAC ROYCO]). The results are summarized in Table 1. In the clean booth, we observed 770 particles per cubic foot greater than 0.3 μm in diameter.

Although we observed more particles initially inside the enclosure, after closing the lid of the enclosure to isolate from the clean booth, the number of particles drastically reduces with time. After 7 min, no particle greater than 80 nm in diameter is detected. This verifies that extremely clean local environment is realized in a compact fashion. This extremely clean environment is suitable for reliable nano-processing without using high-cost super-clean room and we believe that such a compact system can widely be used in many places such as university laboratories.

## 4. Application of our prototype

To further demonstrate our prototype tool, we also fabricated 2D patterns, dot and hole arrays, as shown in Fig. 8a and b. We confirmed a good uniformity over an area of $50 \times 50\ \mu m^2$. These patterns are typical of nano-devices, such as nano-optical devices (Photonic Crystal, Sub-Wavelength Structure), nano-electrical devices (Single electron transistor, Quantum dot laser), and nano-bio devices (Plasmon biosensors, DNA molecule filter). Therefore, these results suggest that our prototype tool based on our basic concept can serve as a useful fabrication tool for a wide range of nano-scale device fabrication.

## 5. Summary

We demonstrated the prototype of the near-field lithography system based on the proven concepts of a simple nano-fabrication tool with high resolution at low cost. The resist patterns with sub-50 nm features were fabricated on the entire surface of the 4-in. silicon wafer by using the step and repeat exposure. We realized the ultra-clean environment by making use of the dual clean system, which is crucial for reliable nano-processing. The 2D resist pat-

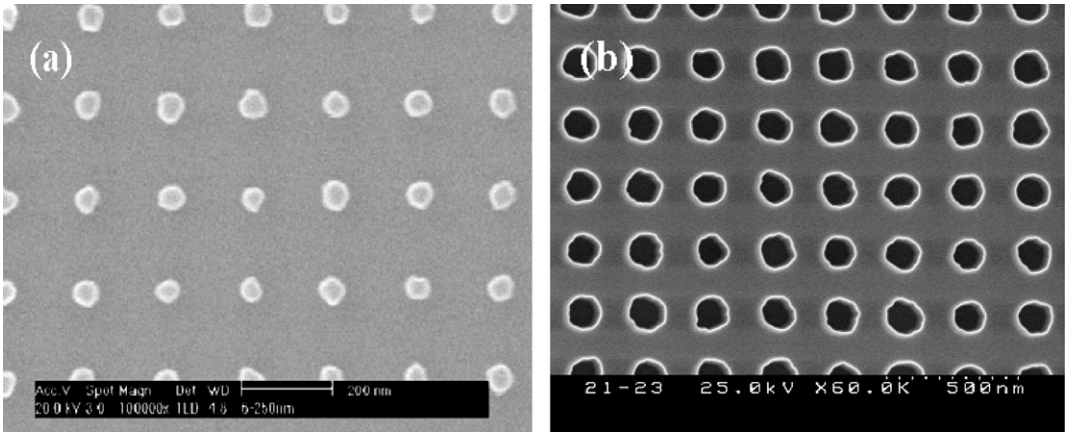


Fig. 8. SEM images of resist pattern, (a) dot array pattern whose pitch is 200 nm and diameter is 60 nm, (b) hole array patter whose pitch is 250 nm and diameter is 150 nm.

terns suitable for a variety of applications were also demonstrated.

## Acknowledgement

This study has been supported by Ministry of Education, Culture, Sports, Science and Technology (MEXT), Japan.

## References

[1] R. Kuroda et al, Canon Inc., USP6171730, 1997 (prior Japanese Patent filing).
[2] T. Ito et al., J. Photopolym. Sci. Technol. 18 (2005) 435–441.
[3] T. Ito et al., Appl. Phys. Lett 89 (2006) 033113.
[4] M.M. Alkaisi et al., Appl. Phys. Lett 75 (1999) 3560–3562.

Available online at www.sciencedirect.com
ScienceDirect
Journal of Luminescence 122–123 (2007) 230–233
JOURNAL OF LUMINESCENCE
www.elsevier.com/locate/jlumin

# Nonadiabatic photochemical reaction and application to photolithography

Hiroki Yonemitsu[a,*], Tadashi Kawazoe[b], Kiyoshi Kobayashi[c], Motoichi Ohtsu[a,b]

[a]*Department of Electronics Engineering, University of Tokyo, Bunkyo-ku, Tokyo 113-8656, Japan*
[b]*Japan Science and Technology Agency, Machida, Tokyo 194-0004, Japan*
[c]*Tokyo Institute of Technology, Meguro-ku, Tokyo 152-8550, Japan*

Available online 10 March 2006

**Abstract**

We introduce a unique photochemical reaction, i.e., nonadiabatic photochemical reaction (NPR) described by exciton–phonon polariton model, which seems to violate the Franck–Condon principle. We demonstrated a novel photolithography using optical near field which is based on the NPR. The UV-photoresist was exposed to visible and red light, while the used photoresist are low or non sensitive for visible light. This method in photolithography drastically reduce the problems, coming from wave properties of light, such as diffraction limit, interference fringes, and so on. Finally, we exposed electron-beam resist, which is completely insensitive for light, and succeeded in fabrication of a 50-nm structure.


*Keywords:* Photolithography; Nanophotolithography; Nonadiabatic photochemical reaction; Nanofabrication.

We have studied the application of optical near field (ONF) to nanostructure fabrication using its novel properties, e.g., higher resolution than diffraction limit and unique photochemical reaction [1]. This unique photochemical reaction is called a nonadiabatic photochemical reaction (NPR) [1], and can be explained by the exciton–phonon polariton (EPP) model [2,3]. In the previous work of Chemical Vapor Deposition, we demonstrated the unique photodissociation involving multiple-step excitation via molecular vibration modes based on EPP model. Following from this process, in this paper, we have applied the NPR to photolithography. Here, we call this novel method of photolithography 'Nonadiabatic Photolithography'.

Recently, to satisfy the demand for mass production of photonic and electronic devices, various methods of nanofabrication are contrived [4–6]. Among all, nonadiabatic photolithography is widely used because it enables conventional photolithographic components and systems for nanofabrication beyond the diffraction limit of light. The wave properties of light can cause problems for nanometric photolithography, including not only the diffraction limit, but also coherency and polarization dependence. In photolithography of high-density nanometric arrays, the optical coherent length is longer than their separation between adjacent corrugations, even when an Hg lamp is used, and there is not enough photoresist absorption to suppress fringe interference of scattered light due to the narrow separations. The transmission intensity of light passing through a photomask strongly depends on its polarization, so the design of photomask structures must include such effects. The largest advantage of nonadiabatic photolithography is free from these problems coming from wave properties of light.

Fig. 1 illustrates schematic drawings of potential curves of an electron in molecular orbital and the EPP model. For an optical far field, the light wavelength is much longer than the size of molecules and the field intensity is uniform in a neutral molecule. Thus, only electrons in the molecule respond to the electric field with the same phase and intensity. In such case, an optical far field cannot excite the higher molecular vibrational state, and the light source

*Corresponding author. Tel.: +81 42 788 6030; fax: +81 42 788 6031.
*E-mail address:* yonemitsu@nanophotonics.t.u-tokyo.ac.jp (H. Yonemitsu).

0022-2313/$ - see front matter © 2006 Elsevier B.V. All rights reserved.
doi:10.1016/j.jlumin.2006.01.115

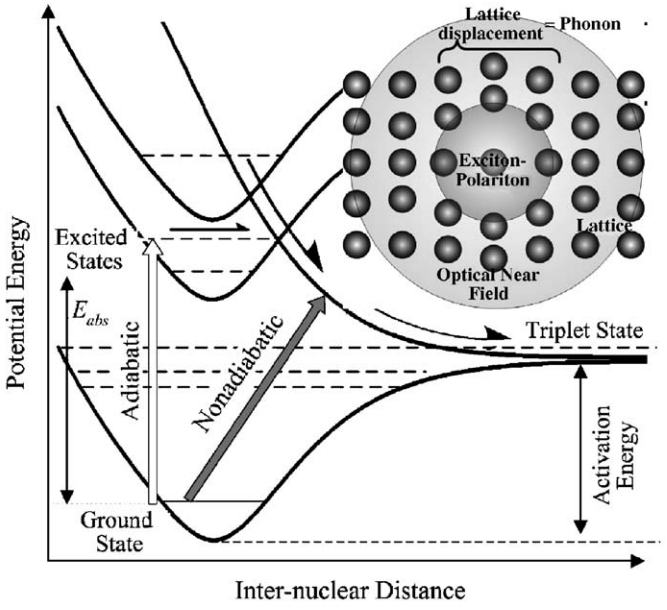


Fig. 1. Schematic drawings of (a) potential curves of an electron in molecular orbital and (b) the exciton–phonon polariton (EPP) model.

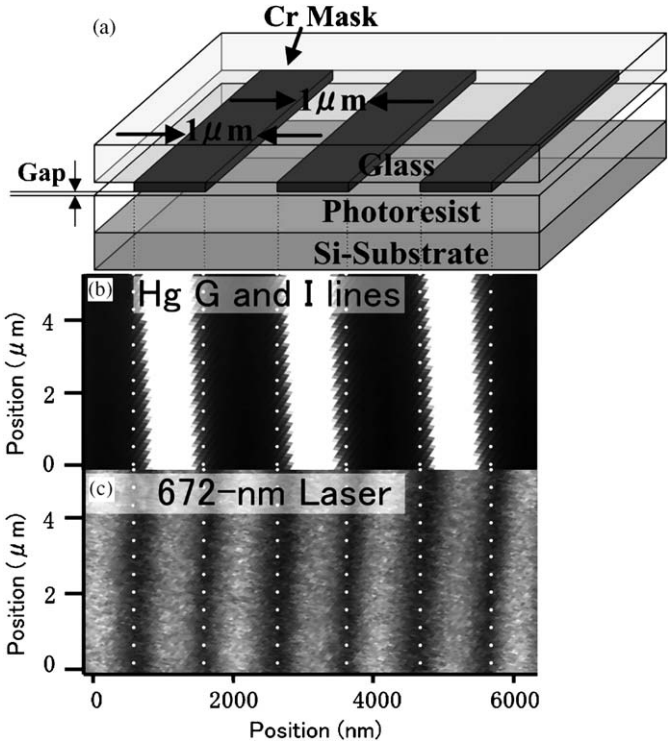


Fig. 2. (a) A schematic of the photomask and the Si-substrate spin coated with photoresist (OFPR-800) during the exposure process, (b) atomic force microscopy images of photoresist OFPR-800 exposed to the g-line of a Hg lamp for 3 s, (c) atomic force microscopy images of photoresist OFPR-800 developed after a 4-h exposure to a 672-nm laser.

must resonate to the energy from the electronic ground state to an excited state for the photoactivation. By contrast, an optical near field has the steeply spatial gradient of optical intensity, and the electrons in the molecule feel nonuniform field intensity. As a result of this non-uniform response of the electrons, the molecular orbital changes and the molecules are polarized. Finally the molecular vibration mode is excited, as shown in Fig. 1(a). In this situation, even the light with low photon energy can activate the molecule via multi-step transition. We propose the EPP model to quantify this excitation process. The EPP is a quasi-particle, which is an exciton–polariton trailing the phonon (lattice vibration) generated by the steep spatial gradient of its optical field, as shown in Fig. 1(b).

An ONF is a highly mixed state with material excitation rather than a propagating light field. When the creation (annihilation) operators for photon, exciton and phonon are denoted $a_{\mathrm{p}}^{\dagger}(a_{\mathrm{p}}), b_{\mathrm{p}}^{\dagger}(b_{\mathrm{p}})$ and $c_{\mathrm{p}}^{\dagger}(c_{\mathrm{p}})$, respectively, the Hamiltonian for the system where photon and exciton, or exciton and phonon interact with each other is written as

$$H=\sum_{p}\hbar\left[\omega_{\mathrm{p}}a_{\mathrm{p}}^{\dagger}a_{\mathrm{p}}+\omega_{\mathrm{p}}^{\mathrm{ex}}b_{\mathrm{p}}^{\dagger}b_{\mathrm{p}}+\frac{i\Omega_{\mathrm{c}}}{2}\left(a_{\mathrm{p}}^{\dagger}b_{\mathrm{p}}-a_{\mathrm{p}}b_{\mathrm{p}}^{\dagger}\right)\right]+\sum_{p}\hbar\,\Omega_{\mathrm{p}}c_{\mathrm{p}}^{\dagger}c_{\mathrm{p}}+\sum_{p,q}\left\{i\hbar\,M(p-q)\,b_{\mathrm{p}}^{\dagger}b_{\mathrm{p}}\left[c_{p-q}+c_{q-p}^{\dagger}\right]+\mathrm{h.c.}\right\} \tag{1}$$

where $p$ or $q$ is the momentum of each particle, $\omega_{\mathrm{p}}$, $\omega_{\mathrm{p}}^{\mathrm{ex}}$ and $\Omega_{\mathrm{p}}$ are the frequency of photon, exciton and phonon, respectively, $\Omega_{\mathrm{c}}$ and $M(p-q)$ are the coupling coefficient between phonon and exciton, and, exciton and photon, respectively, h.c. is the Hermite conjugate.

This Hamiltonian for the ONF probe can be diagonalized using the mean field approximation and unitary transformation, and expressed in such a quasi-particle (EPP) representation as

$$H=\sum_{p}\hbar\,\omega(p)\,\xi_{\mathrm{p}}^{\dagger}\xi. \tag{2}$$

Here the creation (annihilation) operator for EPP and the frequency are denoted $\xi_{\mathrm{p}}^{\dagger}(\xi)$ and $\omega(p)$, respectively. The detailed discussion of EPP model was reported in previous works e.g. [1].

Fig. 2(a) shows a schematic configuration of the photomask used and the Si-substrate on which the photoresist (OFPR-800: Tokyo-Ohka Kogyo Co.) was spin coated. These were used in contact mode. Figs. 2 (b) and (c) show atomic force microscopy (AFM) images of the photoresist surface after the development. Fig. 2(b) shows the developed result, in the conventional setup of photolithography. We used g-line (436-nm) light source for g-line photoresist of OFPR800. The obtained corrugated pattern was the same as the shape of the photomask. On the other hand, in the nonadiabatic photolithography, the developed grooves on the photoresist appeared along the edges of the Cr mask pattern, as shown in Fig. 2(c). We used 672-nm light for OFPR800 in the nonadiabatic photolithography. The optical power density and the

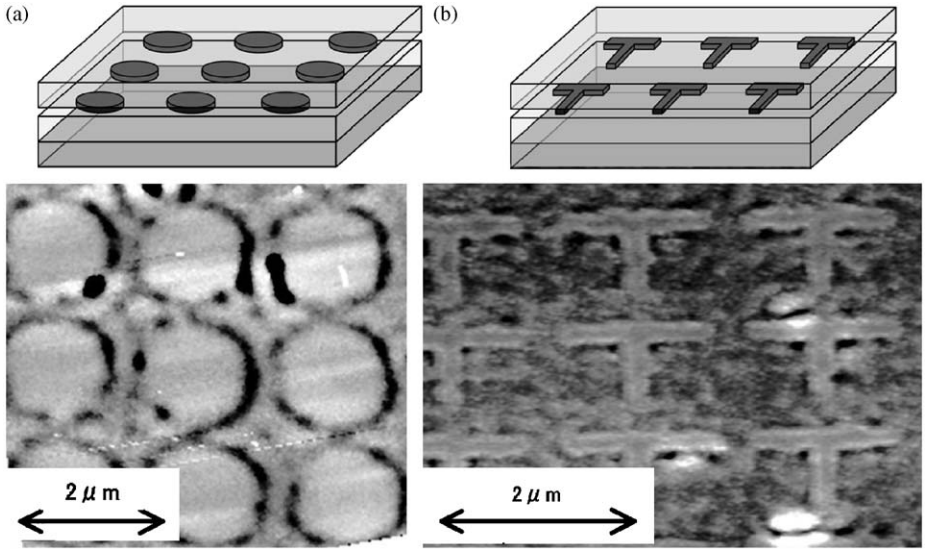


Fig. 3. (a) AFM images of photoresist TDMR-AR87 exposed to the polarized g-line of a Hg lamp for 10 s using a circle-shaped array photomask, (b) AFM images of photoresist OTDMR-AR87 developed after a 40-s exposure to the g-line of a Hg lamp using a T-shaped array photomask.

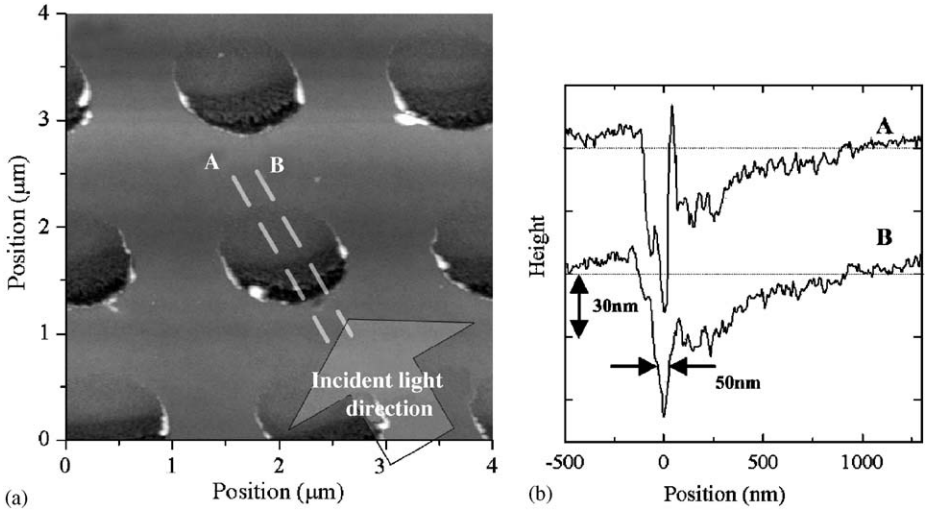


Fig. 4. (a) Atomic force microscopy images of Electron-Beam resist exposed for 5 min using the Q-switched laser (355 nm) and a circle-shaped (1 μm diameter) array photomask, (b) cross-sectional profiles of the developed pattern along broken lines A and B in Fig. 4(a).

exposure time were 1 W/cm$^2$ and 4 h, respectively. The corrugated pattern was 30 nm deep and 150 nm wide, much smaller than the wavelength of the light source. In this region, a steeply spatial gradient of optical energy that indicates the existence of an optical near field is expected, and direct irradiation of 672-nm light cannot expose the photoresist. The formation of the pattern never comes from the thermal effect. This is because it is difficult to make such minute temperature distribution corresponding to the corrugated pattern by the CW-light source that we used. These results indicate that the nonadiabatic process using ONF can expose the photoresist.

Fig. 3 shows atomic force microscopy (AFM) images of the photoresist surface after exposure and development. Fig. 3(a) shows corrugated pattern on the photoresist TDMR-AR87 (Tokyo-Ohka Kogyo Co.) using a linearly polarized g-line light. TDMR-AR87 is the photoresist for an i-line (365-nm) light source, whose sensitivity reacts for g-line is little. The conventional photolithography using a photomask with a periodically nanometric array has strong harmful effects on polarization of light and interference fringes. We confirmed the difficulties due to these harmful effects experimentally. However, using nonadiabatic photolithography method, we succeeded in transfers of the 2D nanometric arrays of circles and T-shapes; as shown in Figs. 3(a) and (b). The grooves on the photoresist appear along the ridge lines of the Cr mask pattern. While the used light source was non-polarized, the harmful effects were

drastically reduced. Thus, usefulness of nonadiabatic photolithography is evident.

We also attempted the exposure of electron beam resist (EB: ZEP-520: ZEON Co. Ltd.) optically. Fig. 4(a) shows AFM image of the developed EB resist surfaces after nonadiabatic exposure. The light source was the third harmonic generation of a Q-switched Nd:YAG laser and the exposure duration was 5 min. The pulse energy density, the pulse duration, and repetition frequency were 250 μJ/cm$^2$, 10 ns, and 20 Hz, respectively. We succeeded in patterning even the EB resist, while it never exposed by the propagating light. The developed pattern of 50 nm structures had the pit depth of 70 nm, which is deep enough for the later process, i.e., the etching of substrate, to reach the Si substrate. The fabricated structure, which had a diameter of 1 μm, was asymmetrical because the light incident angle was 70°. In contact mode lithography, the degree of contact between a photomask and resist is very important, because the ONF localizes in a extremely minute area. Since the EB resist has high smooth surface, the degree of contact was improved.

This result shows the possibility that we can choose and use the best material without considering whether it is active or inactive to the light.

We found the nonadiabatic photochemical reaction in the exposure process of photolithography, which originated from the steep spatial gradient of ONF, and described that process using the EPP model. We call this unique technique "nonadiabatic photolithography", which has several advantages, e.g., no interference and no polarization dependence. Finally we succeeded in exposing even the EB resist optically.

## References

[1] T. Kawazoe, et al., Appl. Phys. Lett. 79 (2001) 1184.
[2] T. Kawazoe, et al., J. Chem. Phys 122 (2005) 024715.
[3] T. Kawazoe, M. Ohtsu, Proc. SPIE. 5339 (2004) 619.
[4] S.Y. Chou, P.R. Krauss, P.J. Renstrom, Appl. Phys. Lett. 67 (1995) 3114.
[5] M.M. Alkaisi, R.J. Blaikie, S.J. McNab, R. Cheung, D.R.S. Cumming, Appl. Phys. Lett. 75 (1999) 3560.
[6] John A. Rogers, et al., Appl. Phys. Lett. 70 (1997) 2658.

OPTICAL REVIEW Vol. 13, No. 4 (2006) 225–227

# Electroless Nickel Plating under Continuous Ultrasonic Irradiation to Fabricate a Near-Field Probe Whose Metal Coat Decreases in Thickness toward the Tip

Yuichi SAITO*, Shuji MONONOBE[1†], Motoichi OHTSU[2] and Hideo HONMA

*Graduate School of Engineering, Kanto Gakuin University, Mutsuurahigashi, Kanazawa-ku, Yokohama 236-8501, Japan*
[1]*Kanagawa Academy of Science and Technology, KSP East 409, 3-2-1 Sakado, Takatsu-ku, Kawasaki 213-0012, Japan*
[2]*Department of Electronics Engineering, University of Tokyo, Hongo, Bunkyo-ku, Tokyo 113-8656, Japan*

(Received November 15, 2005; Accepted December 16, 2005)

This paper describes a size-dependent electroless plating method to fabricate a new type of probe with a locally decreasing thickness of metal and a tiny tip size for a combined high resolution shear-force and near-field optical microscope. In this method, the tip size and decreasing thickness profile, which affect the resolution capabilities of the microscopes, are controlled by adding a continuous ultrasonic wave with a frequency of 1 MHz to a nickel plating bath. The probe with a tip radius of curvature of 25 nm was successfully fabricated at an ultrasonic power density of 1.6 W cm$^{-2}$, its metal thickness gradually decreased from 850 to 20 nm toward the distal tip. 

**Key words:** electroless plating, metallization, ultrasonic wave, optical fiber, SNOM, NSOM, etching, non-contact atomic force microscope

## 1. Introduction

A combined near-field optical and shear-force microscope employing an apertured probe is widely applied to nano-optical imaging, spectroscopy, and processing,[1,2] where the shear-force feedback system is used for simultaneous topographic imaging and for distance regulation of the probe and the sample. However, the resolution capability of a shear-force microscope is limited to a large probe size of submicrons. To improve the topographic resolution of the combined microscope, one should fabricate a probe having both a small tip diameter and metal coat. We have proposed a fiber probe whose metal thickness locally decreases toward the distal tip [Fig. 1(a)], and have developed a fabrication method based on size-dependent electroless nickel plating under ultrasonic irradiation. In this paper, we describe the probe with a decreasing metal thickness profile and its fabrication method, and then discuss the size-dependence of electroless plating.

## 2. Fiber Probe with a Decreasing Thickness Profile of Metal

Figures 1(a) and 1(b) show an schematic illustrations of (a) a probe with a decreasing thickness profile of metal and (b) an apertured probe, respectively. In (a), the radial thickness of the metal coating gradually decreases from submicrons or more to subsubmicrons. $r_1$ is the tip radius of curvature, and $\theta$ and $\phi$ are the cone angles of the fiber and probe, respectively. In (b), $d_1$ ($> 2r_1$) is the distal diameter of an apertured probe. In both figures, $z$ is the distance of the sample and probe, and the hatched curves schematically represent the shear-force scanning operations in relation to the two probes, respectively. For the probe with a decreasing thickness profile, the operation successfully works as a constant distance mode as shown in (a). However, in (b), the precisely topographic variation of the step-like structure cannot be obtained with the apertured probe due to a poor

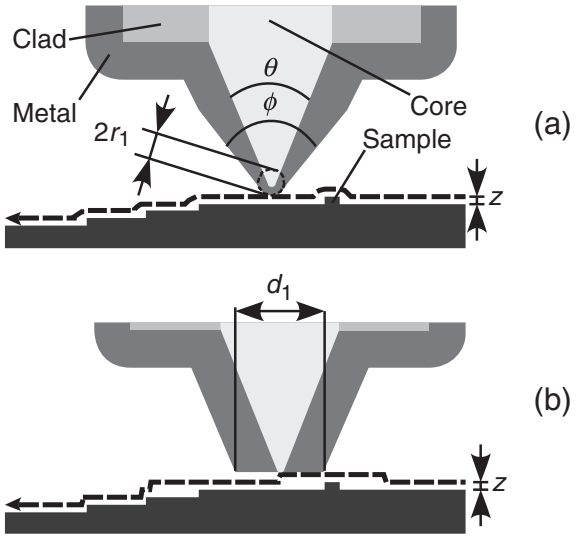


Fig. 1. Schematic illustrations of (a) the probe with a decreasing metal thickness profile and (b) apertured probe, respectively. Here, $r_1$ shows the radius of curvature, $\theta$ and $\phi$ are the full cone angles of the tapered fiber and metal coating, respectively, and $d_1$ is distal diameter of the metallized flat end of the apertured probe. In (a), the metal coating of the probe body has a constant metal thickness which is fairly thick in comparison to the skin depth. In a distal portion, the thickness gradually decreases toward the tip.

*Present address: Surface Engineering Research Institute, Kanto Gakuin University, 4-4-1 Ikeda-cho, Yokosuka, Kanagawa 239-0806, Japan.
†Present address: Department of Mechanical Engineering, Toyo University, Kawagoe, Saitama 350-8585, Japan.

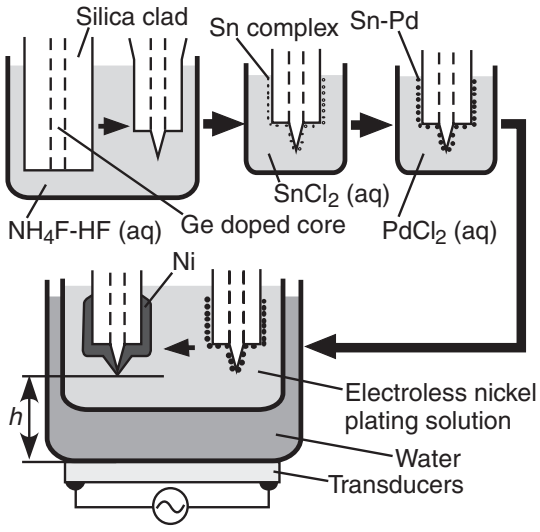


Fig. 2. (a) Schematic illustration of the method involving four steps: tapering a fiber, sensitizing, activating, and electroless nickel plating. The size-dependence of electroless plating which is caused by ultrasonic irradiation results in the decreasing thickness profile of nickel. $h = 220$ mm.

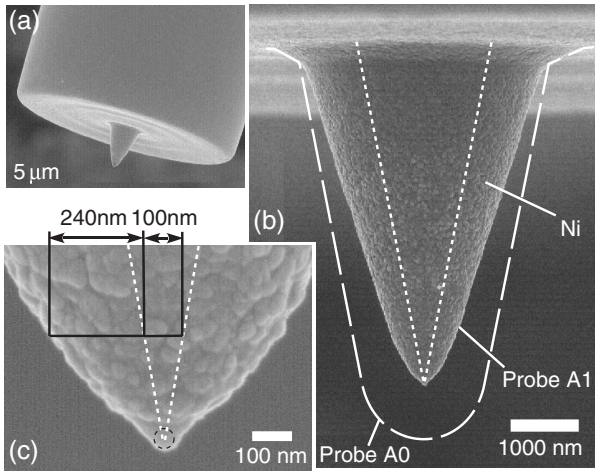


Fig. 3. (a) Scanning electron micrographs of the fabricated probe (probe A1), (b) its conical taper, and (c) magnified tip region. During the plating, a continuous ultrasonic wave with a frequency of 1 MHz and an electric power density of $1.6\,\mathrm{W\,cm^{-2}}$ was irradiated to the plating solution as shown in Table 1. In b and c, the dotted lines represent the cross-sectional profiles of the tapered fiber, respectively. The hatched curve shows another profile of the entirely coated probe (probe A0), plated without ultrasonic irradiation.

aspect ratio, although constant height mode is realized against the dot-like protrusion. As a result, the fiber probe with a decreasing metal thickness profile is found to be very effective in development of a high resolution shear-force/near-field optical microscope.

## 3. Sized-Dependent Electroless Plating Method

Figure 2 shows a schematic illustration of the plating method for fabricating the probe as in Fig. 1(a). The method involves tapering a fiber, sensitizing, activating, and electroless nickel plating with ultrasonic agitation. By this method, we fabricated a fiber probe with a radius of $r_1 = 25$ nm in a decreasing metal thickness profile as shown in Fig. 3(a). In the following, the method is described for this probe. First, a $GeO_2$-doped silica fiber with a core diameter of 2 μm, clad diameter of 125 μm, and an index difference of 2% was consecutively immersed in buffered HF with volume ratios of $40\%NH_4F : 50\%HF : H_2O = 1.7 : 1 : 1$ for 80 min and in $10 : 1 : 1$ for 120 min. The temperatures of two etching solutions were kept at around 25 °C. The obtained fiber probe has a conical tapered core with a cone angle of $\theta = 20^\circ$ and an apex diameter less than 10 nm. The tapered core is protruding from the flat clad end with a diameter of 25 μm. Next, the fiber probe was consecutively immersed in $0.1\,\mathrm{g\,dm^{-3}}$–$SnCl_2$ solution for 3 min and in $5\,\mathrm{mg\,dm^{-3}}$–$PdCl_2$ solution for 3 min. This sensitizing and activating was repeated twice. Finally, the nickel coating was done by an electroless plating unit with an ultrasonic generator (Honda Electronics, W357 HP). The plating time was 15 min. The compositions of the used plating solution is summarized in Table 1. The ultrasonic generator has four ceramic transducers from which a continuous ultrasonic wave with a frequency of around 1 MHz are radiated directionally. The total area of the transducers is $126 \times 110\,\mathrm{mm^2}$. For details of the ultrasonic generator, see Mononobe *et al.*[3] The delay time between the start of plating and the start of ultrasonic agitation was around 5 s. The electric power density for adding ultrasonic agitation to the plating solution is $1.6\,\mathrm{W\,cm^{-2}}$. This autocatalytic plating, which involves several chemical reactions in the solution, is affected by agitation and chemical species such as dissolved oxygen. To form nickel coating with the decreasing profile, the ultrasonic power density must be controlled to keep the local dissolved oxygen concentration of the thickness-decreasing region higher than those of the other regions.

Table 1. Composition of the nickel plating bath.

| | |
|---|---|
| $NiSO_4{\cdot}6H_2O$ ($\mathrm{mol{\cdot}dm^{-3}}$) | 0.1 |
| $CH_3COONH_4$ ($\mathrm{mol{\cdot}dm^{-3}}$) | 0.4 |
| $NaPH_2O_2{\cdot}H_2O$ ($\mathrm{mol{\cdot}dm^{-3}}$) | 0.2 |
| pH | 5.0 |
| Temperature (°C) | 62 |

## 4. Results and Discussion

The probe, which is called probe A1, has a conical taper and a distal tip as shown in Figs. 3(b) and 3(c), respectively. Here, the dotted lines correspond to the cross-sectional profiles of the tapered fiber. From the figures, the nickel radial thickness in the cross-sectional portion of the foot of the conical taper and the radius $r_1$ are estimated to be around 850 and 25 nm, respectively. The cone angle $\phi$ is around 80° in the tip region. In (b), the hatched curve shows cross-section of an entirely coated probe, which was plated without ultrasonic irradiation. The entirely coated probe is called probe A0. By comparing probe A1 with A0, it is

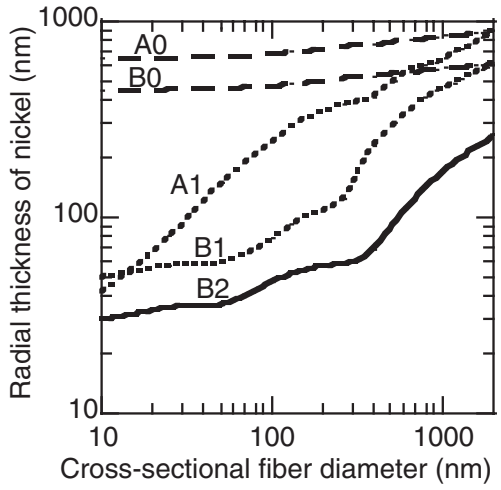


Fig. 4. Dependence of the radial nickel thickness profiles of five probes on the cross-sectional diameter of fiber. Here, curve A0 and curve A1 corresponds to the profiles of probes A0 and A1 as appeared in Fig. 2(b). For curves B0–B2, the nickel plating solution with a temperature of 60 °C was agitated by the ultrasonic wave with power densities of 0, 1.6, and 2.2 W cm$^{-2}$, respectively. The plating times of the five probes is 15 min.

found that the size dependence is caused in a tapered portion with a cross-sectional diameter of 2000–10 nm by using ultrasonic irradiation with a frequency of 1 MHz and electric power density of 1.6 W cm$^{-2}$.

Figure 4 shows the dependencies of five probes which on the radial nickel thickness were fabricated by various plating conditions. Here, curves A0 and A1 are those of probes A0 and A1, respectively. For curves B$i$ ($i = 0$–2), we used the nickel plating solution at a temperature 60 °C lower than the 62 °C for probes A0 and A1. The numbers $i = 0$, 1, and 2 are defined as ultrasonic power densities of 0, 1.6, and 2.2 W cm$^{-2}$, respectively. They are represented by dotted and solid curves, respectively. The plating times of the five probes are 15 min. The curve B0 is 0.67 times the thickness of probe A0. It was difficult to control the size-dependence by varying the temperature and coating rate without ultrasonic irradiation. The radius $r_1$ of probe B1 is 2 times larger than probe A1. Although the radius $r_1$ is smaller than probe A1, the nickel thickness in the foot region of the taper is too thin to block the unwanted propagating light in near-field optical imaging. Among these probes, probe A1 with a decreasing thickness profile of nickel coating and small tip radius of curvature $r_1 = 25$ nm is essentially effective in the combined shear-force and near-field optical microscope.

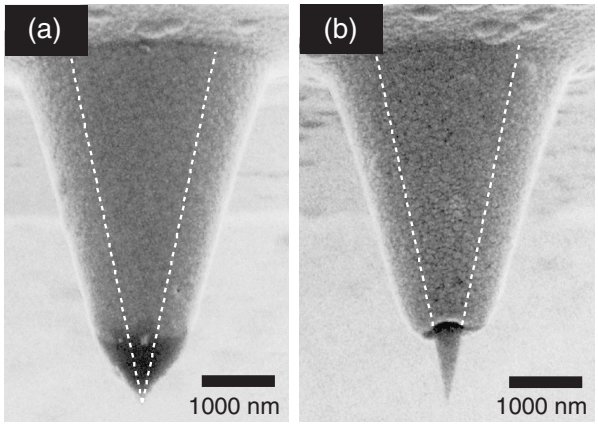


Fig. 5. Scanning electron micrographs of nickel-coated probes, obtained using a mechanical stirrer with speeds of (a) 100 and (b) 300 rpm for agitation of the plating solution, respectively.

To demonstrate the reproducibility of ultrasonic agitation, we plated using a mechanical stirrer instead of the ultrasonic generator. Figures 5(a) and 5(b) show scanning electron micrographs of nickel-coated probes. They were plated while adding agitation with stirrer speeds of 100 and 300 rpm to the plating solution, respectively. However, we could not control the decreasing metal thickness profile due to low reproducibility.

## 5. Conclusion

We fabricated a near-field optical probe with a decreasing thickness profile of nickel coating based on size-dependent electroless plating under continuous ultrasonic irradiation. The fabricated probe has a small radius of curvature of 25 nm and cone angle of 80°, and is suitable for a high resolution shear-force/near-field optical microscope. To fabricate such probes, we kept the ultrasonic power density at around 1.6 W cm$^{-2}$.

A part of this work was supported by the Kunitake "Organization and Function" Research Area, PRESTO, the Japan Science and Technology Agency, Japan.

### References

1) *Near-Field Optics*, ed. D. W. Pohl and D. Coujorn (Kluwer, Dordrecht, 1993) NATO ASI Series E, Vol. 242.
2) *Near-Field Nano/Atom Optics and Technology*, ed. M. Ohtsu (Springer-Verlag, Tokyo, 1998).
3) S. Mononobe, Y. Saito, M. Ohtsu and H. Honma: Jpn. J. Appl. Phys. **43** (2004) 2862.

OPTICAL REVIEW Vol. 13, No. 4 (2006) 222–224

# Near-Field Evaluation of a Quantum Size Effect in Self-Aligned GaN Whiskers Fabricated Using Photochemical Etching

Kokoro KITAMURA[1*], Takashi YATSUI[2] and Motoichi OHTSU[1,2]

[1]*School of Engineering, The University of Tokyo, 7-3-1 Hongo, Bunkyo-ku, Tokyo 113-8656, Japan*
[2]*Solution-Oriented Research for Science and Technology (SORST), Japan Science and Technology Agency, 687-1 Tsuruma, Machida, Tokyo 194-0004, Japan*

(Received November 1, 2005; Accepted December 16, 2005)

We fabricated nanoscale GaN whiskers using photochemical etching. The fabricated GaN whiskers were conjugated and aligned perpendicular to the incident light polarization used for photochemical etching in a self-assembling manner. Their far-field photoluminescence spectra exhibited a blue-shifted photoluminescence peak at 3.60 eV. Near-field photoluminescence spectra of individual GaN whiskers were obtained, for the first time. The evaluation of the near-field spectra identified several peaks from individual whiskers, corresponding to a diameter range of 5–10 nm, and revealed a stepwise change in the diameter along the axis of individual whisker. 

**Key words:** photochemical etching, quantum size effect, whisker, near-field photoluminescence, nanophotonic device

## 1. Introduction

For future optical transmission and signal-processing systems with high data transmission rates and capacity, we have proposed nanometer-sized photonic integrated circuits (i.e., nanophotonic ICs).[1)] As a representative device, the low-temperature operation of a nanophotonic switch was demonstrated by controlling the dipole forbidden optical energy transfer among resonant energy states in closely spaced CuCl quantum cubes via an optical near field.[1)] The switch was made from three CuCl quantum cubes with a size ratio of $1 : \sqrt{2} : 2$ on a sub-10-nm scale.

GaN is a promising material for room-temperature nanophotonic switches, due to its large exciton binding energy[2)] and chemical stability.[3)] Considering the amount of the energy shift of the single exciton state in GaN nanocrystallites as a result of the quantum confinement effect at room temperature, it is estimated that the size inaccuracy in GaN nanocrystallites must be as low as $\pm 10\%$ in order to realize efficient near-field energy transfer among the resonant energy state in a nanophotonic switch composed of 5-, 7-, and 10-nm-quantum dots.[4)] To realize this nanoscale controllability, electron beams[5)] and scanning probe microscopes[6–8)] have been used to control the site on the substrate. However, these techniques have a low throughput ratio for production, since they use a scanning beam or probe.

To realize the mass-production of a nanophotonic switch, we propose a self-assembling method of photochemical etching, in which high size controllability is realized using size-selective excitation due to the quantum size effect in GaN nanocrystallites.[9)] As the photochemical etching proceeds, the size of the GaN nanocrystallites decreases and the band gap energy of the GaN increases due to the quantum size effect. Finally, the photochemically etched size stops decreasing when the band gap energy of GaN reaches the photon energy of the illumination. High controllability in position is also realized using a nanoscale template and the subsequent optical near-field distribution generated on the template.

In this letter, as a preliminary experiment in self-assembly, we fabricated GaN whiskers using photochemical etching with a propagation light to check the size controllability. In order to evaluate the promising optical properties of the fabricated GaN whiskers, we observed near-field photoluminescence (PL) spectra of individual GaN whiskers for the first time.

## 2. Experimental

A 10-μm-thick GaN layer (n-type) was grown on a sapphire substrate using metal organic chemical vapor deposition (MOCVD). Photochemical etching was then carried out using a 1 : 1 solution of 50% HF and 30% $H_2O_2$ at room temperature, under the illumination of a He–Cd laser ($\lambda = 325$ nm). Adding an oxidizing agent ($H_2O_2$) to the solution eliminated the need for a counter electrode, which is usually used in photochemical etching.[10)] We deposited a Cr island on the GaN surface to increase the etching rate by catalysis.[11)] The etched surface morphology was evaluated using scanning electronic microscopy (SEM). The optical properties of the whiskers were examined using a collection-mode near-field optical microscope with a He–Cd laser ($\lambda = 325$ nm) for excitation at 15 K, in which we used a UV fiber probe with a 20-nm-thick aluminum coating.

## 3. Results and Discussion

Figures 1(a) and 1(b) show SEM images of the GaN surface etched for 1 and 30 min, respectively. The GaN whiskers were conjugated and the separation of the ridges ($W$) and height ($H$) both increased as the etching proceeded. Figure 1(c) is a schematic of the aligned whiskers in (b). Figure 1(d) shows a magnified SEM image of (b), in which individual whiskers forming the ridge are recognized. Figure 1(e) shows a magnified SEM image of the surface after etching for 60 min, in which the smallest whisker diameters are less than 10 nm. Furthermore, the direction of the ridge was perpendicular to the incident light polarization

*E-mail: kitamura@nanophotonics.t.u-tokyo.ac.jp

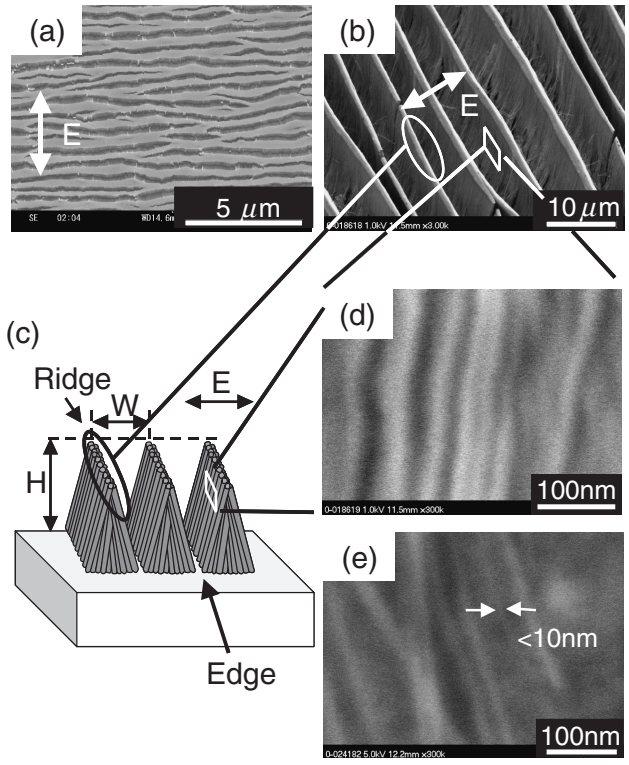


Fig. 1. SEM images of the surface morphology after etching for (a) 1 and (b) 30 min. (c) Schematic diagram of aligned whiskers. (d) Magnified SEM image of (b). (e) Magnified SEM images of the surface etched for 60 min.

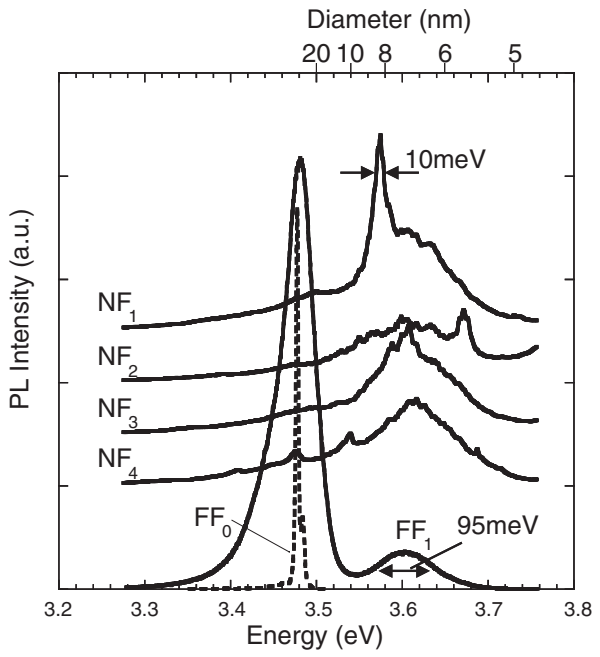


Fig. 2. Far-field [$FF_0$: unetched substrate, $FF_1$: substrate etched for 60 min [Fig. 1(c)]] PL spectra and near-field ($NF_0$–$NF_4$) PL spectra of substrate etched for 60 min.

[see the arrows in Figs. 1(a) and 1(b)]. The conjugated whiskers were aligned perpendicular to the ridge [Fig. 1(e)]. From this dependence on the light polarization, we concluded that the linear alignment of whiskers originates from the linearly polarized light of the He–Cd laser. We arrived at this conclusion for the following reasons: (1) Light that is polarized perpendicular to the slit has a greater transmission efficiency through the slit in comparison with parallel polarization, as is well known in optics. (In our photochemical etching process, the fabricated grooves between the ridges serve as the slit.) (2) By localizing the carriers at the bottom of the groove (i.e., this slit) with perpendicular polarization, a deeper groove is fabricated for the perpendicular polarization. The greater transmission (1) enhances the carrier localization (2), and the resultant deeper groove further increases the carrier localization. This positive feedback process leads to the formation of self-aligned whiskers perpendicular to the light polarization. By contrast, note that for the ridge structures formed using a Hg lamp,[11] the fabricated ridges were oriented randomly.

In order to estimate the whisker diameters, we obtained far-field PL spectra. Curve $FF_1$ in Fig. 2 shows the low-temperature (5 K) far-field PL spectral profile from a sample etched for 60 min. Note that the peak of this curve was blue-shifted to 3.60 eV in comparison with the far-field PL spectrum of unetched GaN, which has a single peak at 3.48 eV (curve $FF_0$). Since the observed whisker diameter was smaller than the exciton Bohr radius of GaN (11 nm[12]), we predicted that the blue-shifted peak originates from the quantum size effect in the GaN whiskers. This prediction is supported by the calculation using the effective mass approximation ($m_e = 0.2$,[13] $m_h = 0.8$[14]), in which the blue-shifted peak at 3.60 eV corresponds to the PL from a whisker 7.2 nm in diameter. The large spectral width of 95 meV in curve $FF_1$ arises from the fluctuation in the diameter of the whiskers. To evaluate the spectral width of an individual whisker, we measured the near-field PL at several points in conjugated whiskers at 15 K (curves $NF_1$–$NF_4$ in Fig. 2). Since the decrease in whisker diameter must stop at 4.3 nm, the point at which the band gap energy of GaN reaches the photon energy of the He–Cd laser (3.81 eV), the sharp peaks (10 meV width) in curves $NF_1$–$NF_4$ correspond to the PL from whiskers with diameters of 5–10 nm. This result suggests that a longer etching time is required to realize photon energy control of the whisker diameter. The details of the dependence of the whisker diameter on etching time and the photon-energy are currently under study.

Figures 3(a) and 3(b) show the spatial distributions of the near-field PL intensity at 3.69 and 3.67 eV, respectively. These images show the drastic variation in the PL intensity along the whisker axis, in which the two intensity distributions are anti-correlated along the axis, and the bright areas in the images have a single linear shape. Furthermore, since the spatial distribution of the near-field PL intensity at 3.67 eV, corresponding to the whisker with 5.7 nm in diameter, is much larger (0.4 μm width along a whisker axis) than Bohr radius of GaN (11 nm), quantum confinement effect along the whisker axis is negligible. Thus, we concluded that the two intensity distributions at 3.69 and

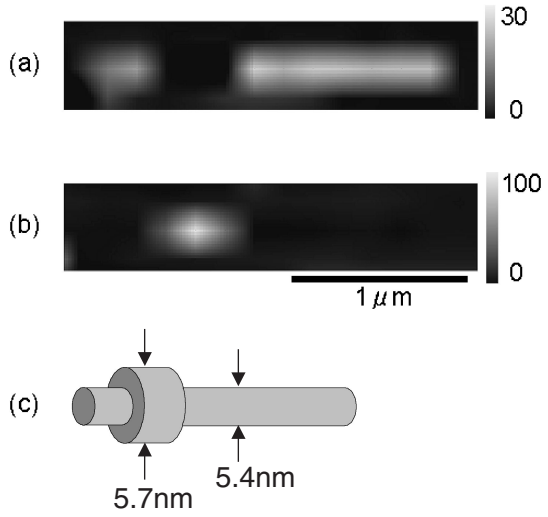


Fig. 3. Spatial distribution of the near-field PL intensity at (a) 3.69 and (b) 3.67 eV. (c) Schematic explanation of the stepwise change in whisker diameter along its axis.

3.67 eV are originated from quantum confinement effect due to the stepwise change in the whisker diameter, as explained schematically in Fig. 3(c). The stepwise change in the whisker diameter originated from fluctuation in the etching rate. A more detailed examination of the dependence on the etching conditions (optical power used for etching, etching time, and so on) should clarify the origin of this phenomenon and facilitate control of the stepwise change in the whisker diameter.

## 4. Conclusion

In conclusion, we fabricated nanoscale GaN whiskers using photochemical etching. We found that the carrier-localization dependence on the polarization resulted in the self-alignment of whiskers. The fabricated whiskers exhibited a blue-shifted peak at 3.60 eV in the far-field PL spectra. We succeeded in obtaining the first near-field PL spectra of individual GaN whiskers. The near-field PL spectra exhibited sharp peaks from individual whiskers, which corresponded to diameters from 5 to 10 nm. Furthermore, the near-field evaluation revealed a stepwise change in the diameter along the axis of an individual whisker. The use of the self-alignment method will dramatically increase the throughput of the production of nanoscale structures, which will be required by future systems. Our results suggest the possibility of realizing an one-dimensional nanophotonic device in a single whisker by controlling the diameter along the whisker axis.

## References

1) M. Ohtsu, K. Kobayashi, T. Kawazoe, S. Sangu and T. Yatsui: IEEE J. Sel. Top. Quantum Electron. **8** (2002) 839.
2) R. Senger and K. Bajaj: Phys. Rev. B **68** (2003) 205314.
3) J. R. Mileham, S. J. Pearton, C. R. Abernathy, J. D. MacKenzie, R. J. Shul and S. P. Kilcoyne: J. Vac. Sci. Technol. A **14** (1996) 836.
4) T. Kawazoe, K. Kobayashi, S. Sangu and M. Ohtsu: Appl. Phys. Lett. **82** (2003) 2957.
5) T. Ishikawa, S. Kohmoto and K. Asakawa: Appl. Phys. Lett. **73** (1998) 1712.
6) S. Kohmoto, H. Nakamura, T. Ishikawa and K. Asakawa: Appl. Phys. Lett. **75** (1999) 3488.
7) M. Ara, H. Graaf and H. Tada: Appl. Phys. Lett. **80** (2002) 2565.
8) T. Yatsui, T. Kawazoe, M. Ueda, Y. Yamamoto, M. Kourogi and M. Ohtsu: Appl. Phys. Lett. **81** (2002) 3651.
9) H. Koyama and N. Koshida: J. Appl. Phys. **74** (1993) 6365.
10) J. A. Bardwell, J. B. Webb, H. Tang, J. Fraser and S. Moisa: J. Appl. Phys. **89** (2001) 4142.
11) D. J. Díaz, T. L. Williamson, I. Adesida and P. W. Bohn: J. Appl. Phys. **94** (2003) 7526.
12) Y. Xie, Y. Qian, W. Wang, S. Zhang and Y. Zhang: Science **272** (1996) 1926.
13) A. M. Witowski, K. Pakuła, J. M. Baranowski, M. L. Sadowski and P. Wyder: Appl. Phys. Lett. **75** (1999) 4154.
14) J. I. Pankove, S. Bloom and G. Harbeke: RCA Rev. **36** (1975) 163.

OPTICAL REVIEW Vol. 13, No. 4 (2006) 218–221

# Evaluating the Quantum Confinement Effect of Isolated ZnO Nanorod Single-Quantum-Well Structures Using Near-Field Ultraviolet Photoluminescence Spectroscopy

Takashi YATSUI[1]*, Motoich OHTSU[1,2], Sung Jin AN[3], Jinkyoung YOO[3] and Gyu-Chul YI[3]

[1]*Solution-Oriented Research for Science and Technology (SORST), Japan Science and Technology Agency, 687-1 Tsuruma, Machida, Tokyo 194-0004, Japan*
[2]*School of Engineering, The University of Tokyo, 7-3-1 Hongo, Bunkyo-ku, Tokyo 113-8656, Japan*
[3]*National CRI Center for Semiconductor Nanorods and Department of Materials Science and Engineering, Pohang University of Science and Technology (POSTECH), San 31 Hyoja-dong, Pohang, Gyeongbuk 790-784, Korea*

(Received November 15, 2005; Accepted January 20, 2006)

Using low-temperature near-field spectroscopy, we obtained spatially and spectrally resolved photoluminescence (PL) images of individual ZnO nanorod single-quantum-well structures (SQWs) with a spatial resolution of 20 nm. We observed the dependence of the quantum confinement effect of the PL peak on the well width ($L_{aw}$), from which the linewidths of near-field PL spectra of ZnO nanorod SQWs ($L_{aw} = 2.5$ and 3.75 nm) were determined to be as narrow as 3 meV. However, near-field PL spectra of individual SQWs with $L_{aw} = 5.0$ nm exhibited two PL peaks, presumably due to strains or defects in the ZnMgO in the nanorod SQWs. Since the exciton in a quantum structure is an ideal two-level system with long coherence times, our results provide criteria for designing nanophotonic devices. 

**Key words:** ZnO, nanorod, single-quantum-well structures, quantum confinement effect

## 1. Introduction

Future optical transmission systems will require nanophotonic integrated circuits[1)] composed of nanometer-scale dots to increase data transmission rates and capacity. ZnO nanocrystallite is a promising material for realizing room-temperature nanophotonic devices, owing to its exciton binding energy, which is as large as 110 meV in quantum structures,[2)] and large oscillator strength.[3)] Furthermore, the recent demonstration of a semiconductor nanorod quantum-well (QW) structure enabled us to fabricate nanometer-scale electronic and photonic devices on single nanorods.[4–6)] Recently, ZnO/ZnMgO nanorod multiple-QW structures (MQWs) exhibiting the quantum confinement effect have also been fabricated.[7)] Further improvement in the fabrication of nanorod heterostructures has resulted in the observation of significantly enhanced photoluminescence (PL) intensity, even from ZnO/ZnMgO nanorod single-QW structures (SQWs).[8)] Furthermore, spatially resolved near-field PL spectra of individual nanorod ZnO QWs have been measured to realize nanophotonic devices using low-temperature near-field optical microscopy (NOM).[9)]

## 2. Experimental

ZnO/ZnMgO SQWs were fabricated on the ends of ZnO nanorods with a mean diameter of 40 nm using catalyst-free metalorganic vapor phase epitaxy.[10)] The average concentration of Mg in the ZnMgO layers used in this study was determined to be 20 at. %. The average ZnO well layer thicknesses in the substrate, $L_{aw}$, investigated in this study were 2.5, 3.75, and 5.0 nm, while the thicknesses of the ZnMgO bottom and top barrier layers in the SQWs were fixed at 60 and 18 nm, respectively. These thicknesses were determined by the transmission electron microscopy (TEM) measurement. After growing ZnO nanorod SQWs on sapphire (0001) substrate, they were dispersed on a flat sapphire substrate to measure the near-field PL of isolated nanorod QWs [Fig. 1(a)].

Far-field PL spectra were obtained using a He–Cd laser ($\lambda = 325$ nm) before dispersing the ZnO/ZnMgO nanorod SQWs. The emission signal was collected with an achromatic lens ($f = 50$ mm). The optical properties of individual ZnO SQWs were investigated by collection-mode NOM at 15 K, using a He–Cd laser ($\lambda = 325$ nm) for excitation and an UV fiber probe with an aperture diameter of 30 nm to detect the PL signals [Fig. 1(b)]. In contrast to the naturally formed quantum dot (QD) structure formed in a two-dimensional (2D) narrow QW,[11–13)] the barrier and cap layers laid on the substrate allowed the probe tip to access the PL source, which reduced carrier diffusion in the ZnO SQWs and the subsequent linewidth broadening, thereby resulting in high spatial and spectral resolution. The excitation source, which had a spot size of approximately 100 μm in diameter was focused on a nanorod sample laid on the substrate.

## 3. Results and Discussion

The solid curves in Fig. 2 show the near-field PL spectra of the isolated ZnO SQW nanorods with well-layer widths ($L_{aw}$) of 5.0 ($NF_a$), 3.75 ($NF_b$), and 2.5 ($NF_c$) nm. In these spectra, the emission peaks around 3.365 ($I_2^{ZnO}$) and 3.555 ($I^{ZnMgO}$)[7,8)] eV are associated with neutral–donor bound excitons in the ZnO stem, and the excitons in the $Zn_{0.8}Mg_{0.2}O$ layers, respectively, which correspond to the peaks in the respective far-field spectra [dashed curves $FF_a$, $FF_b$, and $FF_c$ in Fig. 2(a)]. Blue-shifted PL emission peaks

*E-mail address: yatsui@ohtsu.jst.go.jp

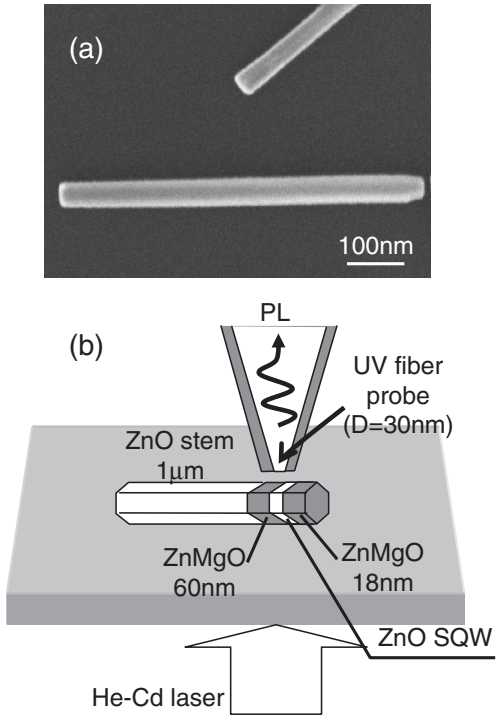


Fig. 1. (a) Scanning electron micrograph of the dispersed ZnO/ZnMgO nanorod SQWs. (b) Schematic of near-field spectroscopy of isolated ZnO SQWs on the ends of a ZnO nanorod.

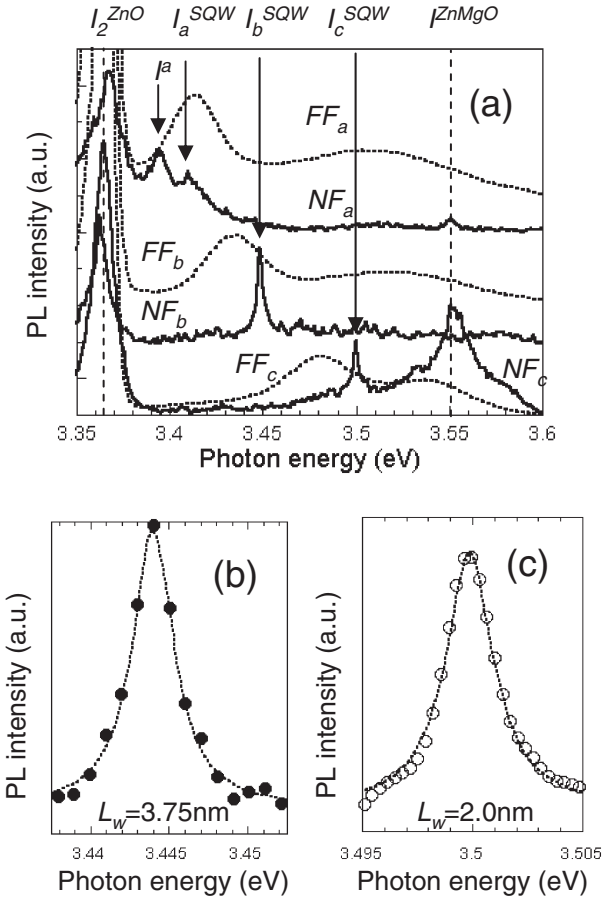


Fig. 2. (a) Size-dependent PL spectra of isolated ZnO nanorod SQWs with $L_{aw} = 5.0$ ($FF_a, NF_a$), 3.75 ($FF_b, NF_b$), and 2.5 ($FF_c, NF_c$) nm, obtained at 15 K. *FF*: far-field spectra of vertically aligned ZnO nanorod SQWs. *NF*: near-field PL spectra of the isolated ZnO SQWs obtained at the well layer. Respective magnified near-field PL spectra of the isolated ZnO SQWs of (b) $L_{aw} = 3.75$ and (c) $L_{aw} = 2.5$ nm.

were observed at 3.410 ($I_a^{SQW}$ for $L_{aw} = 5.0$ nm), 3.444 ($I_b^{SQW}$ for $L_{aw} = 3.75$ nm), and 3.499 ($I_c^{SQW}$ for $L_{aw} = 2.5$ nm) eV. Since these peak energies are comparable to the predicted ZnO well layer thicknesses, $L_w$, of 4.6 ($I_a^{SQW}$), 3.8 ($I_b^{SQW}$), and 2.7 ($I_c^{SQW}$) nm, respectively, calculated using the finite square-well potential of the quantum confinement effect in the ZnO well layer, we strongly believe that peaks $I_a^{SQW}$, $I_b^{SQW}$, and $I_c^{SQW}$ originated from the ZnO SQWs. For the theoretical calculation, we used $0.28m_0$ and $1.8m_0$ as the effective masses of an electron and a hole in ZnO, respectively, at a ratio of conduction- and valence-band offsets ($\Delta E_c/\Delta E_v$) of 9, and a band-gap offset ($\Delta E_g$) of 250 meV.[8] Note that the Lorentzian functions indicated by the dashed curves in Figs. 2(b) and 2(c) fit the respective spectrum shapes at $I_b^{SQW}$ ($L_{aw} = 3.75$ nm) and $I_c^{SQW}$ ($L_{aw} = 2.5$ nm) well, and the spectral widths of the ZnO SQWs (3.2 meV for $L_{aw} = 3.75$ nm and 2.6 meV for $L_{aw} = 2.5$ nm) are much narrower than those of the far-field spectra (40 meV).

The near-field PL spectrum of the nanorod SQWs with $L_{aw} = 5.0$ nm ($NF_a$) had a broader spectral width of $I_a^{SQW}$ with an additional peak at 3.395 eV ($I_a$). In order to determine the origin of the $I_a$ emission peak, we obtained spatially resolved near-field PL spectra along the axial direction of ZnO SQWs of $L_{aw} = 5.0$ nm (Fig. 3). Curves 1 to 14 shown in Fig. 3(a) correspond to the near-field PL spectra obtained every 18 nm from the left- to right-hand side along the dashed white line in Fig. 3(b). Curve 10 of *NF* and curve *FF* in Fig. 3(a) are the same as curves $NF_a$ and $FF_a$ in Fig. 2(a), respectively. Figures 3(b)–3(f) show the spatially and spectrally resolved PL images at 3.365, 3.393, 3.400, 3.410, and 3.550 eV, respectively. Several conclusions can be drawn from these spatial distributions. First, the full width at half maximum of the linearly shaped distribution of $I_2^{ZnO}$ at 3.365 eV [Fig. 3(b)] was as small as 20 nm, which is comparable to the width of the nanorod [40 nm, see Fig. 1(a)]. This result confirms that this distribution originates from the isolated ZnO SQWs nanorod. Second, a comparison of the cross-sectional profiles along the dashed white lines in Figs. 3(b) and 3(e) reveals that the peak intensity at 3.365 eV ($I_2^{ZnO}$) from the ZnO stem decreased, while the emission at 3.410 eV from the SQW ($I_a^{SQW}$) remained at the end of the nanorod [also see curves B and E in Fig. 3(g)]. This result supports the postulate that the blue-shifted emission at 3.410 eV ($I_a^{SQW}$) was confined to the end of the ZnO stem, surrounded by the ZnMgO barrier layers [see curve F in Fig. 3(g)]. Third, the emission peak of $I_a$ was split into two peaks of 3.393 eV [$I_{a1}$: Fig. 3(c)] and 3.400 eV [$I_{a2}$: Fig. 3(d)], and the peak intensity of $I_{a1}$ decreased at the end of the nanorod, while that of $I_{a2}$ increased. From the corresponding cross-sectional profiles [curves C and D in

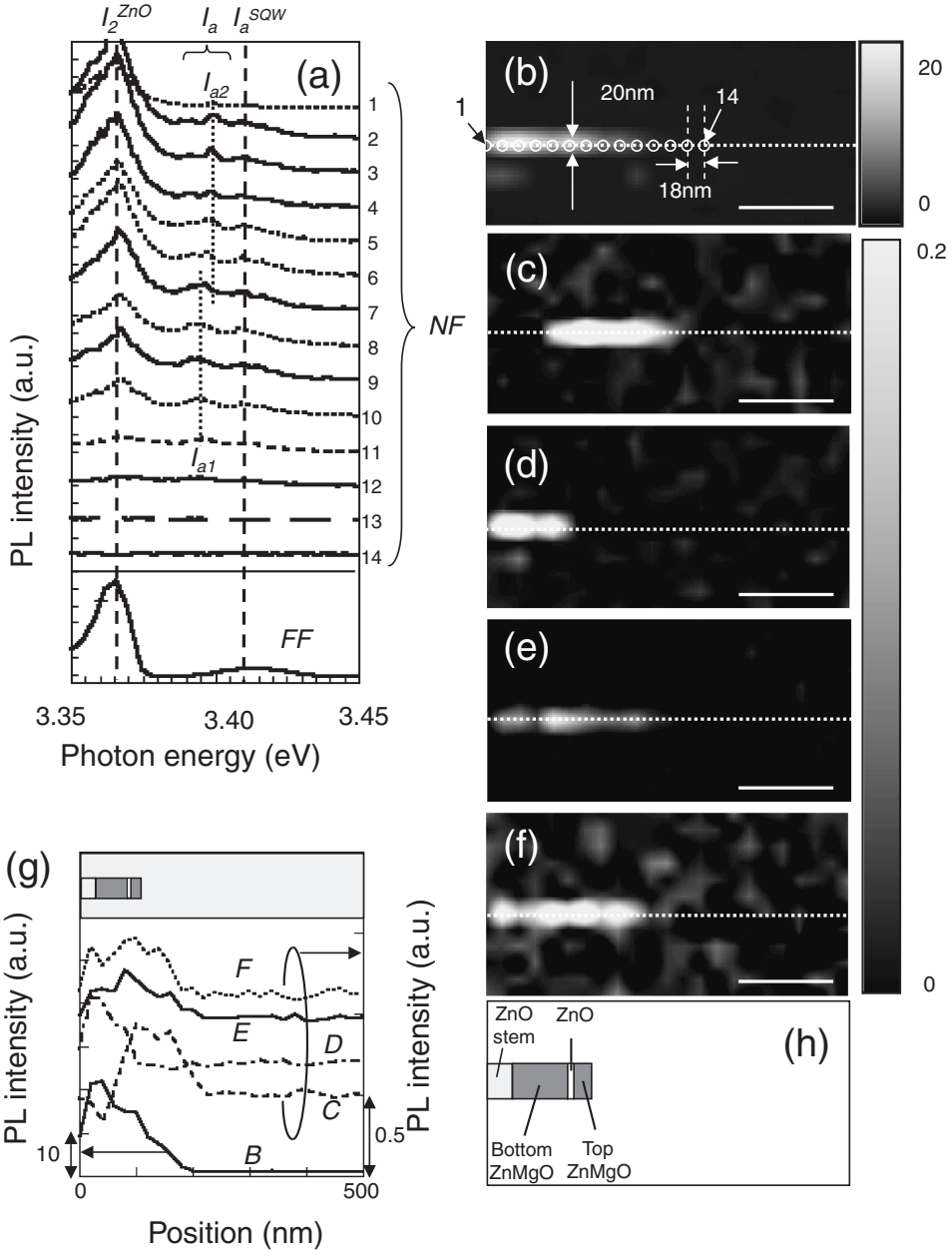


Fig. 3. (a) Low-temperature (15 K) far-field PL spectra of vertically aligned ZnO nanorod SQWs (*FF*) and near-field PL spectra (*NF*) of the isolated ZnO SQWs ($L_{aw} = 5.0$ nm). The spatial distributions at the peaks at (b) 3.365 ($I_2^{ZnO}$), (c) 3.393 ($I_{a1}$), (d) 3.400 ($I_{a2}$), (e) 3.410 ($I_a^{SQW}$), and (f) 3.550 eV ($I^{ZnMgO}$). Scale bars: 100 nm. (g) Curves B–F show the cross-sectional profiles along the dashed white lines in (b)–(f). (h) Schematic of the ZnO nanorod SQWs.

Fig. 3(g)], we found that these peaks were located in the top and bottom ZnMgO layers, respectively [as shown in Fig. 3(h)]. Since the ZnO QW thickness in the individual ZnO nanorod, $L_w$, was atomically flat, the two peaks are presumably originated from strains or defects in the ZnMgO layers. Detailed origins of these peaks are currently under studied using a fiber probe with a smaller aperture.

## 4. Conclusion

In summary, low-temperature near-field spectroscopy determined that the linewidth of near-field PL spectra of individual ZnO nanorod SQWs ($L_{aw} = 2.5$ and 3.75 nm) was as narrow as 3 meV. Furthermore, near-field PL spectra of individual SQWs with $L_{aw} = 5.0$ nm exhibited two PL peaks, resulting from strains or defects in the ZnMgO in the nanorod SQWs. The results shown here provide criteria for realizing nanophotonic devices using a two-level system.[14,15] As a representative device, a nanophotonic switch can be realized by controlling the dipole forbidden optical energy transfer among the resonant energy levels of nanometer-scale QDs via an optical near field.[16] By considering the amount of the energy shift of the single exciton state in ZnO nanocrystallites resulting from the quantum confinement effect at room temperature, we

estimate that the size accuracy of ZnO nanocrystallites must be as low as $\pm 10\%$ in order to realize efficient near-field energy transfer among the resonant energy states in a nanophotonic switch composed of 5-, 7-, and 10-nm QDs.[16] Accordingly, the near-field PL measurement of isolated SQWs described above is a promising step toward designing a nanophotonic switch and related devices.

**Acknowledgment**

The work at POSTECH was supported by the National Creative Research Initiative Project, Korea and AOARD 05-84 (Quotation No. FA5209-05-T0369), United States.

**References**

1) M. Ohtsu, K. Kobayashi, T. Kawazoe, S. Sangu and T. Yatsui: IEEE J. Sel. Top. Quantum Electron. **8** (2002) 839.
2) H. D. Sun, T. Makino, Y. Segawa, M. Kawasaki, A. Ohtomo, K. Tamura and H. Koinuma: J. Appl. Phys. **91** (2002) 1993.
3) D. C. Reynolds, D. C. Look, B. Jogai, C. W. Litton, G. Cantwell and W. C. Harsch: Phys. Rev. B **60** (1999) 2340.
4) Y. Wu, R. Fan and P. Yang: Nano Lett. **2** (2002) 83.
5) M. T. Björk, B. J. Ohlsson, C. Thelander, A. I. Persson, K. Deppert, L. R. Wallenberg and L. Samuelson: Appl. Phys. Lett. **81** (2003) 4458.
6) M. S. Gudiksen, L. J. Lauhon, J. Wang, D. C. Smith and C. M. Lieber: Nature **415** (2002) 617.
7) W. I. Park, G.-C. Yi, M. Y. Kim and S. J. Pennycook: Adv. Mater. **15** (2003) 526.
8) W. I. Park, S. J. An, J. L. Yang, G.-C. Yi, S. Hong, T. Joo and M. Kim: J. Phys. Chem. B **108** (2004) 15457.
9) T. Yatsui, M. Ohtsu, J. Yoo, S. J. An and G.-C. Yi: Appl. Phys. Lett. **87** (2005) 033101.
10) W. I. Park, D. H. Kim, S.-W. Jung and G.-C. Yi: Appl. Phys. Lett. **80** (2001) 4232.
11) K. Matsuda, T. Saiki, S. Nomura, M. Mihara, Y. Aoyagi, S. Nair and T. Takagahara: Phys. Rev. Lett. **91** (2003) 177401.
12) J. R. Guest, T. H. Stievater, G. Chen, E. A. Tabak, B. G. Orr, D. G. Steel, D. Gammon and D. S. Katzer: Science **293** (2001) 2224.
13) T. Guenther, C. Lienau, T. Elsaesser, M. Clanemann, V. M. Axt, T. Kuhn, S. Eshlaghi and A. D. Wieck: Phys. Rev. Lett. **89** (2002) 057401.
14) A. Zrenner, E. Beham, S. Stufler, F. Findeis, M. Bichler and G. Abstreiter: Nature **418** (2002) 612.
15) Z. Yuan, B. E. Kardynal, R. M. Stevenson, A. J. Shields, C. J. Lobo, K. Cooper, N. S. Beattie, D. A. Ritchie and M. Pepper: Science **295** (2002) 102.
16) T. Kawazoe, K. Kobayashi, S. Sangu and M. Ohtsu: Appl. Phys. Lett. **82** (2003) 2957.

# [II] PRESENTATIONS

## IN INTERNATIONAL CONFERENCES

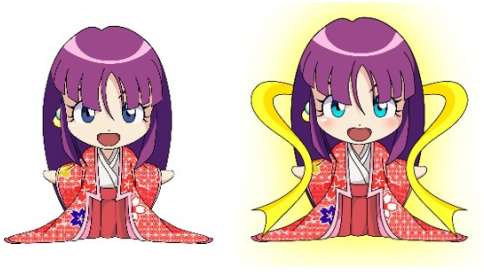

# Nanophotonics

**M. Ohtsu**

*Department of Electronics Engineering, the University of Tokyo*
*2-11-16 Yayoi, Bunkyo-ku, Tokyo 113-8656, Japan, http://uuu.t.u-tokyo.ac.jp*

This presentation reviews nanophotonics, which has been proposed by Ohtsu in 1993[1]. It is a novel optical nanotechnology utilizing local electromagnetic interactions between nanometric elements via optical near fields. The true nature of nanophotonics is to realize "*qualitative innovation*" in photonic devices, fabrications, and systems by utilizing novel functions and phenomena caused by optical near field interactions, which are impossible as long as conventional propagating light is used. As the evidence of such innovation, novel nanophotonic devices, nanophotonic fabrications, and nanophotonic systems are demonstrated.

For nanophotonic devices, the optical near field is used as a carrier to transmit the signal. As key devices, we demonstrate a nanophotonic switch [2], logic gates including a not-gate [3], and an optical nano-fountain [4] based on optical near field energy transfer between quantum dots. Fabrication processes of practical devices are also presented.For nanophotonic fabrications, we demonstrate photochemical vapor deposition of nanometric particles based on the photo-dissociation of gas-phase metal-organic molecules using optical near fields under nonresonant condition, which is possible by multiple-step excitation via molecular vibration modes [5, 6]. Such a nonadiabatic process violates the Franck-Condon principle, and can be applied to other photochemical phenomena in order to open a new field of nano-fabrication. As an example, we demonstrate the patterning by the near-field photo-lithography using a visible light for UV photoresist[7]. It enables fabricating a replica of electronic circuit pattern, multiple exposures, nanophotonic devices, and so on. An architectural approach to nanophotonic information and communication systems is also discussed. Finally, the future prospects are presented.

## Reference:

[1]: M. Ohtsu(Ed): "Preface to Volume *V*" in *Progress in Nano-Electro-Optics V* (Spinger-Verlag, Berlin, 2006)

[2]: T. Kawazoe, et al., "Demonstration of a nanophotonic switching operation by optical near-field energy transfer", Appl. Phys. Lett., vol.82, p.2957 (2003)

[3]: T. Kawazoe, et al., "Demonstration of nanophotonic NOT gate using near-field optically coupled quantum dots", Appl. Phys. B, vol.84, p.243 (2006)

[4]: T. Kawazoe, K. Kobayashi, and M. Ohtsu, "Optical nanofountain: A biomimetic device that concentrates optical energy in a nanometric region", Appl. Phys. Lett., vol.86, p.103102 (2005)

[5]: T. Kawazoe, Y. Yamamoto, and M. Ohtsu, "Fabrication of a nanometric Zn dot by nonresonant near-field optical chemical vapor deposition", Appl. Phys. Lett., vol.79, p.1184 (2001)

[6]: T. Kawazoe, et al., "Nonadiabatic photodissociation processs using an optical near field", J. Chem. Phys., vol.122, p.024715 (2005)

[7]: H. Yonemitsu, et al., "Nonadiabatic photochemical reaction and application to photolithography", J. Luminescence, vol.122/123, p.230 (2007)

# Single-Photon Excitation Energy Transfer between Quantum Dots via an Optical Near-Field Interaction

**Tadashi Kawazoe[1], Shunsuke Tanaka[2], and Motoichi Ohtsu[1,2]**

*1Japan Science and Technology Agency, Room 213, Bld. 9, The University of Tokyo,2-11-16 Yayoi, Bunkyo-ku, Tokyo 113-8656, Japan*

*2Department of Electronics Engineering, The University of Tokyo, Bunkyo-ku, Tokyo 113-8656, Japan*

kawazoe@ohtsu.jst.go.jp

**Topics:** Nanophotonics, Single photon source

Recently, many single photon sources using quantum dots (QDs) were reported for quantum communication technology [1]. Nanophotonic devices, which we have proposed, operate by a single photon [2-5], namely, they have potential as controllable single photon sources. An excitation energy transfer between quantum dots is one of the most important mechanisms for the operation of the nanophotonic devices. In this presentation, we report the first observation of single photon QD source by optical near-field spectroscopy and an evidence for a single photon excitation energy transfer between CuCl QDs.Figure1 (a) shows two different sized CuCl QDs coupled with an optical near-field interaction. When their size ratio is 2:1 , the excitation input light generates single (1,1,1:quantum numbers)-exciton only in the QD-A. This is because the transition to the (2,1,1)-exciton level in QD-B is optically forbidden [2]. The exciton in QD-A is transfered to QD-B by optical near-field interaction and relaxes to the (1,1,1) exciton sublevel. Finally, it recombines in QD-B. If multiple excitons are generated, the relaxation process changes due to the exciton-exciton interaction. Thus the finally emitted photon is single.

In the experiment, we used SHG of a modelocked Ti:sapphire laser with a pulse duration of 1 ps and a repetition rate of 80 MHz as the excitation light source. The photons emitted from QD-B were collected using an optical near-field fiber probe. Number of photon state was measured by HanburyTwiss method [6] and the single photon emission from QD-B was verified. Figure 1(b) shows the experimental result. Synchronous counting peaks appeared in the cycle of 12.5ns of delay time which corresponds to 1/80MHz. However, there was no synchronous counting at the time origin, as shown by the arrow. This result indicates QD-B acts as a single photon source. Its accuracy is more than 98 % estimated from the statistical point of view.

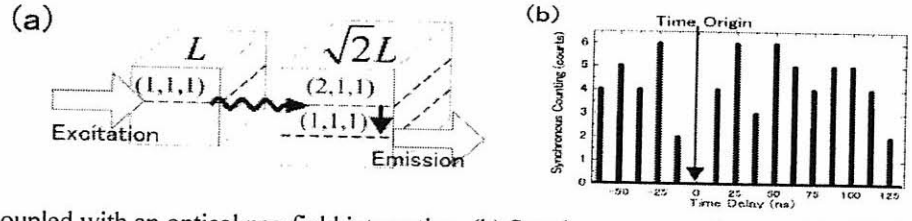


Fig.1 (a) QDs coupled with an optical nearfield interaction. (b) Synchronous counting result by Hanbury-Twiss method.

## Reference:

[1] J.I. Cirac, P. Zoller, H.J. Kimble and H. Mabuchi, Phys. Rev. Lett. 78, 3221 (1997).

[2] T. Kawazoe, K. Kobayashi, J. Lim, Y. Narita, and M. Ohtsu, Phys. Rev. Lett. 88, 067404 (2002).

[3]T. Kawazoe, K. Kobayashi, S. Sangu, and M. Ohtsu, Appl. Phys. Lett., 82, 2957 (2003).

[4] T. Kawazoe, K. Kobayashi, and M. Ohtsu, Appl. Phys. Lett., 86, 103102 (2005).

[5] T. Kawazoe, K. Kobayashi, K. Akahane, M. Naruse, N. Yamamoto, and M. Ohtsu, Applied Physics B, 84,243 (2006).

[6] R. Hanbury Brown and R. Q. Twiss, Nature 178 1447 (1956).

# Progress in developing nanophotonic integrated circuits.

Takashi YATSUI[1], Gyu-Chul YI[2], and Motoichi OHTSU[1,3].

*1 SORST, Japan Science and Technology Agency, Bunkyo-ku, Tokyo, 113-8656 Japan*

*2 School of Engineering, The University of Tokyo, Bunkyo-ku, Tokyo 113-8656, Japan*

*3 National CRI Center for Semiconductor Nanorods and Department of Materials Science and Engineering Pohang University of Science and Technology (POSTECH), San 31 Hyoja-dong, Pohang, Gyeongbuk 790-784, Korea*

In this paper, we review recent progress in developing nanophotonic devices using optical near-field interaction. ZnO nanocrystallites are potentially ideal components for realizing room-temperature operation of nanophotonic devices because of their high exciton-binding energy and great oscillator strength. To confirm this promising optical property of ZnO, we report the near-field time-resolved spectroscopy of ZnO nanorod double-quantum-well structures (DQWs). First, we observed nutation of the population between the resonantly coupled exciton states of DQWs, in which the coupling strength of the near-field interaction was found to be decreased exponentially as the separation increased. Furthermore, we successfully demonstrated the switching dynamics of a dipole-forbidden optical energy transfer among resonant exciton states. Our results provide criteria for designing nanophotonic devices. The success of time-resolved near-field spectroscopy of isolated DQWs described here is a promising step toward realizing a practical a nanometer-scale photonic switch and related devices.

# Observation of the dark states of near-field coupled InAs quantum dots using optical near-field microscopy

**Tadashi Kawazoe[1)], Kazuhiro Nishibayashi[2)], Kouichi Akahane[3)], Naokatsu Yamamoto[3)], and Motoichi Ohtsu[1,2)]**

[1)] *SORST, Japan Science and Technology Agency, Tenkoh building 17-4F, 687-1 Tsuruma, Machida, Tokyo 194-0004, Japan. Telephone:+81-42-788-6039, fax:+81-42-788-6031, e-mail: kawazoe@ohtsu.jst.go.jp*

[2)] *.Department of Electronics Engineering, University of Tokyo, 7-3-1 Hongo, Bunkyo-ku, Tokyo 113-8656, Japan.*

[3)] *National Institute of Information and Communications Technology, Koganei, Tokyo 184-8795, Japan.*

**Abstract:** We observed the dark states of coupled InAs quantum dots via an optical near-field. The experimental results show that the dipoles of near-field coupled InAs quantum dots are distributed with an anti-parallel configuration.



**OCIS codes:** (230.1150) All-optical devices s; (300.6470) Spectroscopy, semiconductors

A coupled quantum dot (QD) system has a number of more interesting and unique properties than does a single QD system. The optical near-field interaction is one of the mechanisms used to couple QDs. It is possible to control the coupling strength of the optical near-field coupling QDs, and to realize unique optical devices. So far, we have observed the optically forbidden energy transfer between neighboring cubic CuCl QDs via an optical near field [1] and demonstrated several kinds of nanometric optical device based on the optical near-field coupling of QDs [2-4]. In our previous experiments, the carrier lifetime increased with the optical near-field interaction between QDs [5]. This means that the dipoles of near-field coupled QDs distribute with an anti-parallel configuration. Such a dipole pair has a property like a quadrupole, which results in a dark state. In this presentation, we observe the luminescence from the dark state of near-field coupled InAs QDs using a near-field spectrometer.

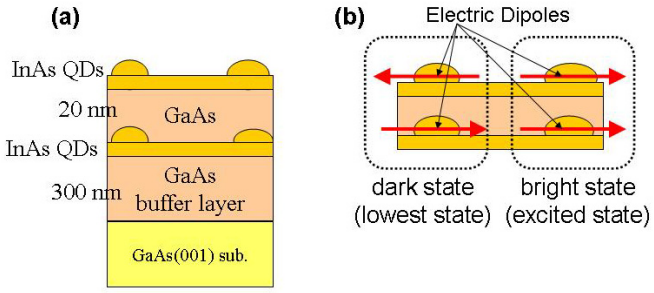


**Fig. 1**. Schematic drawing of the sample structure (a) and an explanation of the dark stage in a coupled QD system via an optical near field.

Figure 1 shows a schematic drawing of the sample structure and explains the dark state in the coupled QD system. To realize the coupled QD system, double InAs quantum-dot layers were grown. The mean quantum-dot size was 5 nm high and 30 nm in diameter. Using molecular beam epitaxy in SK-mode growth, the quantum dots could be aligned vertically, and the sheet density of the quantum dots was less than $10^{10}$ $cm^2$. Therefore, the horizontal distance between quantum dots was about 100 nm, and the vertical coupling of QDs was expected via the optical near-field interactions, given that their vertical separation was close to their diameter. In the near-field coupled system, the directions of the electric dipole of the lowest state distribute as shown in Fig. 1(b) and the result looks like an electric quadrupole. Therefore, the lowest state of the coupled QD system becomes a dark state. The luminescence intensity from such dark states is weak in far-field measurements, but it should be enhanced in near-field measurements because the quadrupole system can be resolved into the two individual dipoles in the near-field region.

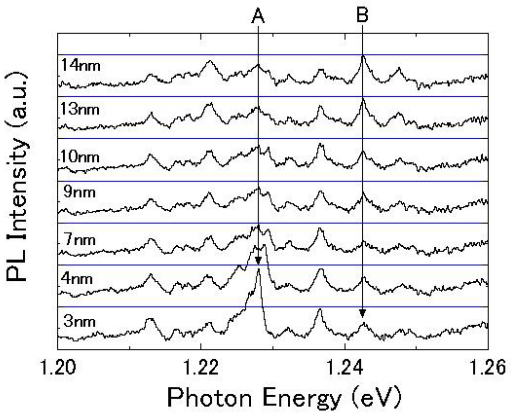


**Fig. 2**. Near-field photoluminescence spectra for separations ranging from 14 to 3 nm between the near-field probe and coupled QD system.

Figure 2 shows near field photoluminescence spectra of near-field coupled QDs for separations of 14–3 nm between the QD system and near-field probe. In the experiment, a He-Ne laser ($h\nu$=1.959 eV) was used as the light source, and the sample temperature was 20 K. Peak A corresponds to the lowest state of the coupled QDs, i.e., the dark state, and peak B corresponds to the excited level, *i.e.*, the parallel dipoles state. Peak A increased and peak B decreased as the separation decreased. These tendencies can be explained as follows. With a large separation, the photo-excited carriers in the lowest dark state (peak A) could not relax and the carriers accumulated. In the end, they did relax from the excited state (peak B). In addition, with the narrow separation, the near-field probe modifies the relaxation from the lowest dark state (peak A), and the carrier accumulation effect becomes small and peak B decreases. These experimental results support the coupling of the InAs QDs via the optical near-field interaction, enabling them to act as nanophotonic devices.

[1] T. Kawazoe, K. Kobayashi, J. Lim, Y. Narita, and M. Ohtsu, Phys. Rev. Lett. **88**, 067404 (2002).
[2] T. Kawazoe, K. Kobayashi, S. Sangu, and M. Ohtsu, Appl. Phys. Lett., **82**, 2957 (2003).
[3] T. Kawazoe, K. Kobayashi, and M. Ohtsu, Appl. Phys. Lett., **86**(10), 103102 (2005).
[4] T. Kawazoe, K. Kobayashi, K. Akahane, M. Naruse, N. Yamamoto, and M. Ohtsu, Applied Physics B, **84**, 243 (2005).
[5] T. Kawazoe, K. Kobayashi, and M. Ohtsu, IEICE Trans. on Electron., Vol. E**88**-C, 1845 (2005).

# Nanophotonic switch using one-dimensional ZnO double-quantum-well structures

**T. Yatsui,[*] S. Sangu,[†] T. Kawazoe,[*] and M. Ohtsu,[*,‡]**
*[*] SORST, Japan Science and Technology Agency, 687-1 Tsuruma, Machida, Tokyo, Japan 194-0004*
*+81 42-788-6040, +81 42-788-6031*
*[†] Advanced Technology R&D Center, Ricoh Co., Ltd.,16-1, Shinei-cho, Tsuduki-ku, Yokohama, Kanagawa, Japan 224-0035*
*+81 45-590-1431, +81 45-590-1894*
*[‡] School of Engineering, The University of Tokyo, 2-11-16 Yayoi, Bunkyo-ku, Tokyo, Japan 113-8656*
*+81 3-5841-1189, +81 3-5841-1140*
yatsui@ohtsu.jst.go.jp
**S. J. An, J. Yoo, and G.-C. Yi**
*National CRI Center for Semiconductor Nanorods and Department of Materials Science and Engineering, POSTECH*
*San 31 Hyoja-dong, Pohang, Gyeongbuk 790-784, Korea*
*+82 54-279-2155, +82 54-279-8635*

**Abstract:** We observed spectral switching and evaluated its dynamics by controlling the dipole-forbidden optical near-field energy transfer among resonant exciton states using 1D-ZnO nanorod double-quantum-well structures.

**OCIS codes:** (320.7130) Ultrafast processes in condensed matter, including semiconductors, (260.2160) Energy transfer

Systems of optically coupled quantum dots (QDs) are expected to be applicable to quantum information processing [1]. Additional functional device, called nanophotonic devices [2], can be realized by controlling exciton excitation in the energy levels in QDs. One representative device is a nanophotonic switch using CuCl [3], in which the switching dynamics are controlled by dipole-forbidden optical near-field energy transfer among resonant energy levels in the QDs. ZnO is a promising material for realizing room-temperature nanophotonic devices, owing to its large exciton binding energy [4] and recent achievements in the fabrication of nanorod heterostructures [5]. Here, we report near-field time-resolved spectroscopy of ZnO nanorod double-quantum-well structures (DQWs). We evaluated the switching dynamics using the dipole-forbidden optical energy transfer among resonant exciton states, and our results provide criteria for designing nanophotonic devices.

Figures 1a and 1b explain the "OFF" and "ON" states of the proposed nanophotonic switch. Two QWs, $QW_1$ and $QW_2$, are used as the input/output and control ports of the switch, respectively. Assuming well widths, $L_w$, of 3.2 and 3.8 nm with $Zn_{0.8}Mg_{0.2}O$ barrier layers, the ground exciton energy level in $QW_1$ and the first excited energy level in $QW_2$ resonate with each other. In the "OFF" operation (Fig. 1(a)), all the exciton energy in $QW_1$ is transferred to the ground energy level in the neighboring $QW_2$. Consequently, the input energy escapes to $QW_2$, and consequently, no optical output signals are generated from $QW_1$. In contrast, in the "ON" state (Fig. 1(b)), the escape route to $QW_2$ is blocked by the excitation of $QW_2$, due to state filling in $QW_2$ by applying the control signal; therefore, the input energy is transferred to $QW_1$ and an optical output signal is generated.

To confirm the switching dynamics between the ZnO/ZnMgO DQWs with $L_w$ = 3.2 and 3.8 nm with 3 nm separation were fabricated on the ends of ZnO nanorods with a mean diameter of 80 nm using catalyst-free metalorganic vapor phase epitaxy (Fig. 1(c)) [5]. The optical properties of individual ZnO DQWs were observed under a near-field optical microscope at 15K, using a UV fiber probe with a 30-nm aperture diameter.

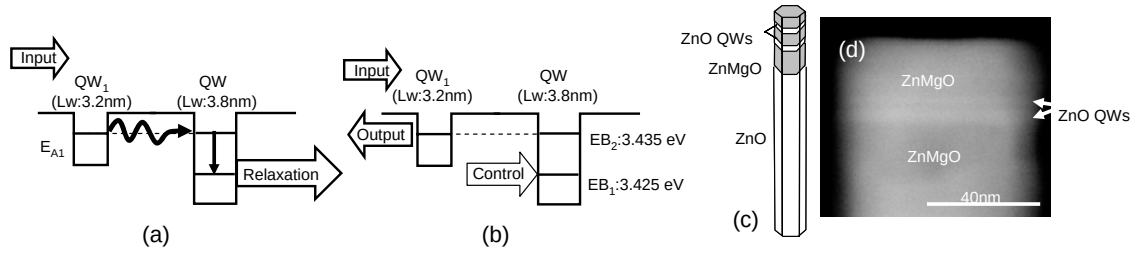


Fig. 1 Controlling the near-field energy transfer. Schematic of the nanophotonic switch of (a) "OFF" state and (b) "ON" state. (c) and (d) Fabricated ZnO nanorod DQWs.

As shown in curve $NF_{OFF}$ in Fig.2(a) [the near-field photoluminescence (PL) with continuous input light excitation from a He-Cd laser (3.814 eV) alone], no emission from the exciton ground level of $QW_1$ ($EA_1$) or the excited level of $QW_2$ ($EB_2$) at a photon energy of 3.435 eV was not observed. This indicates that the excited energy in $QW_1$ was transferred to the excited state of $QW_2$. Furthermore, the excited state of $QW_2$ is a dipole-forbidden level. Curve $NF_{Control}$ in Fig. 2(a) shows the near-field PL signal obtained with a control light excitation of 3.425 eV via second harmonic generation of a mode-locked Ti-sapphire laser with a pulse duration of 10 ps, emission from the ground state of $QW_2$ at a photon energy of 3.425 eV was observed. Both input and control light excitation resulted in an output signal with an emission peak at 3.435 eV, in addition to the emission peak at 3.425 eV (curve $NF_{ON}$), which corresponds to the ground state of $QW_2$. Since the excited level of $QW_2$ is a dipole-forbidden level, the observed emission at 3.435 eV indicates that the energy transfer from the ground state of $QW_1$ to the excited state of $QW_2$ was blocked by the excitation of the ground state of $QW_1$. In other words, the dipole-forbidden optical energy transfer among resonant energy levels in ZnO QWs via an optical near field was confirmed directly.

Next, we evaluated the dynamic properties of the nanophotonic switch. We observed time-resolved near-field PL signals at 3.435 eV with both input and control laser excitation (see Fig. 2(b)). The decay time constant was 483 ps. The output signal increased synchronously, within 100 ps, with the control pulse, which agrees with the theoretically expected result based on the quantum mechanical density matrix formalism [6].

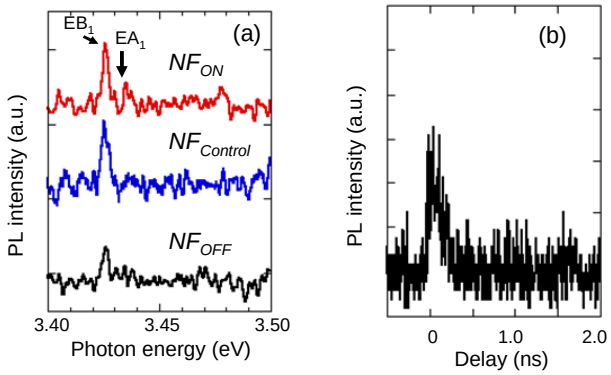


Fig. 2 (c) $NF_{ON}$, $NF_{Control}$, and $NF_{OFF}$ show near-field PL signal obtained with the illumination of Input laser along, Control laser alone, and Input and Control laser, respectively. (b) Near-field time-resolved PL signal with "ON" state.

For room-temperature operation, since the spectral width reaches thermal energy (26 meV), a higher Mg concentration in the barrier layers and narrower wells are required so that the spectral peaks of the first excited state ($E_2$) and the ground state ($E_1$) do not overlap. We believe that this requirement can be achieved using two QWs with 1.5-nm ($QW_1$) and 2-nm well ($QW_2$) widths with a Mg concentration of 50 %, in which the energy difference between $E_2$ and $E_1$ in $QW_2$ is about 50 meV [7].

**References**


1. M. Bayer, P. Hawrylak, K. Hinzer, S. Fafard, M. Korkusinski, Z. R. Wasilewski, O. Stern, and A. Forchel, "Coupling and entangling of quantum states in quantum dot molecules application to quantum information processing," Science **291**, 451-453 (2001).
2. M. Ohtsu, K. Kobayashi, T. Kawazoe, S. Sangu, and T. Yatsui, "Nanophotonics: design, fabrication, and operation of nanometric devices using optical near fields," IEEE J. Select. Top. Quant. Electron. **8**, 839-862 (2002).
3. T. Kawazoe, K. Kobayashi, S. Sangu, and M. Ohtsu, "Demonstration of a nanophotonic switching operation by optical near-field energy transfer," Appl. Phys. Lett. **82**, 2957-2959 (2003).
4. A. Ohtomo, K. Tamura, M. Kawasaki, T. Makino, Y. Segawa, Z. K. Tang, G. K. L. Wong, Y. Matsumoto, and H. Koinuma, "Room-temperature stimulated emission of excitons in ZnO/(Mg, Zn)O superlattices," Appl. Phys. Lett. **77**, 2204-2206 (2000).
5. W. I. Park, S. J. An, J. L. Yang, G.-C. Yi, S. Hong, T. Joo, and M. Kim, "Photoluminescent properties of ZnO/$Zn_{0.8}Mg_{0.2}O$ nanorod single-quantum-well structures," J. Phys. Chem. B **108**, 15457-15460 (2004).
6. K. Kobayashi, S. Sangu, T. Kawazoe, and M. Ohtsu, "Exciton dynamics and logic operations in a near-field optically coupled quantum-dot system," J. Lumin. **112**, 117-121 (2005).
7. W. I. Park, G.-C. Yi, and M. Jang, "Metalorganic vapor-phase epitaxial growth and photoluminescent properties of $Zn_{1-x}Mg_xO$ (0<x<0.49) thin films," Appl.. Phys. Lett. **79**, 2022-2024 (2001).

# Hierarchy in Optical Near-Fields by Nano-Scale Shape Engineering and its Application to Traceable Memory

**Makoto Naruse[1),2)], Takashi Yatsui[3)], Jun Hyoung Kim[2)], and Motoichi Ohtsu[2)]**
*1) National Institute of Information and Communications Technology, 4-2-1 Nukui-kita, Koganei, Tokyo 184-8795, Japan*
naruse@nict.go.jp
*2) The University of Tokyo, 2-11-16 Yayoi, Bunkyo-ku, Tokyo 113-8656, Japan*
*3) Japan Science and Technology Agency, 687-1 Tsuruma, Machida, Tokyo 194-0004, Japan*

**Abstract:** We numerically and experimentally studied the hierarchy of optical near-fields by engineering the shape of metal plates at nanometer-scale. Combined with localized energy-dissipation, this hierarchy should enable novel functionality, such as traceability of optical memories.

**OCIS codes:** (999.9999) Optical near-field; (210.4680) Optical memories; (190.0190) Nonlinear optics; (070.6020) Signal processing; (180.5810) Scanning microscopy

## 1. Introduction

Optical near-fields allow localized interactions at scales smaller than the diffraction limit of light [1], opening the door to novel nanometer-scale devices and technologies [2]. Optical near-fields have other unique physical features in addition to the ability to break through the diffraction limit; one notable feature is their intrinsic hierarchical nature, meaning that they exhibit different physical behavior at different scales [3,4]. Nano-scale fabrication technology for metals [5], quantum structures, and so forth has been advancing rapidly. In this paper, we describe a numerical and experimental study of the hierarchy of optical near-fields by engineering the shape of metal plates at nanometer scale. Specifically, we deal with a two-layer system, where (i) at smaller scale, which we call *Layer 1*, the system should exhibit a unique response, and (ii) at a larger scale, called *Layer 2*, the system should output two different signals. Such a hierarchical response can be applied to functions like traceability of optical memory in combination with a localized energy dissipation process. Optical access to this memory will be automatically recorded due to energy dissipation occurring locally in Layer 1, while at the same time, information will be read out based on the Layer 2 behavior [6]. Therefore, such hierarchy enables traceability of optical storage, which will be important for the security and management of digital content. We experimentally demonstrate the principle of the hierarchy using triangular gold nanostructures, and we discuss its theoretical basis by means of the two-dipole model.

## 2. Hierarchy in optical near-field by shape-engineering and its application to traceable memory

We begin with a numerical analysis of the hierarchical optical response by shape-engineering of metal nanostructures. Here, we assumed two types of shapes. The first one (*Shape I*) has two triangular metal plates aligned in the same direction; and the other one (*Shape II*) has them facing each other, as shown in Fig. 1(a). We assumed that the metal was gold, the gap between the two apexes was 50 nm, the horizontal length of one triangular plate was 173 nm, the angle at the apex was 30 degree, and the thickness was 30 nm. We assumed an incident uniform plane wave with a wavelength of 680 nm. The polarization was parallel to the *x* axis in Fig. 1(b). It is well-known that a strong electro-magnetic field is excited due to excitation of a plasmon induced in a metal nanostructure, particularly at the position of the apex, due to the interaction of charges concentrated at that point [7]. In fact, as

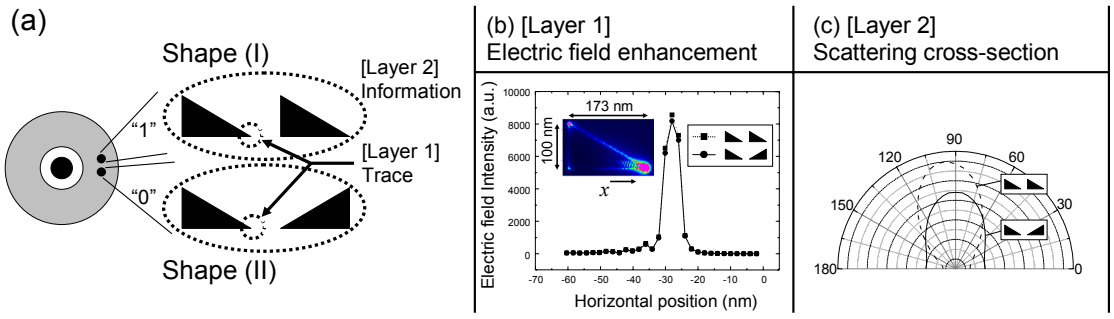


Fig. 1 (a) Hierarchy in optical near-fields by engineering the shape of metal plates at nanometer scale. (b) In Layer 1, both shapes exhibit comparable electric-field enhancement, and (c) in Layer 2 they exhibit different system responses.

shown Fig. 1(b), the electric field near the surface (1 nm away from the metal surface) shows an intensity nearly five orders of magnitude higher than the surrounding area. It should also be noted that nearly comparable electric-field enhancements are observed near the apexes of Shapes I and II, which are respectively denoted by the squares and circles in Fig. 1(b).

On the other hand, the two shapes exhibit different responses when the Layer 2 signal is associated the entire structure composed of the two triangles. As shown in Fig. 1(c), Shape I exhibits larger scattering cross-section compared to Shape II. This indicates that a digital output is retrievable by observing the scattering from the entire structure, where, for example, digital 1 and 0 are respectively associated with Shape I and Shape II.

### 3. Analysis and experiment

One physical reason for the different Layer 2 signals from those shapes is the following. As shown in Fig. 2(a), the phases of the *x*-component of the electric field inside the metal differ by almost 180 degree between the apex and the opposite side. Therefore, the system is approximated by two dipoles orientated in the same directions and in opposite directions for Shapes I and II, respectively. Based on the electric field formula:

$$\boldsymbol{E}^{(0)}(\boldsymbol{R}) = \left(\frac{iK^3}{4\pi\varepsilon_0}\right)\left\{-\frac{1}{3}\left[\boldsymbol{d}^{(0)} - 3\left(\boldsymbol{n}_0 \bullet \boldsymbol{d}^{(0)}\right)\boldsymbol{n}_0\right]h_2^{(1)}(KR) + \frac{2}{3}\boldsymbol{d}^{(0)}h_0^{(1)}(KR)\right\} \tag{1}$$

where $h_n^{(1)}$ represents spherical Hankel functions of the first kind and $\boldsymbol{n}_0$ is a unit vector from the position of dipole $\boldsymbol{d}^{(0)}$ to observation position $\boldsymbol{R}$, the electric-field intensity from the identically oriented dipoles increases rapidly compared to that from the oppositely oriented dipoles as the distance between the dipole and the observation position increases (Fig. 2(b)). In other words, we see that Shapes I and II effectively behave as a dipole and a quadrupole, respectively. Fig. 2(b) also indicates that comparable intensities are obtained for both shapes when the observation position is close to the dipoles, which is the intended system response in Layer 1.

In order to experimentally demonstrate the principle, we fabricated Shapes I and II in gold metal plates on a glass substrate by a liftoff technique using electron-beam lithography. We used a near-field optical microscope in an illumination collection setup with an apertured fiber probe having a diameter of 530 nm, as shown in Fig. 2(c). The light source used was a laser diode with an operating wavelength of 690 nm. The distance between the substrate and the probe was maintained at 450 nm. Fig. 3(d) shows the electric field intensity depending on the shape of the metal plates, where the Shape I series exhibited larger values compared to the Shape II series, as expected from the simulation and the theory. The insets in Fig. 2(d) are SEM pictures of each sample, where the horizontal length of a single triangle ranged from about 300 to 400 nm.

In summary, we have demonstrated the hierarchy of optical near-fields by shape-engineering of metal nanostructures, and we have discussed its theoretical origin based on induced dipoles.

References

[1] D. W. Pohl and D. Courjon eds., *Near Field Optics* (Kluwer, Dordrecht, 1993).
[2] M. Ohtsu and K. Kobayashi, *Optical Near Fields* (Springer, Belin 2004).
[3] M. Naruse, et. al., "Hierarchy in optical near-fields and its application to memory retrieval," Optics Express **13**, 9265-9271 (2005).
[4] M. Naruse, T. Inoue, and H. Hori, "Analysis of Hierarchy in Optical Near-Fields Based on Angular Spectrum Representation," in Integrated Photonics Research and Applications/ Nanophotonics 2006 Technical Digest (Optical Society of America, Washington, DC, 2006), NFB6.
[5] S.A. Maier, M.L. Brongersma, P.G. Kik, S. Meltzer, A.A.G. Requicha, H.A. Atwater, "Plasmonics - A route to nanoscale optical devices," Adv. Mater. **13**, 1501-1505 (2001).
[6] M. Naruse, et. al., "Nanophotonic traceable memory based on energy localization and hierarchy of optical near-fields," 2006 Sixth IEEE Conference on Nanotechnology (IEEE NANO 2006).
[7] T. Matsumoto, T. Shimano, H. Saga, H. Sukeda, and M. Kiguchi, "Highly efficient probe with a wedge-shaped metallic plate for high density near-field optical recording," J. Appl. Phys. **95**, 3901-3906 (2004).

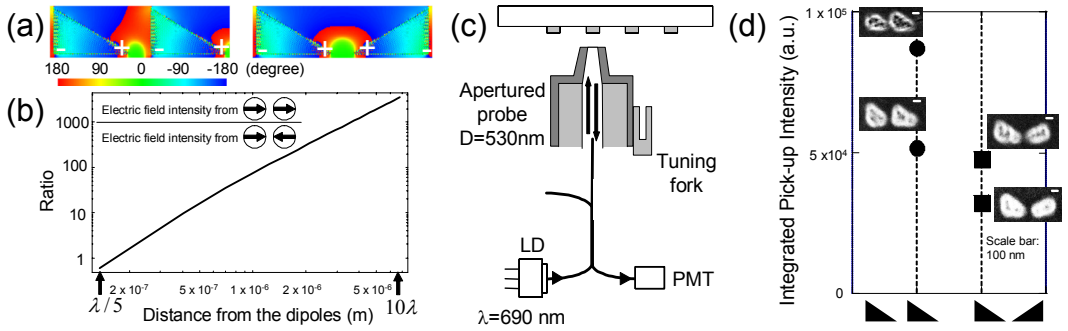


Fig. 2 (a) Profiles of the *x*-component of phase in induced electric field in the metal. (b) The difference between the electric field intensities grows rapidly as the distance between the observation position and the dipoles increases. (c) Experimental setup. (d) Electric field intensity for Layer 2 signals for both Shapes I and II.

# Nanophotonic devices using excitation energy transfers

*Tadashi Kawazoe[1], Yatsui Takashi[1], and Motoichi Ohtsu[1, 2]*

*[1] Japan Science and Technology Agency, Tenkoh Building 17-4F, 687-1 Tsuruma, Machida, Tokyo 194-0004, Japan.*

*[2] Department of Electronics Engineering, The University of Tokyo, 7-3-1 Hongo, Bunkyo-ku, Tokyo 113-8656, Japan.*

Recently, several kinds of nanometric photonic device have been studied for large-capacity communication systems and data-transfer bridges in personal computers (PCs). However, there is insufficient discussion on "*true*" nanophotonic devices. We have proposed a "*true*" nanophotonic device using excitation energy transfer[1]. First, we will discuss the features of a nanophotonic device based on a comparison of electronic devices used for large-scale integration, conventional photonic devices, and nanophotonic devices. The important points are how the device transfers signals and how one determines the device status, *i.e.*, whether it is ON or OFF.

Figure 1 shows typical electronic and photonic devices. In an electronic device (Fig. 1(a)), electrons act as signal carriers and the resistance in each device determines the device status. These features enable the miniaturization and integration of such devices. By contrast, a detector outside the device determines the status of a conventional photonic device (Fig. 1(b)). Consequently, the total device size increases and its integration is difficult. A "*true*" nanophotonic device (Fig. 1(c)) contains an optical source and a system for determining device status. Therefore, it is smaller than electronic devices and integration becomes possible.

The interaction that causes the transfer of excitation energy is an optical near field. This is not a wave, but is a local electromagnetic field that is coupled with excitation in the nanomaterial. We believe that the electronic and photonic phenomena in a nanomaterial should be described by the optical near-field interaction, since they are indeed physical phenomena caused by the local electromagnetic field coupled with excitation in the nanomaterial. Next, we will introduce the optical near-field interaction and unique phenomena based on it.

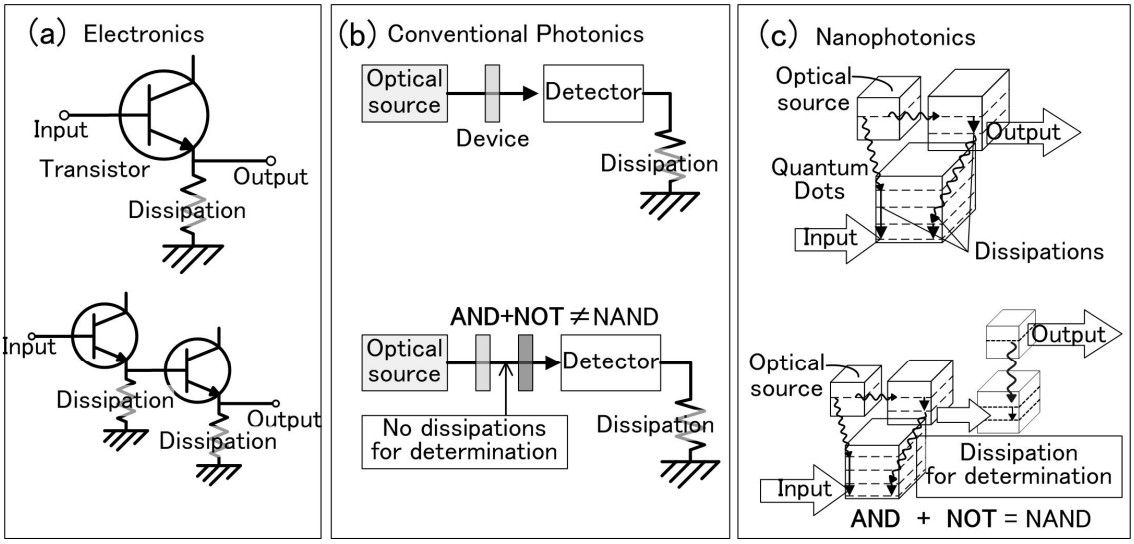


**Fig.1**. The configurations of (a) electronic devices, (b) conventional photonic devices, and (c) nanophotonic devices.

[1] M. Ohtsu et al, IEEE J. Sel. Top. Quant. Electron **8**, 839 (2002). T.kawazoe, et al., Phys. Rev. Lett. **88**, 067404 (2002).; Appl. Phys. Lett., **82**, 2957 (2003).; Appl. Phys. Lett., **86**, 103102, (2005).; Appl. Phys. B, **84**, 241 (2006).

**Direct Observation of the Optical Near - field Energy Transfer Among the Resonant Energy States Between ZnO Nanorod Double - quantum - well Structures.**

T.Yatsui[1]; S.Sangu[2]; T.Kawazoe[1]; M.Ohtsu[3,1]; J.Yoo[4,5]; S.An[4,5]; G.Yi[4,5]. 1. SORST, JST, Machida, Japan; 2. Advanced Technology R&D Center, Ricoh Co., Ltd., Yokohama, Kanagawa, Japan; 3. School of Engineering, University of Tokyo, Bunko-ku, Tokyo, Japan; 4. Department of Materials Science and Engineering, POSTECH, Pohang, Gyungbuk, South Korea; 5. National CRI Center for Semiconductor Nanorods, Pohang, Gyungbuk, South Korea.

**Abstract Number:** Q19.3

**Presentation Time:** Thursday, Nov. 30, 4:00 PM - 4:15 PM

**Location:** Room 312 (Hynes)

Nanometer-scale ZnO is a promising material for realizing nano-scale photonic devices at room temperature, due to its large exciton binding energy (60 meV). Furthermore, spatially- resolved near-field photoluminescence (PL) spectra of individual nanorod ZnO quantum-well structures (QWs) have been measured to realize nanophotonic devices using low-temperature near-field optical microscopy (NOM). To observe the optical interaction between the ZnO QWs, we measured the time-resolved near-field PL signals of ZnO double-quantum-well structures (DQWs).

$ZnO/Zn_{0.8}Mg_{0.2}O$ QWs were fabricated on the ends of ZnO nanorods with a mean diameter of 40 nm. They were grown vertically from the sapphire (0001) substrate using catalyst-free metalorganic vapor phase epitaxy, in which the ZnO nanorod was grown in the c orientation. Three samples were prepared for this study: single-quantum-well structures (SQWs) with a well layer thickness, $L_w$, of 3.0 nm, DQWs with $L_w$ = 3.5 nm with 6 nm separation, and three pairs of DQWs with $L_w$ = 2.0 nm with different separations (3, 6, and 10 nm), in which each DQW was separated by 30 nm. Using collection-mode NOM with an apertured (diameter of 50 nm) UV fiber probe, we obtained time-resolved near-field PL spectra at 15 K using the 4.025-eV ($\lambda$ = 308 nm) third harmonic generation of a mode-locked Ti-sapphire laser with a pulse duration of 10 ps to excite the ZnO QWs. We compared the time-resolved near-field PL signals at photon energies corresponding to the emission from excitons confined in the ZnO QWs. The decay time constants were found to be 390, 440, and 160 ps for the (1) SQWs, (2) DQWs, and (3) three-pair DQWs, respectively. To check whether these spectral intensities decrease monotonically or have some oscillator components, we performed Fourier analysis. While the power spectrum of the SQWs did not exhibit any peak, indicating that it decreases monotonically, the power spectrum of the DQWs had a strong peak at a frequency of 2.6 $ns^{-1}$. We believe that this peak originated from the nutation of the population among the resonant energy states between the DQWs via optical near-field energy transfer. Furthermore, we found that the power spectra of the three pairs of DQWs had three peaks, at frequencies of 1.9, 4.7, and 7.1 $ns^{-1}$. Since the degree of the coupling strength, which is proportional to the frequency of the nutation, should increase as the separation decreases, we believe that these peaks correspond to the signals from the respective DQWs with different separations of 10 (1.9 $ns^{-1}$), 6 (4.7 $ns^{-1}$), and 3 nm (7.1 $ns^{-1}$). The exponential decay in the value of the frequency with the separation increase also supports the postulate that the peaks in the power spectra originate from the localized field interaction between the quantum wells. The results presented here provide criteria for realizing nanophotonic devices using one-dimensional ZnO nanorod QWs.

**Low - temperature ( ~270°C ) Growth of Vertically Aligned ZnO Nanorods Using Photo - assisted Metal Organic Vapor Phase Epitaxy.**

K.Kitamura[1]; T.Yatsui[2]; M.Ohtsu[1,2]; T.Nakamata[1]; J.Lim[3]; G.Yi[4]. 1. Graduate School of Engineering, The University of Tokyo, Bunkyo-ku, Tokyo, Japan; 2. Solution-Oriented Research for Science and Technology, Japan Science and Technology Agency, Machida, Tokyo, Japan; 3. Interdisciplinary Graduate School of Science and Engineering, Tokyo Institute of Technology, Yokohama, Japan; 4. Department of Materials Science and Engineering, Pohang University of Science and Technology, Pohang, South Korea.

**Abstract Number:** K2.6

**Presentation Time:** Monday, Nov. 27, 4:00 PM - 4:15 PM

**Location:** Room 200 (Hynes)

ZnO nanocrystallites are a promising material for realizing nanophotonic devices at room temperature, owing to their large exciton binding energy and large oscillator strength. Furthermore, ZnO/ZnMgO nanorod heterostructures have been fabricated and the quantum confinement effect from single-quantum-well structures (SQWs) was observed. Nanophotonic device applications using ZnO quantum-well structures require a high Mg concentration in the ZnMgO layers, which results in strong localization of the photons in the quantum-well layers. To realize this, a lower growth temperature is required to avoid the interdiffusion of Mg. To obtain high-quality crystallinity at a low growth temperature, we used photo-induced metal organic vapor phase epitaxy (MOVPE). ZnO nanocrystallites were grown on Si(100) substrates using a low-pressure MOVPE system without using any metal catalysts. Diethylzinc (DEZn) and oxygen were used as the reactants and argon was used as the carrier gas. To decrease the growth temperature, we used a He-Cd laser ($\lambda$= 325 nm, 300 $\mu$W) as the light source during MOVPE growth, yielding reactive Zn and O radicals via photolysis. To examine the temperature dependence of the morphology of the deposited film, we realized nanoparticle growth inside the laser spot only, even at room temperature. Furthermore, when the growth temperature was increased to 270°C, vertically aligned nanorod structures measuring 1 $\mu$m in length and 200 nm in diameter were obtained under He-Cd laser irradiation. Although the photoluminescence (PL) spectra (measured at 5K) of the nanoparticles grown at room temperature did not show any peaks, those of the nanorods grown at 270°C resulted in strong PL emission at 3.37eV, corresponding to the emission from a neutral-donor bound exciton in ZnO. The emission peak energy of room temperature PL (3.29 eV) agreed with the reported value (3.26 eV), which corresponds to the spontaneous emission from the free exciton in high-quality ZnO nanocrystallites. The full width at half maximum of the PL spectra was about 105 meV, which is comparable with the 100 meV of high-quality ZnO nanorods grown using MOVPE at 400°C. In addition, high-resolution transmission electron microscopic images of the nanorod structure grown at 270°C revealed hexagonally packed single-crystalline growth with (0001) direction. These results imply that the ZnO nanorods grown using photo-induced MOVPE at low temperature (270°C) were composed of single-crystalline ZnO nanocrystallites. Decreasing the growth temperature using photo-assisted MOVPE should realize a higher Mg concentration in the ZnMgO layers.

# Effect of additive chloride ion on submicron size-dependence of electroless nickel plating

Shuji MONONOBE[1,2] and Motoichi OHTSU[3]

[1] *Department of Mechanical Engineering, School of Engineering, Toyo University, Kawagoe-shi, Saitama 350-8585, Japan*

[2] *Special Res. Lab. for Optical Sci., Kanagawa Academy of Science and Technology, KSP East 409, 3-2-1 Sakado, Takatsu-ku, Kawasaki-shi, Kanagawa 2130012, Japan*

[3] *Department of Electronic Engineering, Tolyo University, 7-3-1 Hongo Bunkyo-ku, Tokyo 113-8656, Japan*

## 1. INTRODUCTION

Recently, near-field optical microscope (NSOM) [1,2] employing shear-force feedback technique, which provides simultaneous topographic and NSOM imaging, has been applied as a powerful tool for nano-optical imaging and local spectroscopy. To develop a high resolution NSOM/ shear-force microscopy, we have proposed a new type of probe tip having a metal film whose thickness gradually decreases toward the apex.[3] We previously fabricated fiber probes with a decreasing metal film by adding lead ion with an extremely low concentration to a nickel-plating bath. However, some of them have a dip-like structure around the foot of a protruding fiber tip (see Fig. 1(a).). In this paper, we present a new method using nickel-plating bath with chloride ion to avoid generation of dip-like structure.

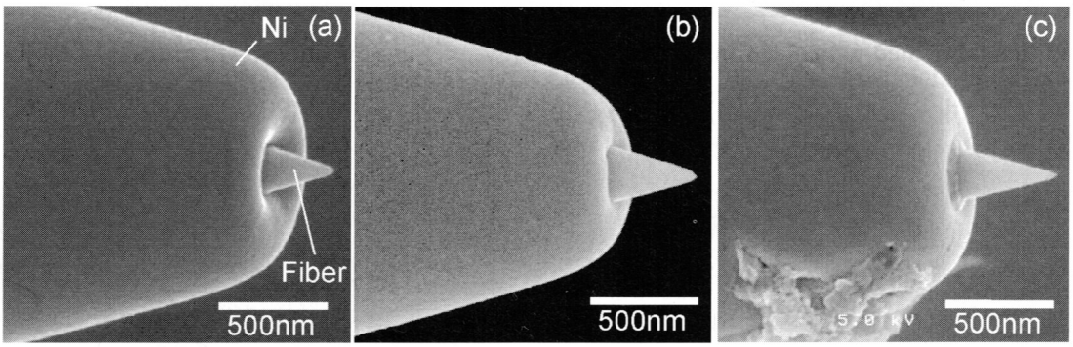


**Fig.1** Scannning electron micrographs of three protruding probes, which were plated in electroless nicke plating solutions with (a) $[Cl^-]=0mol/dm^3$, (b) $[Cl^-]=0.75mol/dm^3$, (c) $[Cl^-]=1mol/dm^3$, respectively.

## 2. EXPERIMENTAL

The method involves tapering an optical fiber, surface activation, and electroless nickel plating. Firstly, a $GeO_2$-doped fiber with a core diameter of 2 μm and a relative refractive index difference of 2% was etched in buffered HF. The obtained probe has a

conical tapered core and a clad diameter of 25 μm. The cone angle of $\theta$=20° and the apex diameter less than 10 nm. Next, the tapered fiber was coated with a palladium by a sputter unit. The thickness corresponds to a few nanometers. Finally, we plated the tapered probe in a nickel plating bath at a temperatures of 64-68°C. The plating bath includes 0.04mg/dm$^3$-$Pb^{2+}$, 0.01mol/dm$^3$-$Ni^{2+}$ and 0.1mol/dm$^3$-$CH_3COO^-$, 2mol/dm$^3$-$NH_4^+$, and 0.15mol/dm$^3$-$PH_2O_2^-$. To vary the concentration of $Cl^-$ from 0 to 1.5 mol/dm$^3$, ammonium chloride $NH_4Cl$ was added. Further, $(NH_4)_2SO_4$ was added for control of the total concentration $NH_4^+$ of a plating solution.

## 3. RESULT

Figures 1(a), 1(b), and 1(c) show scanning electron micrographs of the magnified top regions of the nickel-coated probes fabricated using plating solutions with [$Cl^-$] = 0, 0.75, and 1.5 mol/dm$^3$, respectively. In a-c, the conical fiber tips are protruded from nickel film. The foot diameters of the protruding tips are estimated to be a constant value of 240nm. As appeared in Figs. 1(a) and 1(b), dip-like structure of nickel coat is formed in a region of [$Cl^-$]<1mol/dm$^3$. At [$Cl^-$]=0 mol/dm$^3$, the height of dip-like structure is estimated to be more than 130nm from Fig. 1(a). Using a plating solution with a high concentration of [$Cl^-$]=1.5 mol/dm$^3$, the height is decreased down to a small value of 20-30nm.

## 4. SUMMARY

W proposed a submicron-size-dependent plating method using a new plating bath with a chloride ion concentration of motre than 1mol/dm$^3$ for near-field optical microscopy probe. By applying this plating to a tapered fiber, we reproducibly succeeded in fabricating a protruding NSOM probe with a foot diameter of 240 nm.

## REFERENCES


[1] M.Ohtsu, *Near-field Nano/Atom Optics and Technology*, (Springer-Verlag, Berlin, 1998).

[2] S. Mononobe, "Near-field optical probes and the imaging applications", In: *Progress in Nano-Electro-Optics III* (ed. Ohtsu, M.) (Springer-Verlag, Berlin, 2005).

[3] S. Mononobe, Y. Saito, M. Ohtsu, H. Honma, "Fabrication of a near-field optical fiber probe based on electroless nickel plating under ultrasonic irradiation", *Jpn. J. Appl. Phys.*, **43** (5B), 2862-2863, (2005).

# Near-Field Lithography as prototype nano-fabrication tool

Yasuhisa Inao [a], Shinji Nakasato [a], Ryo Kuroda [a], Motoichi Ohtsu [b]
[a] Canon Research Center, Canon Inc., Ohta-ku, Tokyo 146-8501, Japan
phone: +81-3-5732-2575 e-mail: inao.yasuhisa@canon.co.jp
[b] Department of Electronics Engineering, University of Tokyo, Bunkyo-ku, Tokyo 113-8656, Japan

Key word: near-field, lithography, clean environment, tri-layer resist process, nano-optical elements

Nano-scale fabrication techniques suitable for semiconductor electronic devices and nano-optical components are intensively studied. However, the requirements to their resolution and soaring costs are demanding. Near-field lithography (NFL) has been proposed as a low cost fabrication tool with nano-resolution [1-3]. NFL makes use of optical near field generated around the photomask to expose a photoresist, which is in close contact with the mask. After the demonstration of near-field printing of sub wavelength structures [1], we have developed the tri-layer resist process particularly suitable for NFL using a very thin photoresist, and successfully fabricated very fine resist patterns [2, 3].

We have been developed prototype of NFL system is shown in Fig. 1. The system has i-line (365 nm) of a mercury lamp as a light source. Note that this wavelength is much greater than the line and space patterns of less than 100 nm that we use. The whole system is enclosed in dual clean environment. Some of the features of our system are described below.

a) Fine resolution over the whole mask with step and repeat exposure

In NFL, the distance between the mask and the photoresist shuld be as short as possible. In order to accomplish a perfect physical contact between the mask and the wafer, we attach the mask to the bottom of a pressure vessel and pressurise it. The mask is then deformed and fits to the wafer. To obtain a large contact area greater than 5 x 5 $mm^2$, the initial distance between the mask and the wafer was set to be ~50 μm. This also helps us minimise the mask deformation. As shown in Fig. 2, we are able to fabricat a resist pattern with the features smaller than 50 nm. By comparing the patterns at the centre and near the edge, we confirmed an excellent uniformity (see Fig. 4). We also successfully fabricated 25 patterns on a 4-inch silicon wafer by successive exposure (Fig. 3).

b) Ultrafine particle control by dual clean system

Our prototype is designed for use in normal environment without expensive clean room equipment. In order to prevent any particles from interfering the physical contact between the mask and the wafer, the system is set in a compact clean booth and clean air through ULPA filters is circulated inside the prototype. No particle greater than in 80 nm diameters are detected by using a commercial particle counter indicating that extremely clean local environment is realised in a compact fashion.

We also fabricated hole and dot arrays as examples of two-dimensional patterns, useful for sub-wavelength structures and photonic crystals, as shown in Fig. 5, by using our system. These results demonstrate good fidelity of the NFL process and its great capability of high-resolution pattern transfer with low cost, showing interesting opportunities for novel nano-device fabrication.

This study has been supported by Ministry of Education, Culture, Sports, Science and Technology.

[1] M. M. Alkaisi, et al, *Appl. Phys. Lett.*, **75** , 3560-3562 (1999 )
[2] T. Ito et al, *J. Photopolymer Sci, and Tecnol.*, **18** P.435-441(2005)
[3] T. Ito et al, *Appl. Phys. Lett.*, ( to be published )

# Near-Field Lithography as prototype nano-fabrication tool

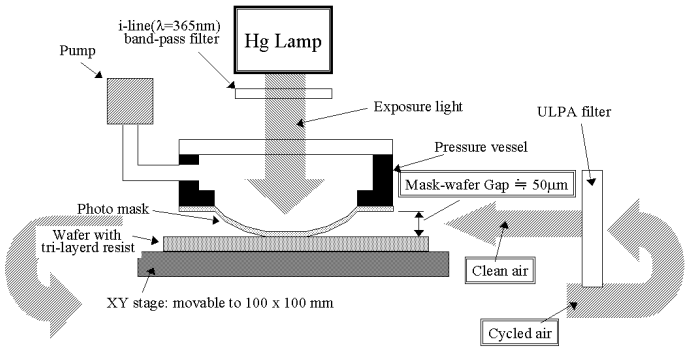


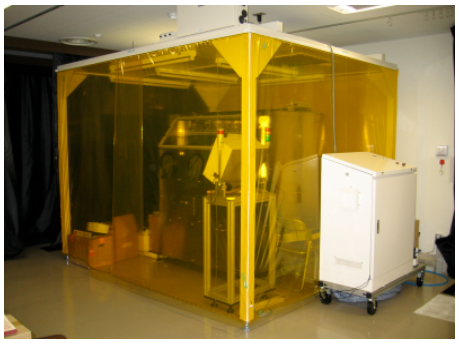

Fig. 1 Schematic illustration and photograph of our prototype

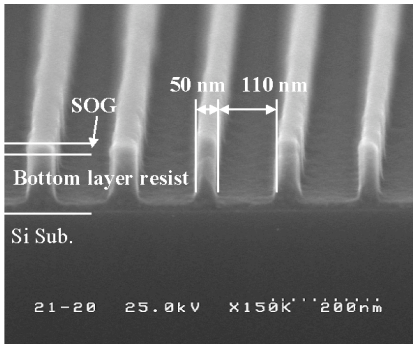


Fig. 2 Resist pattern (cross-sectional view)

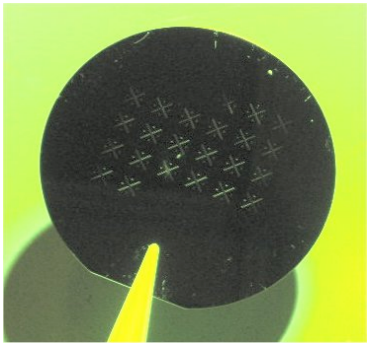

Fig. 3 Resist pattern
fabricated by step and repeat scheme

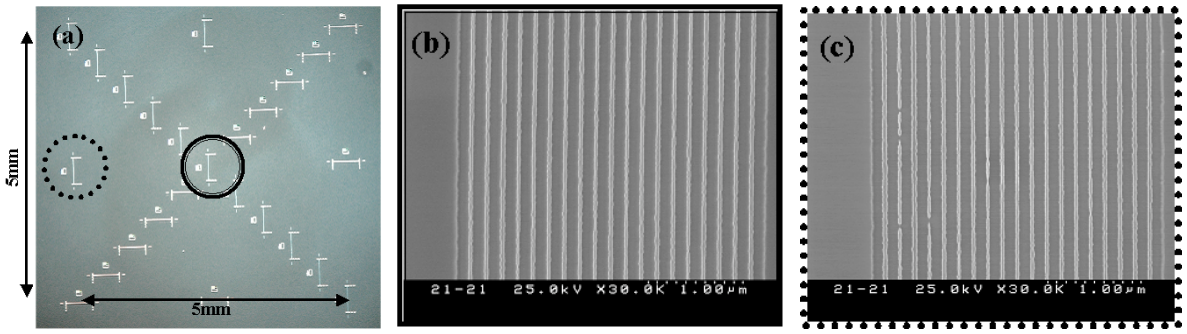


Fig. 4 (a) Resist patterns fabricated in 5x5mm area,
(b) pattern at the centre, (c) pattern at the edge of 5 x 5 $mm^2$ area

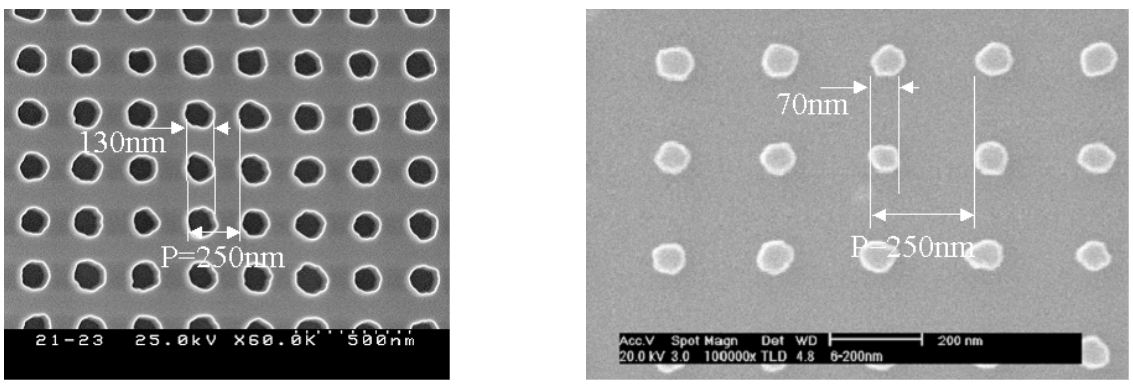


Fig. 5 Resist patterns of hole and dot array

# Nanophotonic Devices using InAs Quantum Dots

*T. Kawazoe*
*Japan Science and Technology Agency, Machida, Tokyo 194-0004, Japan*

*K. Akahane and N. Yamamoto*
*NICT, Koganei, Tokyo 184-8795, Japan*

*K. Nishibayashi and M. Ohtsu*
*University of Tokyo, Bunkyo-ku, Tokyo, 113-8656, Japan*

An optical near-field generated on a nanometric element, is free from the diffraction of light and enables the operation and integration of nanometric optical devices. By using the localized optical near-field as the signal carrier, which is transmitted from one nanometric element to another, a nanoscale photonic device can be realized. The primary advantage of nanophotonics is the capacity to achieve novel functions that are based on local electromagnetic interactions, while realizing nanometer-sized photonic devices. Based on this idea, we observed an optically forbidden energy transfer between cubic CuCl quantum dots (QDs) and proposed several nanometric optical devices: a nanometric AND-gate, a nanometric NOT-gate, and an optical nanofountain [1].

However, CuCl QDs are unsuitable for the actual integration owing to their size and position inhomogeneity and chemical instability. In order to obtain the size- and position-controllability of QDs, III-V semiconductor QDs were selected. Toward the actual integration in nanophotonic modules, we prepared the InAs QDs using MBE method. Figure 1 shows the sample structure, near-filed PL spectrum of the sample, and its near-field image at 15 K. This sample structure enables a nanophotonic NOT-gate operation. In the presentation, we will discuss the experimental results of the device operation using this sample.

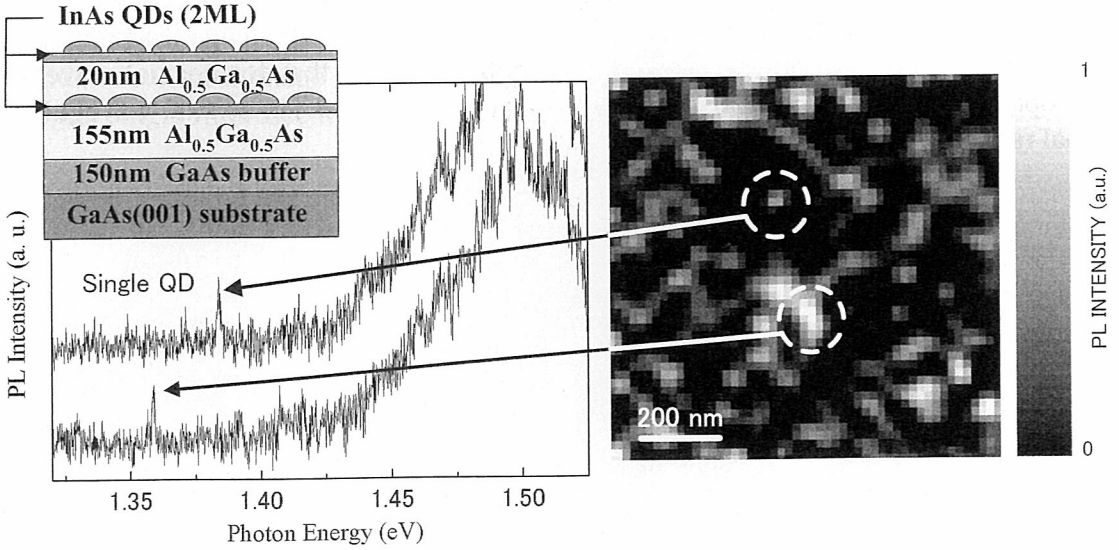


**Fig. 1**: Sample Structures (InAs/AlGaAs QDs) for NOT-gate operation, near-field PL spectra of the sample, and the near-field PL image.

[1] T.kawazoe, et al., *Phys. Rev. Lett.* **88**, 067404 (2002).; *Appl. Phys. Lett.*, **82**, 2957 (2003).; *Appl. Phys. Lett.*, **86**, 103102, (2005).; *Appl. Phys. B*, in press (2006).

# Nanophotonics using Optical Near-field

*T. Kawazoe*
*Japan Science and Technology Agency, Machida, Tokyo 194-0004, Japan*

*M. Ohtsu*
*University of Tokyo, Bunkyo-ku, Tokyo, 113-8656, Japan*

Nanophotonics is defined as a technology that utilizes local electromagnetic interactions between a small nanometric element and an optical near field. Since an optical near field is free from the diffraction of light due to its size-dependent localization and size-dependent resonance features, nanophotonics using optical near field enables the operation of nanometric optical device and the nanometric fabrication [1]. The primary advantage of an optical near field is its capacity to realize novel functions based on local electromagnetic interactions. I introduce these novel functions with the interesting experimental results. It should be noted that some of the conventional concepts of wave-optics, such as interference, become not essential in nanophotonics, and the nanophotonics using optical near field brings qualitative innovation to the optical technology.

Here, I explain about the novel optical switch using an optical near field as an example. Figures 1 illustrates the OFF and ON states of the proposed nanophotonic switch using three QDs [2]. The QD-I, O, and C are used as the input, output, and control ports of the switch, respectively. The typical size of this switch is less than 20 nm. The quantized energy sublevels (1,1,1) in QD-I, (2,1,1) in QD-O, and (2,2,2) in QD-C resonate with each other. Additionally, the energy sublevels (1,1,1) in QD-O and (2,1,1) in QD-C also resonate. Almost all the energy of the excitation in the QD-I transfer to the energy sublevels (1,1,1) in the neighboring QD-O, and finally, it transfers to the energy sublevels (1,1,1) in the QD-C, although the energy transfers between QDs are optically forbidden. In the OFF state, the input energy escapes to the QD-C, and then the output signal is obstructed. In the ON state, the escape passes to the QD-C are blocked by the excitation of the QD-C, and thus the input energy goes through the QD-O giving an output signal. This device is not achieved without optical near-field features. The basic concept of this device is applicable to several other functional nanophotonic devices.

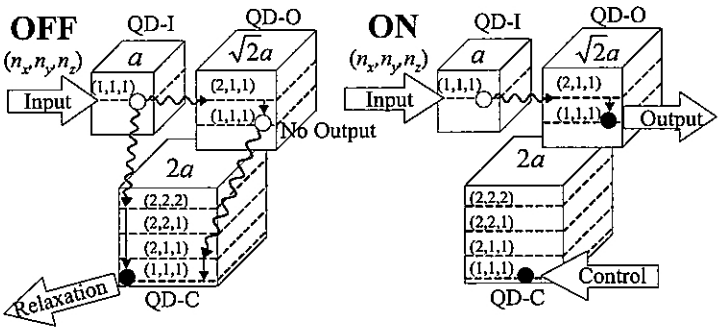


Fig.1.

The nonadiabatic photochemical processes using an optical near field are useful and interesting. We had demonstrated optical CVD and photolithography using visible and red light source [2,3]. Since, in the nonadiabatic photochemical reaction, molecules are exposed only to the optical near field, a more accurate fabrication becomes possible.

[1] T.kawazoe, et al., *Phys. Rev. Lett.* **88**, 067404 (2002).; *Appl. Phys. Lett.*, **82**, 2957 (2003).; *Appl. Phys. Lett.*, **86**, 103102, (2005).; *Appl. Phys. B*, in press (2006).
[2] T. Kawazoe, K. Kobayashi, S. Takubo, and M. Ohtsu, J. Chem. Phys. **93**, 2937 (2005).
[3] H. Yonemitsu, T. Kawazoe, K. Kobayashi and M. Ohtsu, J. Luminescence in press, Available online 10 March 2006.

# Deposition of 5nm-diameter Zn-nanodot using near field optical CVD with optically inactive $Zn(acac)_2$

*T. Kawazoe*
*Japan Science and Technology Agency, Machida, Tokyo 194-0004, Japan*

*K.Kobayashi*
*Tokyo Institute of Technology, 2-12-1 Ookayama, Meguro-ku, Tokyo 152-8551, Japan*

*M. Ohtsu*
*University of Tokyo, Bunkyo-ku, Tokyo, 113-8656, Japan*

Spatial localized nature of the optical near field can be used for novel nano-fabrication. For example, we have found in the near-field optical chemical vapor deposition (NFO-CVD) that the metal organic molecules are photodissociated by a nonresonant optical near field with photon energy lower than the dissociation energy of the molecule[1]. This unique photodissociation is explained by the nonadiabatic photochemical process and the exciton-phonon polariton model which we have developed [2].

In the experiment, $Zn(acac)_2$ was used as the source of the reacting molecular gas. An $Ar^+$ laser ($\lambda$ = 457 nm) was used as the light source. The fiber probe used for NFO-CVD was a high-throughput single-tapered fiber probe, which was fabricated by pulling and etching a pure silica core fiber. The cone angle of the fabricated fiber probe was 30 degrees and its apex diameter was 30 nm. During deposition, the pressure of $Zn(acac)_2$ was 70 mTorr in the CVD chamber.

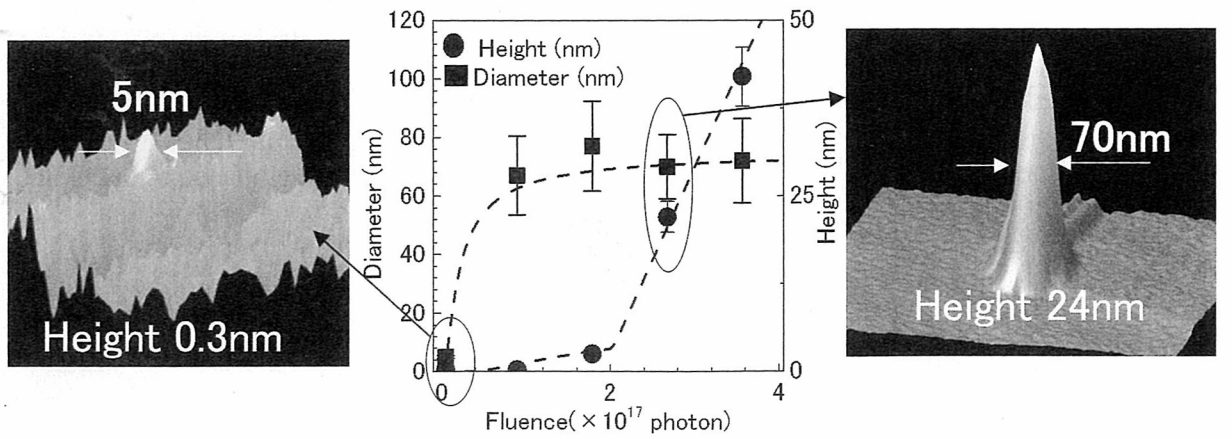


**Fig. 1**: The fluence dependencies of the width and height of deposited Zn-nanodots using NFO-CVD and their shear force microscope images.

Figure 1 shows the experimental results of Zn deposition. Although $Zn(acac)_2$ is optically inactive, we observed the deposition of Zn-nanodots on the substrate just below the apex of the fiber probe using NFO-CVD. Finally, we obtained Zn nanodot of 5-nm in diameter by the optimizations of the incident laser power and the deposition time.

[1] T. Kawazoe, Y. Yamamoto, and M. Ohtsu, *Appl. Phys. Lett.*, **79**, 1184, (2001).
[2] T. Kawazoe, K. Kobayashi, S. Takubo, and M. Ohtsu, *J. Chem. Phys.*, **122**, 024715, (2005).

# Plasmonic circuits for nanophotonic devices

Takashi Yatsui*[a], Makoto Naruse[b, c], Motoichi Ohtsu[a,c]
[a] SORST, Japan Science and Technology Agency, 687-1 Tsuruma, Machida, Tokyo 194-0004 Japan
[b] Photonic Network Group, National Institute of Information and Communications Technology, 4-2-1 Nukui-kita, Koganei, Tokyo 184-8795, Japan
[c] School of Engineering, the University of Tokyo, 2-11-16 Yayoi, Bunkyo-ku, Tokyo 113-8656, Japan
*yatsui@ohtsu.jst.go.jp; phone 81 42 788 6030; fax 81 42 788 6031

## ABSTRACT

To realize the optical devices required by future systems, we have proposed nanometer-scale photonic integrated circuits (i.e., nanophotonic ICs) [1]. These devices consist of nanometer-scale dots, and an optical near field is used as the signal carrier. Since an optical near field is free from the diffraction of light due to its size -dependent localization and resonance features, nanophotonics enables the fabrication, operation, and integration of nanometric devices. To drive a nanophotonic device with an external conventional diffraction-limited photonic device, a far/near-field conversion device is required. Here, we review the use of a nanometer -scale waveguide as such a conversion device for nanophotonic ICs [1-7]. Furthermore, the fabrication of a nanophotonic device using an optical near-field is introduced [8,9].

**Keywords:** Optical near-field, Nanophotonic device, Plasmon, Nano cot coupler, Nanophotonic fabrication

## 1. INTRODUCTION

Future optical transmission and data -processing systems will require integrated advanced photonic devices, in order to increase data processing rates and capacity. These devices will have to be significantly smaller than conventional diffraction-limited photonic devices. To meet this requirement, we have proposed nanometer-scale photonic integrated circuits (nanophotonic ICs) that are composed of nanometer-sized elemental devices (nanophotonic devices) [1]. As a representative device, a nanophotonic switch was proposed and its operation was demonstrated by controlling the dipole forbidden optical energy transfer among resonant energy states in CuCl quantum cubes via an optical near field.

For use in future photonic systems, the nanophotonic devices and ICs must be connected to conventional diffraction-limited photonic devices. This connection requires a far/near-field conversion device, such as a nanometer-scale optical waveguide. The performance parameters required of this device include:

(A) High conversion efficiency

(B) A guided beam width of less than 100nm for efficient coupling of the converted optical near-field to sub-100 nanometer-sized dots.

(C) A propagation length that is longer than the optical wavelength to avoid direct coupling of the propagating far-field light to the nanophotonic device consisting of nanometer-scale dots. (The propagation length $l_t$ is defined as $I(z) = I(0) \exp(-z/l_t)$, where I(z) is the optical intensity and z is the longitudinal position measured from the input terminal (z = 0)).

Plasmonics: Metallic Nanostructures and their Optical Properties IV, edited by Mark I. Stockman,
Proc. of SPIE Vol. 6323, 63230O, (2006) · 0277-786X/06/$15 · doi: 10.1117/12.680108

## 2. PLASMONIC CIRCUITS

### 2.1 A Plasmon Waveguide with a Metallic-Core Waveguide

To meet these requirements, we used a metal-coated Si wedge structure. Figure 1(a) shows our plasmon-waveguide scheme [2]. The main part consists of a silicon dielectric wedge, coated with a thin metal film. Incoming far-field light, which is polarized parallel to the y-axis, is first transformed into the 2 dimensional (2D) surface plasmon mode on side $F_1$ (see Fig. 1(b)). Next, the 2D surface plasmon mode is converted into the 1D TM plasmon mode at the edge between $F_1$ and the plateau. This conversion occurs because of the scattering coupling at the edge [3]. Third, the transverse magnetic (TM) plasmon mode [11] propagates along the plateau in a manner similar to surface plasmon modes using metal strips [12] or edge modes using metal wedges [13]. This propagation occurs because the metal film deposited on the plateau is thicker than that on the other faces ($F_1$, $F_2$, and $F_3$) due to the normal evaporation process (see Fig. 1(c)). Consequently, the plateau acts as a metal-core waveguide. Finally, the TM plasmon mode at the waveguide outlet is converted into an optical near-field so that it couples to the nanometer-scale dots, which are located in close proximity to the outlet.

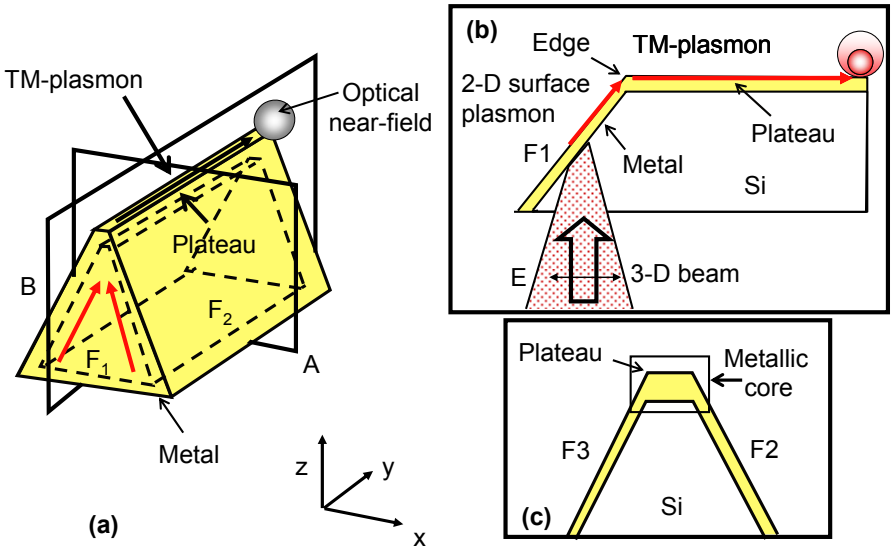


**Fig. 1** (a) Bird's-eye view of a plasmon waveguide. The x- and y-axes are perpendicular and parallel to the plateau axis, respectively. (b) Cross-section along plane B (yz) in (b). (c) Cross-section along plane A (xz) in (b)

The advantages of our waveguide are:

(a) High conversion efficiency from the 2D surface plasmon mode to the 1D TM plasmon mode, due to the scattering coupling [3].

(b) The beam width decreases (as narrow as 1 nm) with the core diameter, since this waveguide does not have a cut-off [11].

(c) The propagation length of the TM-plasmon mode is sufficiently long to meet requirement (C). For example, the propagation length is 1.25 μm (at $\lambda$ = 830 nm) for a TM plasmon with a gold core (diameter D = 40nm) insulated by air [14].

The plasmon waveguide was fabricated using anisotropic etching. The spatial distribution of the electric-field energy throughout the plateau of the metallized Si wedge was measured by scanning with a fiber probe with an aperture diameter of $D_a$ = 60 nm. In order to excite the plasmon mode, linearly polarized light (λ = 830 nm) was focused onto the $F_1$ face. Figures 2(a) and (b) show the observed electric-field energy distributions on wedges with plateau widths W = 1 μm and 150 nm, respectively, for TM polarization (the incident light polarization is parallel to the y-axis). We found that the propagating mode was excited efficiently only by TM polarized incident light. The closed and open circles in Fig. 2(c) and (d) show the cross-sectional profiles along the lines in Fig. 2(a) (A-A' and a-a') and 2(b) (B-B' and b-b'), respectively. Here, transmission was defined as the ratio of the light power detected by the fiber probe to the input light power. From the dotted exponential curve fitting the open circles in Fig. 2(c), the propagation length was estimated to be 1.25 μm for the 150-nm wedge. This value is comparable to the theoretical value for TM plasmon mode in a cylindrical metal-core waveguide with D = 40 nm that consists of a gold core and air cladding (λ = 830 nm) [14]. From the solid

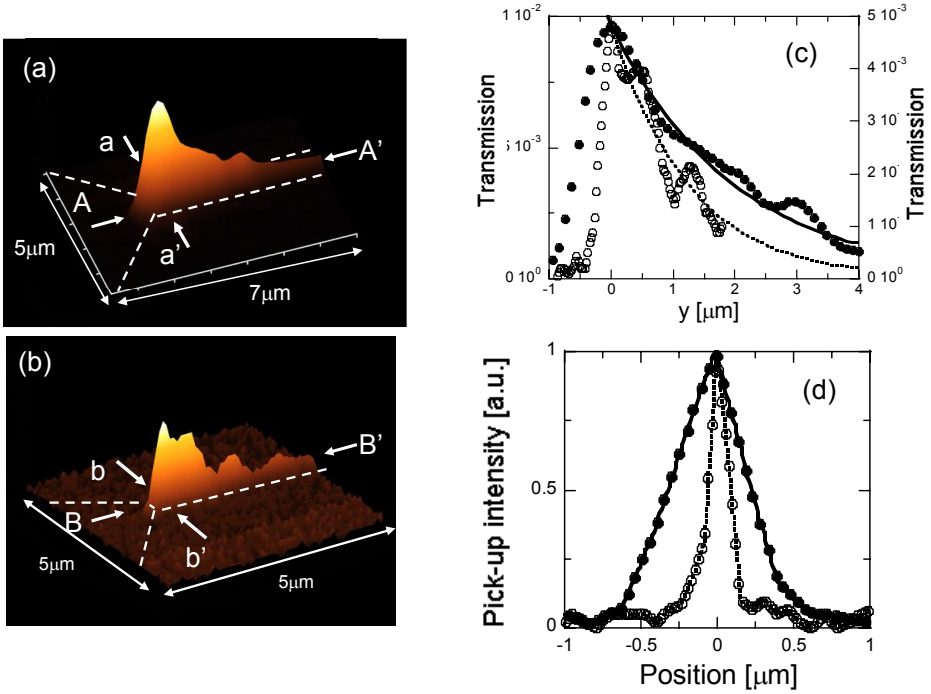


**Fig. 2** Electric-field distribution (λ = 830 nm) on the silicon wedge plateau. TM polarization: (a) W = 1 μm. (b) W = 150nm. (c) Cross-sectional profiles along A–A' (closed circles) and B–B' (open circles) in (a) and (b), respectively. (c) The solid and dotted curves represent the exponential curves fitted to the experimental values. (**d**) Cross-sectional profiles along a–a' (closed circles) and b–b' (open circles) in (**a**) and (**b**), respectively

exponential curve fitting the closed circles in Fig. 2(c), the propagation length for W = 1.0 μm was estimated to be 2.0 μm, which is longer than that for W = 150 nm. This is because, as W increases, the effective refractive index approaches that of the surface plasmon at the planar boundary between gold and air [14]. These experimental results confirm that the observed excitation along the plateau was the TM plasmon mode. Figure 2(d) shows that the full width at half maximum (FWHM) of the cross-sectional profiles was 150nm for W = 150 nm. With minor improvements to the waveguide, this FWHM value should meet requirement (B). Furthermore, note that the transmission was $5.0 \times 10^{-3}$ for W = 150 nm; this is ten times higher than that of a fiber probe with $D_a$ = 150nm [4]. This efficient excitation of the TM plasmon mode can be attributed to the scattering coupling at the edge between $F_1$ and the plateau. This transmission efficiency meets requirement (A). Finally, the propagation length estimated above is longer than the incident light wavelength. This meets requirement (C).

### 2.2 A Nanodot Coupler with a Surface Plasmon Polariton Condenser for Optical Far/Near-Field Conversion

To increase the propagation length, a more promising candidate is a nanodot coupler consisting of an array of closely spaced metallic nanoparticles, because higher transmission efficiency is expected from the plasmon resonance in the closely spaced metallic nanoparticles [5, 15, 16]. The energy transfer along the nanodot coupler relies on the near-field coupling between the plasmon-polariton mode of the neighboring nanoparticles.

To increase the efficiency of exciting localized surface plasmon in the nanodot coupler compared with that excited by propagating far-field light, we equipped the nanodot coupler with a surface plasmon polariton (SPP) condenser for efficient far/near-field conversion. Figure 3 shows the proposed optical far/near-field conversion device [5].

Incoming far-field light is first transformed into the 2D SPP mode on the metallic film. Then, the SPP mode is scattered and focused by the SPP condenser, which consists of several hemispherical metallic submicron particles that are arranged in an arc and work as a phased array [17]. The input terminal of the nanodot coupler is fixed at the focal point of the SPP. Finally, after the localized surface plasmon is transmitted through the nanodot coupler, it is converted into an optical near-field so that it couples to the nanophotonic device.

The advantages of this device are that it has

(a) A high conversion efficiency, from the SPP mode to the localized surface plasmon in the nanodot coupler, owing to the scattering coupling at the inlet metallic nanoparticle [2].

(b) No cut-off diameter for the metallic nanoparticle array, i.e., the beam width decreases with the diameter because the electric field vector, which is dominant in the nanodot coupler, involves a Förster field only[15].

(c) Farther propagation than that of the metallic-core waveguide due to the reduction in the metal content and plasmon resonance in the metallic nanoparticles. For example, the calculation using the finite-difference time domain (FDTD) method estimated a propagation length of $l_t$ = 2 μm (at an optical wavelength λ = 785 nm) for a plasmon-polariton mode with linearly aligned 50-nm dots with 10-nm separation [18].

Advantages (a)-(c) are compatible with meeting requirements (A)–(C), respectively.

To fabricate the nanodot coupler and SPP condenser using a focused ion beam (FIB), we used a silicon-on-insulator (SOI) wafer to avoid ion beam drift. The SPP condenser and nanodot coupler were fabricated using the FIB. A diffraction grating was also fabricated using an FIB milling technique 50 μm below the condenser in order to excite the SPP by the incident optical far-field (a laser beam).

The spatial distribution of the optical near-field energy was observed using a collection mode near-field optical microscope. A light source with a wavelength of λ = 785 nm was used to transmit the far-field light through the 10-μm-thick Si substrate. A sharpened fiber probe with 20-nm-thick gold film was used to enhance the collection efficiency [7].

First, we measured the spatial distribution of the optical near-field energy on a linear nanodot coupler, for which the input terminal was fixed at the focal point of the SPP. Figures 3(a) and (b) show a scanning electron microscope (SEM) image and the spatial distribution of the optical near-field energy on the nanodot coupler, respectively. The black dots in Fig. 3(c) show the cross-sectional profile along the white broken line in Fig. 3(b). Position x = 0 corresponds to the focal point of the SPP condenser. Although not all of the energy couples to the nanodot coupler owing to mode mismatch, the optical near-field intensity has a maximum at each edge of the nanoparticles. This is due to artifact resulting from using the fiber probe in constant height mode. The dips indicated by arrows A and B originate from interference of the localized surface plasmon in the nanodot coupler that arises from reflection at the output terminal. However, the exponential envelope (solid curve of Fig. 3(c)) fitted by neglecting this inference indicates that the propagation length was $l_t$ = 4.0 μm. $l_t$ was five times longer than the wavelength, which meets requirement (C). The beam width was 250 nm, which is comparable to the nanoparticle size. As the size of the nanoparticles is determined by the resolution of the FIB for carbon hemisphere deposition, the beam width can be decreased to a sub-50 nm scale using electron beam lithography, which will meet requirement (B).

Second, we checked whether near-field coupling between the neighboring nanoparticles resulted in lower propagation loss by comparing our device with a metallic-core waveguide. For this purpose, we fabricated a gold-core waveguide the same width as the diameter of the nanoparticles in the nanodot coupler, with its input terminal also fixed

at the focal point of the SPP (Fig. 3(d) and 3(e)). The dashed line in Fig. 3(f) shows the cross-sectional profile of the metallic-core waveguide along the dashed line in 3(e) and the exponential envelope (solid curve in Fig. 3(f)) indicates that the propagation length is $l_t$ = 1.2 μm. To evaluate the observed propagation length, we calculated the theoretical value of our metallic-core waveguide. Since the Au-core waveguide is placed on an Si substrate, we calculated the 1D TM plasmon mode [11] in a cylindrical Au-core waveguide with a diameter of 250 nm ($\varepsilon_{Au} = (0.174 + i4.86)^2 = -23.59 + i1.69$) [19] surrounded by medium with a dielectric constant equal to the average of Si and air [14], $\varepsilon_{cl} = ((3.705+i0.007)^2+1)/2 = 7.36+i0.03$ [19]. Based on these assumptions, the calculated propagation length of our Au-core waveguide is 1.4 μm. Since this is in good agreement with the observed value (1.2 μm), the comparison confirms that nanodot coupler realizes more efficient energy transfer.

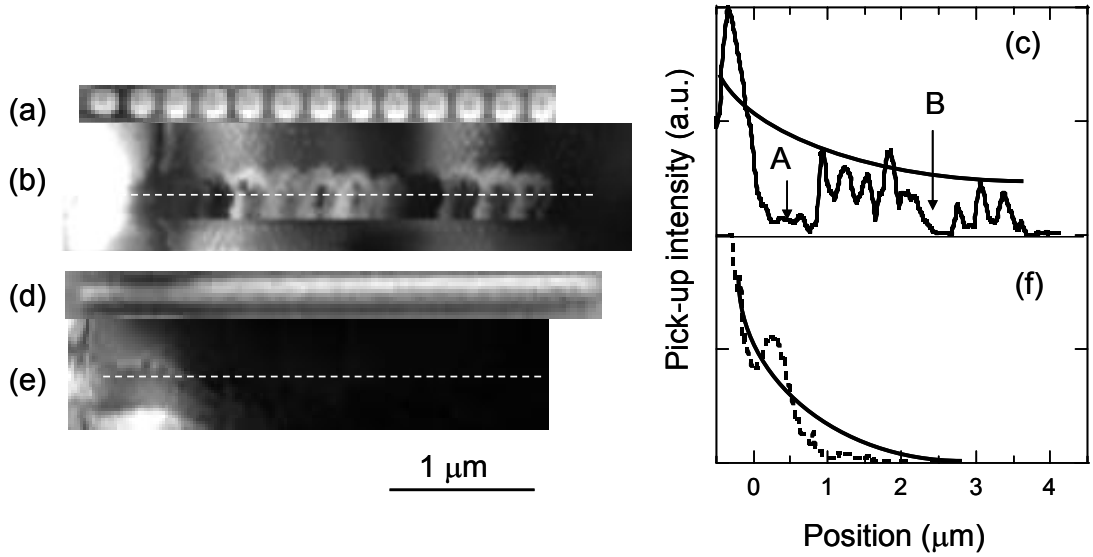


**Fig. 3** SEM image (a) and the near-field energy distribution (b) of a linearly chained nanodot coupler. (c) Solid circles show the cross-sectional profiles along the white dashed line in (b). The solid curve shows the fitted exponential envelope. A and B indicate dips resulting from the length of the nanodot coupler. (c) The solid line shows the cross-sectional profile along the white dashed line in (b). SEM image (d) and the near-field energy distribution (e) of a metallic-core waveguide. (f) The dashed line shows the cross-sectional profile along the metallic-core waveguide and the solid curve shows the fitted exponential envelope.

Finally, we also observed the spatial distribution of the optical near-field energy for zigzag-shaped nanodot coupler (see Fig. 4(a) and (b)). Corners A–D in Fig. 4(c) represent the profiles at locations A–D in Fig. 4 (d), respectively. Comparing adjacent curves, we found that the energy loss at corners A–D was negligible. This is attributed to efficient coupling of the TM and TE localized surface plasmon at the corners. As a result, the propagation length through this zigzag-shaped nanodot coupler was equivalent to that through a linear coupler. Although efficient coupling has been predicted using the point-dipole approximation [15], this is the first experimental confirmation of it. Such high flexibility in the arrangement of nanoparticles is an outstanding advantage for conversion for driving nanophotonic devices.

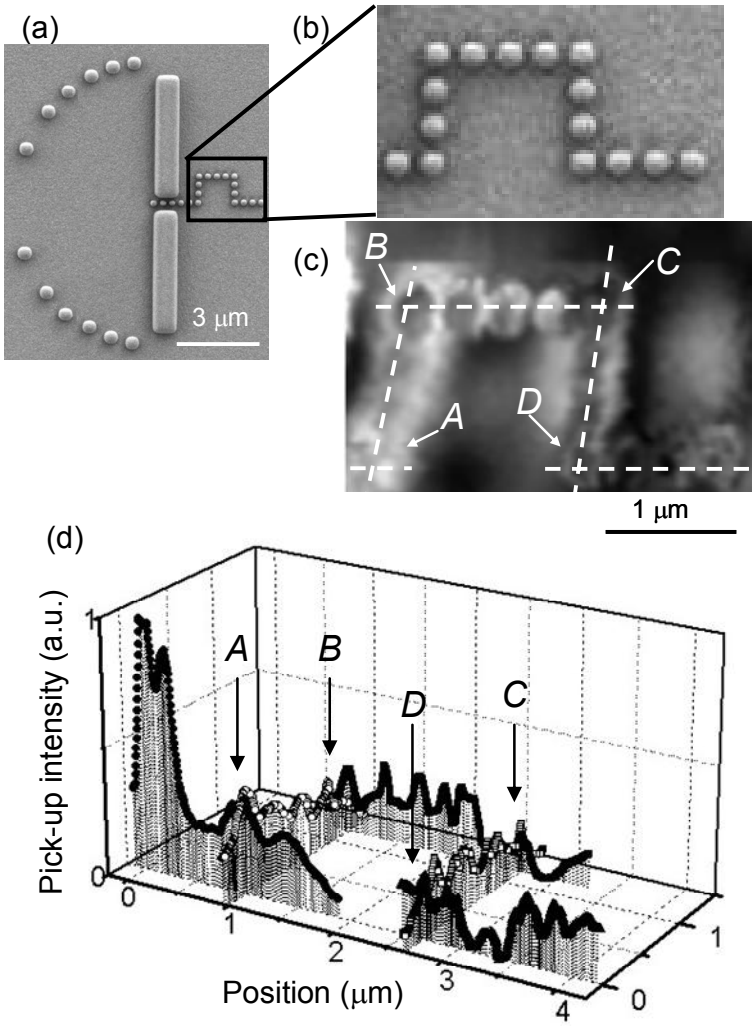


**Fig. 4** (a) and (b) SEM images and the near-field intensity distribution (c) of a zigzag-shaped nanodot coupler. (d) The cross-sectional profiles along the dashed white lines in (c). The arrows A–D indicate the corners

## 3. NANOPHOTONIC FABRICATION FOR NANOPHOTONIC DEVICES

To fabricate nanodot couplers and nanophotonic devices at all scales, we proposed a self-assembling method that builds nanodot chains by controlling the desorption with an optical near-field [8, 9]. Our approach is illustrated schematically in Fig. 5(a). A nanodot chain of metallic nanoparticles is fabricated using radio frequency (RF) sputtering under illumination on glass substrate. To realize self-assembly, a simple groove 100-nm wide and 30-nm deep is fabricated on the glass substrate. During deposition of the metal, linear polarized light illuminating the groove directly from above ($E_{90}$) is used to excite a strong optical near-field at the edge of the groove (see Fig. 5(b)), which induces the desorption of the deposited metallic nanoparticles [8]. A metallic dot has strong optical absorption due to plasmon resonance, which strongly depends on particle size. This can induce desorption of a deposited metallic nanodot when it reaches the resonant diameter [8]. As the deposition of metallic dots proceeds, growth is governed by a trade-off between deposition

and desorption, which determines dot size, depending on the photon energy of the incident light. Consequently, the metallic nanoparticles should align along the groove (Figs. 5(b) and 5(c)).

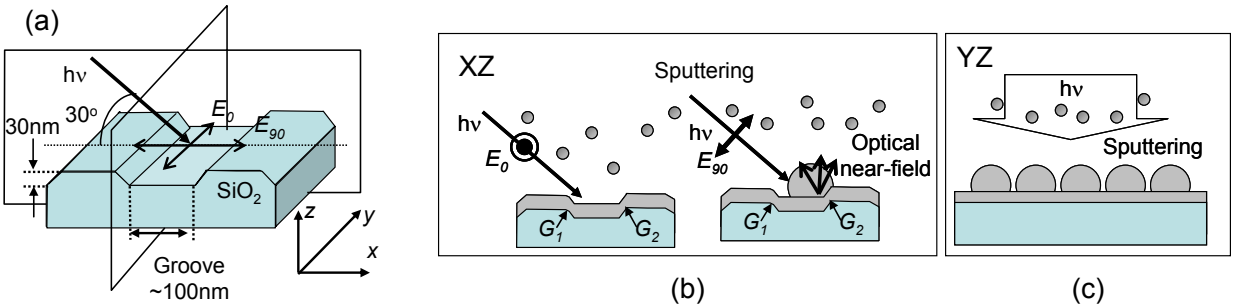


**Fig. 5** (a) Size- and position-controlled ultra-long nanodot chain formation. The slanted light had a spot diameter of 1 mm. The groove parallels the y-axis. $E_{90}$ and $E_0$ are perpendicular and parallel to the y-axis, respectively. (b and c) Cross-sections in planes xz and yz, respectively.

Illumination with 2.33-eV light (50 mW) during the deposition of aluminum resulted in the formation of 99.6-nm-diameter aluminum nanodot chains with 27.9-nm separation that were as long as 100 μm in a highly size- and position-controlled manner (Fig. 6(a)). The deviation of both nanodot size and the separation, determined from SEM images, was as little as 5 nm. The deviation, which was as small 5%, meets the requirement for a nanodot coupler with an efficiency equivalent to 50% of that of an ordered array. To identify the position of the chain, we compared topographic atomic force microscopy (AFM) images of the surface of the glass substrate before and after aluminum deposition, at the same position. Curves α and β in Fig. 6(b) show the respective cross-sectional profiles across the groove. Comparison of these profiles shows that the nanodot chain formed around edge $G_2$. Furthermore, illumination with parallel polarization $E_0$ along the groove resulted in film growth along the groove structure and no dot structure was obtained. Since the near-field intensity with $E_{90}$ was strongly enhanced at the metallic edge of the groove in comparison with $E_0$ owing to edge enhancement of the electrical field (see Fig. 5(b)), a strong near-field intensity results in nanodot chain formation. Dot formation at the one-sided edge originates from the asymmetric electric-field intensity distribution, owing to the slanted illumination.

Aluminum-dot chain formation was also observed with RF sputtering of aluminum under illumination with 2.62-eV light (100 mW) with $E_{90}$ using the same grooved (100-nm wide and 30-nm deep) glass substrate, which resulted in the formation of 84.2-nm nanodots with 48.6-nm separation (Fig. 6(c)). Although the deviation of both nanodot size and the separation was as large as 10 nm, the dot size was reduced in proportion to the increase in the photon energy (99.6 nm × (2.33/2.62) = 88.5 nm ~ 84.2 nm). This result indicates that the obtained size is determined by the photon energy and that the size-controlled dot-chain formation originates from photo-desorption of the deposited metallic nanoparticles [8]. The period under 2.62-eV light illumination (132.8 nm) was longer than that (127.5 nm) for fabrication

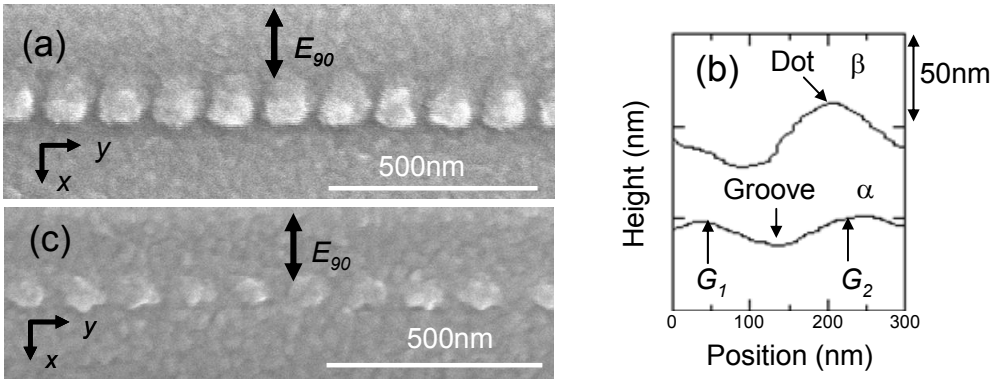


**Fig. 6** (a) SEM image of deposited aluminum with perpendicular polarization $E_{90}$ ($h\lambda$ =2.33 eV). (b) Curves α and β show the respective cross-sectional profiles of AFM images across the groove before and after aluminum deposition, at the same position. (c) SEM image of deposited aluminum with perpendicular polarization $E_{90}$ ($h\lambda$ =2.62 eV).

using the 2.33-eV light. However, the ratios of the center-center distance (d) and radius (a) of the nanodots (d/a = 2.56 and 3.15 obtained under 2.33-eV and 2.62-eV light illumination, respectively) are similar to the optimum value, which is in the range of 2.4-3.0, for the efficient transmission of optical energy along a chain of spherical metal dots calculated using Mie's theory [16]. This is determined by the trade-off between the increase in the transmission loss in the metal and the reduction in the coupling loss between adjacent metallic nanoparticles as the separation increases. Future theoretical analysis, which will include the effect of a continuous metallic film below the nanodot chain, is required to decide the optimum separation of nanoparticles depending on the photon energy. However, our preliminary results imply that the center-center distance was set at the optimum distance for efficient energy transfer of the optical near-field, given that such a strong optical near-field can induce desorption of the deposited metallic nanoparticles and result in position-controlled dot-chain formation.

## 4. SUMMARY

To connect a nanophotonic IC with external photonic devices, we developed a nanometer-scale waveguide using a metal-coated silicon wedge structure. Propagation of the TM plasmon mode was observed using a near-field optical microscope. Illumination ($\lambda$ = 830 nm) of the metal-coated silicon wedge (W = 150 nm) caused a TM plasmon mode with a beam width of 150nm and propagation length of 1.25 μm. The performance was improved further with a nanodot coupler with an SPP condenser. The FWHM of the spatial distribution of the optical near-field energy at the focal point of the SPP was as small as 400nm at $\lambda$ = 785 nm. Furthermore, installing a linear nanodot coupler at the focal point of the SPP realized efficient excitation of plasmon-polariton mode with a transmission length of 4.0 μm. Equivalent energy transfer was observed in zigzag-shaped nanodot couplers. These results confirm that a nanodot coupler with an SPP condenser can be used as the optical far/near-field conversion device required by future systems.

Furthermore, our deposition method is based on a photo-desorption reaction, illumination at multiple photon energies using a simple lithographically patterned substrate could realize the simultaneous fabrication of size- and position-controlled nanoscale structures with different particle sizes, using other metals or semiconductors. The use of this self-assembling method with a simple lithographically patterned substrate will dramatically increase the throughput of the production of the nanoscale structures that will be required by future systems.

## REFERENCES


[1] M. Ohtsu, K. Kobayashi, T. Kawazoe, S. Sangu, and T. Yatsui, "Nanophotonics: Design, Fabrication, and Operation of Nanometric Devices Using Optical Near Fields," IEEE J. Select. Top. Quant. Elect., vol. 8, no. 4, pp.839-862, 2002

[2] T. Yatsui, M. Kourogi, and M. Ohtsu, "Plasmon waveguide for optical far/near-field conversion," Appl. Phys. Lett., vol. 27, no. 27, pp. 4583-4585, 2001

[3] T. Yatsui, M. Kourogi, and M. Ohtsu, "Highly efficient excitation of optical near-field on an apertured fiber probe with an asymmetric structure," Appl. Phys. Lett., vol. 71, no. 13, pp. 1756-1758, 1997

[4] T. Yatsui, M. Kourogi, and M. Ohtsu, "Increasing throughput of a near-field optical fiber probe over 1000 times by the use of a triple-tapered structure," Appl. Phys. Lett., vol. 73, no. 15, pp. 2090-2092, 1998

[5] W. Nomura, M. Ohtsu, and T. Yatsui, "A nanodot coupler with a surface plasmon polariton condenser for optical far/near-field conversion," Appl. Phys. Lett., vol. 86, no. 18, 181108, 2005

[6] W. Nomura, T. Yatsui, and M. Ohtsu, "Efficient optical near-field energy transfer along an Au nanodot coupler with size-dependent resonance," Appl. Phys. B, in press

[7] T. Yatsui, K. Itsumi, M. Kourogi, and M. Ohtsu, "Metallized pyramidal silicon probe with extremely high throughput and resolution capability for optical near-field technology," Appl. Phys. Lett., vol. 80, no.13, pp. 2257-2259, 2002

[8] T. Yatsui, S. Takubo, J. Lim, W. Nomura, M. Kourogi, and M. Ohtsu, "Regulating the size and position of deposited Zn nanoparticles by optical near-field desorption using size-dependent resonance," Appl. Phys. Lett., vol. 83, no. 9, pp.1716-1718, 2003

[9] T. Yatsui, W. Nomura, and M. Ohtsu, "Self-Assembly of Size- and Position-Controlled Ultralong Nanodot Chains using Near-Field Optical Desorption," Nano Lett., vol. 5, no. 12, pp. 2548-2551, 2005

[10] For example, see the International Technology Roadmap for Semiconductors (http://public.itrs.net/)
[11] J. Takahara, S. Yamagishi, H. Taki, A. Morimoto, and T. Kobayashi, "Guiding of a one-dimensional optical beam with nanometer diameter," Opt. Lett., vol. 22, no. 7, pp. 475-477, 1997
[12] J. C. Weeber, J. R. Krenn, A. Dereux, B. Lamprecht, Y. Lacroute, and J. P. Goudonnet, "Near-field observation of surface plasmon polariton propagation on thin metal stripes," Phys. Rev. B, vol. 64, no. 4, 045411, 2001
[13] A. Eguiluz and A. A. Maradudin, "Electrostatic edge modes along a parabolic wedge," Phys. Rev. B, vol. 14, no. 12, pp. 5526-5528. 1976
[14] L. Novotny and C. Hafner, "Light propagation in a cylindrical waveguide with a complex, metallic, dielectric function," Phys. Rev. E, vol. 50, no. 5, pp. 4094-4106, 1994
[15] M. L. Brongersma, J. W. Hartmanm, and H. A. Atwater, "Electromagnetic energy transfer and switching in nanoparticle chain arrays below the diffraction limit," Phys. Rev. B, vol. 62, no. 24, R16356, 2000
[16] I. I. Smolyaninov, D. L. Mazzoni, J. Mait, and C. C. Davis, "Experimental study of surface-plasmon scattering by individual surface defects," Phys. Rev. B, vol. 56, no. 3, pp. 1601-1611, 1997
[17] M. Quinten, A. Leitner, J. R. Krenn, and F. R. Aussenegg, "Electromagnetic energy transport via linear chains of silver nanoparticles," Opt. Lett., vol. 23, no. 17, pp. 1331-1333, 1998
[18] The computer simulations in this paper are performed by a FDTD-based program, Poynting for Optics, a product of Fujitsu, Japan
[19] *Handbook of Optical Constants of Solids*, ed. by E.D. Palik. (Academic, New York 1985)

# [III] REVIEW PAPERS

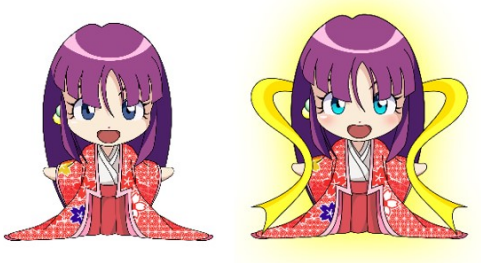

# 近接場相互作用により駆動するナノフォトニックデバイスの進展

八井　崇*・三宮　俊**・大津　元一*,***

近年，光デバイスの微細化の要求は日に日に強くなっており，その寸法は光の回折限界以下になろうとしている．回折限界以下の領域では，従来デバイスを単に微細化するだけでは動作させることは不可能となる．さらには，電子デバイスに関しても同様に微細化が不可欠となっているが，配線などでの熱の発生が問題となり，さらなる微細化が限界に達しようとしている．以上の問題を解決するために，近年半導体微結晶によって構成され近接場光で動作するナノフォトニックデバイスが提唱され，その基本動作検証が報告されている．本稿では，このデバイスの室温動作実現を目指して取り組んでいる酸化亜鉛(ZnO)量子構造を用いた成果について紹介する．

**Keywords : optical near-field, nanophotonic device, ZnO, nanorod**

## 1. まえがき

情報通信の高速化・大容量化により，演算素子の微細化が急務となっている．現在の演算素子を支えるシリコン電子デバイスにおいても，配線などにおける熱の発生が大きな問題となり，微細化の限界がみえ始めている．このような状況において，MIT Microphotonics Center により取りまとめられた2005年版Communications Technology Roadmapに予想されるように，回路の微小化だけでなく既存の電子デバイスから光デバイスの移行が，PC内部のチップ間配線などにおいても必要となってきている．このような光デバイスに求められる寸法は10年以内には100 nm以下になると予測されており，現状の光デバイスを単純に微細化するだけでは，光の回折限界の壁を乗り越えられない．つまり，単に小寸法化という「量的変革」ではなく，伝搬光を用いたのでは実現しないデバイス機能の開発という「質的変革」が求められている[1]．

この問題を解決する有効な手段として，近年，量子ドットによって構成され近接場光によって動作するナノフォトニックスイッチ（波長変換素子）が提案されている[2]．この基本原理を，**図1**を用いて説明する．基本動作は寸法の制御された大小二つの量子構造によって達成される．ここでは，小さい量子箱（$QD_A$）の励起子基底準位（$E_{A1}$）と大きい量子箱（$QD_B$）の励起子第一励起準位（$E_{B2}$）のエネルギーが一致するような寸法比（立方体の場合$1:\sqrt{2}$）となっている．この場合$E_{B2}$の波動関数は奇関数となり，伝搬光では励起することができない光学禁制な準位となる．この系に対して，(**a**)バリア層を励起した場合，$QD_A$と$QD_B$の間隔が十分大きい場合には，それぞれの基底準位からの発光が観測されるが，この間隔が$QD_A$の寸法と同程度になると，エネルギー的に共鳴する$E_{B2}$を通して$E_{B1}$への緩和が発生し，その結果$E_{B1}$からの発光しか観測されないことになる

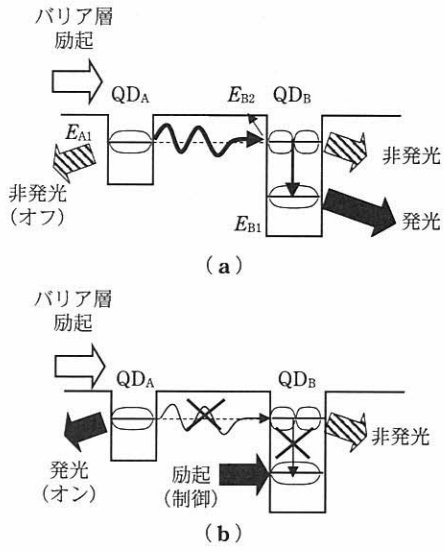


**図1**　ナノフォトニックスイッチの概念図．(**a**)オフ状態，(**b**)オン状態．

* 科学技術振興機構 SORST　〒194-0004　町田市鶴間687-1．e-mail : yatsui@ohtsu.jst.go.jp
** (株)リコー 研究開発本部 先端技術研究所 フォトニクス研究室　〒224-0035　横浜市都筑区新栄町16-1．
*** 東京大学大学院 工学系研究科電子工学専攻　〒113-8656　東京都文京区弥生2-11-16．

分類番号　3.7，6.7

*Progress in nanophotonic devices driven by optical near-field.*

Takashi YATSUI, Suguru SANGU and Motoichi OHTSU.
* SORST, Japan Science and Technology Agency (687-1 Tsuruma, Machida　194-0004)
** Advanced Technology R&D Center, Ricoh Company, Ltd. (16-1 Shinei-cho, Tsuduki-ku, Yokohama　224-0035)
*** Department of Electronics Engineering, University of Tokyo (2-11-16 Yayoi, Bunkyo-ku, Tokyo　113-8656)

($E_{A1}$での発光を観測していると非発光であるために“オフ”状態となる)．次に，(**b**)バリア層を励起しつつ$E_{B1}$に共鳴する光を入射すると，$E_{B1}$が占有されることで，$E_{B2}$から$E_{B1}$へのサブレベル緩和が抑制されるため，$E_{A1}$からの発光が観測される(“オン”状態)．ここで，従来光学禁制である$E_{B2}$は，隣の量子箱における局所的な電場勾配により初めて励起されるものである．つまり，このデバイスは，数nmの量子箱によって構成されているため，非常に寸法が小さいという利点だけでなく，近接場光によってのみ動作するという特長を有する．さらには，このデバイスによって消費されるエネルギーはサブレベル間のエネルギー差($E_{B2}-E_{B1}$)のみであるために，超低消費電力であるという利点がある．以上の基本原理は，3端子に拡張され，CuCl量子箱によりスイッチング動作が実験的に確認されている[3]．

ナノフォトニックデバイスを室温で安定に動作させるために，加工の容易なInAs系量子ドットなどの開発も行われているが[4]，本稿では近年，著者らが研究を進めているZnOを用いた取り組みについて紹介する．

## 2. ZnOナノロッド量子井戸構造

電子デバイスとしても良質な特性を示すZnO[5]の光デバイスとしての特長は，①励起子結合エネルギーが大きい[6](60 meV．量子構造にした場合には，110 meVまで大きくなることが報告されている)，②振動子強度が大きい[7]，ことから室温において強い励起子発光強度が得られることである．

本稿で紹介するZnOの量子構造は，Metalorganic Vapor Phase Epitaxy (MOVPE) 法により作製されたZnOナノロッド先端に作製されている[8,9]．従来，ZnOに限らずさまざまなナノロッドの作製は金属触媒を核としてVapor-Liquid-Solid (VLS) 法により行われていたが[10]，本手法では金属触媒を用いていないために，ナノロッド先端における金属不純物の混入の心配がなく良質な発光特性が得られている[8]．さらには，量子構造を作製するための障壁層の作製にも適しており，ナノロッドの同径方向にも欠陥がまったくみられない良質な量子井戸構造の作製が可能となっている(**図2**)．これにより，ナノロッド先端の単一量子井戸構造とした場合でも，井戸幅に依存して強い励起子発光が観測されている[11,12]．この手法では，量子井戸の幅および間隔を原子層レベルで自在に制御することができるため任意のナノフォトニックデバイス作製が可能となる．

## 3. 近接場エネルギー移動の観測

ZnOナノロッド量子構造における近接場相互作用を観測するために，ナノロッド先端に作製された，①単一量子井戸(SQWs：井戸幅2 nm)，②2重量子井戸(1-DQWs：井戸幅3.5 nm)，③3対のDQWs (3-DQWs：井戸幅2 nm，井戸間隔$D$=3, 6, 10 nmでそれぞれが30 nm分離されている)について近接場分光測定を行った．**図3**(**a**)で示

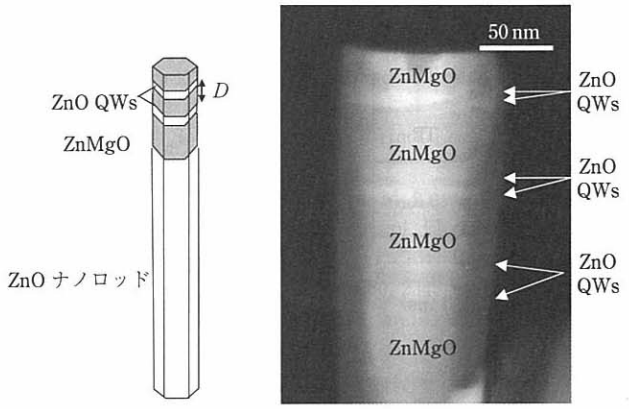


**図2** ZnOナノロッド量子構造の(**a**)概念図，および(**b**)透過型電子顕微鏡像．

すスペクトルは点線・実線がそれぞれ遠方場分光・近接場分光により測定されたものである(測定温度15 K，励起光：He-Cdレーザー($\lambda$=325 nm))．いずれの場合にも369 nm付近におけるロッドの束縛励起子からの発光と，量子井戸からの発光と思われる発光がピークとして現れているのがわかる($I_S$, $I_{1D}$, $I_{3D}$)．また，図3(**b**)は障壁層を$Zn_{0.8}Mg_{0.2}O$として計算された励起子基底準位および励起子第一励起準位の井戸幅依存性を計算した結果である(計算では，電子およびホールの質量を$0.28m_0$・$1.8m_0$，伝導帯・荷電子帯のオフセット比($\Delta E_c/\Delta E_v$)を9，バンドギャップオフセット($\Delta E_g$)を250 meVとして求めた)．このグラフに図3(a)から得られたピーク値をプロットするとよい一致を示すことから，ピーク$I_S$, $I_{1D}$, $I_{3D}$が量子井戸層からの発光であるということがわかる．

次にこのような試料に対して，発光の時間応答を調べるため，近接場時間分解分光測定を行った．測定温度は15 Kに設定し，開口径50 nmの紫外用プローブにより，コレクションモードで観測を行った．DQWsのバリア層を励起す

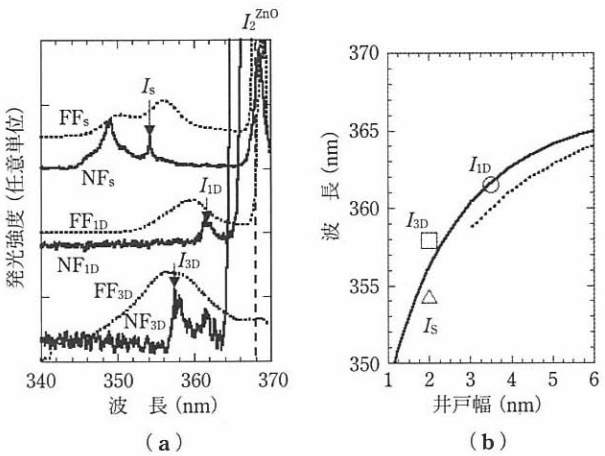


**図3** (**a**)近接場分光(実線)および遠方場分光スペクトル(点線)．$FF_S$・$NF_S$：SQWs，$FF_{1D}$・$NF_{1D}$：1-DQWs，$FF_{3D}$・$NF_{3D}$：3-DQWs．(**b**)励起子基底準位および励起子第一励起準位の井戸幅依存性．

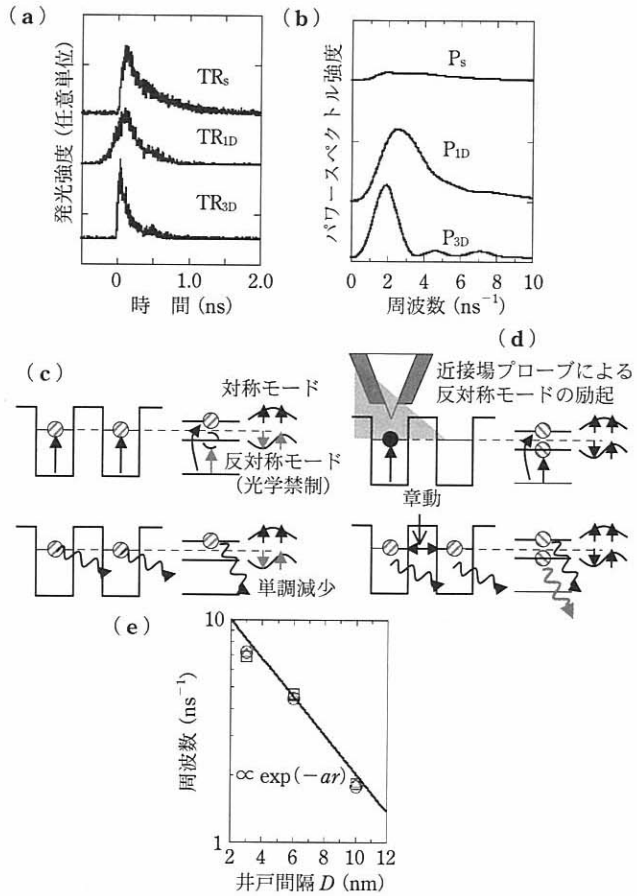


図4　（a）時間発展スペクトル．$TR_S$：SQWs からの発光，$TR_{1D}$：1 DQWs からの発光，$TR_{3D}$：3 DQWs からの発光．（b）$P_S$：$TR_S$，$P_{1D}$：$TR_{1D}$，$P_{3D}$：$TR_{3D}$ のパワースペクトル．（c）結合した DQWs に対する伝搬光励起．（d）結合した DQWs に対する近接場光励起．（e）DQWs の井戸間隔（$D$）依存性．

るために，Ti : Sapphire レーザーの三次高調波（波長 308 nm・パルス幅 2 ps）を用い，井戸層からの発光成分のみを切り出すためにバンドパスフィルターを通して時間応答の観測を行った．その発光の時間波形を**図 4**（**a**）に示す．ここでこれらの時間応答の結果に対して詳細を調べるために，指数関数的な減衰に重畳した揺らぎ成分のフーリエ解析を行った．このパワースペクトを図 4（**b**）に示す．この結果，SQWs の信号（$P_S$）からは周波数のピークがみられなかったのに対して，1-DQWs（$P_{1D}$）では 2.5 $ns^{-1}$ 付近でピークがみられ，3-DQWs（$P_{3D}$）では，2，4.5，7 $ns^{-1}$ 付近の三つのピークが現れるということがわかった．これらの周波数成分は，DQWs でのポピュレーションの章動を観測したものと考えられる．

ここで観測された，章動は近接場測定で特徴的な結果であると考えられる．結合した DQWs では，対称なモードと反対称なモードにエネルギー分離されるが，これが通常の伝搬光励起では光学禁制な反対称モードを励起することができず，ポピュレーションは単調に減少する（図 4（**c**））．これに対して近接場プローブを近接させて観測している本測定では，このプローブによって局所的な電場が生じるこ

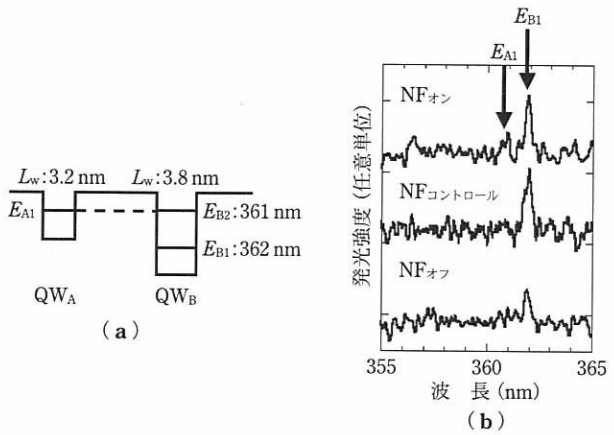


図5　（a）寸法の異なる DQWs の概念図．（b）近接場分光スペクトル．$NF_{オフ}$：入力光のみ入射，$NF_{コントロール}$：制御光のみ入射，$NF_{オン}$：入力光および制御光入射．

とで，DQWs のポピュレーションに偏りが生じ，すなわち，反対称モードも同時に励起されると考えられる．これにより，この対称と反対称のモードの重ね合わせの結果，ポピュレーションが DQWs 間を移動する章動が観測されたのだと考えられる[13]（図 4（**d**））．

さらに，この章動の周期を井戸間隔（$D$）の関数としてプロットした結果を図 4（**e**）に示す．ここでは対称・反対称モードのエネルギー差は井戸間隔 $D$ の減少に伴い大きくなると予測されるので，2, 4.5, 7 $ns^{-1}$ のピークをそれぞれ，井戸間隔 $D$=10，6，3 nm の DQWs からの信号としてプロットした．この結果に示されるように，そのカップリングは井戸間隔が狭くなるにつれ指数関数的に強くなっており，近接場光の急峻な電場勾配をよく表しているといえる．

## 4.　近接場エネルギー移動の制御

以上の結果から，DQWs 間での共鳴する励起準位間において，エネルギー移動の観測が確認されたといえる．さらに，これをスイッチング動作に応用させるためには，エネルギーの移動を一方向に確定する必要がある．この確認のために，DQWs の幅を調整し，拡い井戸幅を有する量子井戸（$QW_B$）の励起子第一励起準位（$E_{B2}$）と狭い井戸幅を有する量子井戸（$QW_A$）の励起子基底準位（$E_{A1}$）が共鳴する寸法で DQWs を作製した（**図 5**（**a**））．これにより，$QW_A$ にポピュレーションを生成させた場合でも，共鳴するエネルギー準位を介してポピュレーションが移動し，この際に失うサブバンド間エネルギーにより，励起が逆流することなく $QW_B$ の基底準位（$E_{B1}$）からの発光のみ観測されることになると期待される．この際，$QW_B$ の第一励起準位は光学禁制であるために，基底準位からの発光しか観測されないと考えられる．

この予測を確認する実験として，まず両者の井戸を励起するために，入力光として He-Cd レーザー（$\lambda$=325 nm）による励起を行った．この状態で得られた近接場光スペクトル（図 5（**b**）の曲線 $NF_{オフ}$）から，362 nm 付近に発光の

ピークを有するスペクトル（$E_{B1}$）が観測された．$QW_A$ と $QW_B$ の井戸が孤立して存在した場合には，それぞれの基底準位に対応する波長 361 nm および 362 nm での発光ピークが観測されるが，この場合には，$QW_B$ の基底準位に相当するピークからの発光しか観測することができなかった．これは，先に予測したように，共鳴する励起子準位間でのエネルギー移動を示す結果であるといえる（図1(a)の“オフ”状態に対応）．次に，このエネルギーの流れを止めるために，制御光として $E_{B1}$ を共鳴励起(図5(b)の曲線 $NF_{コントロール}$．制御光は Ti: Sapphire レーザーの二次高調波：波長 362 nm・パルス幅 2 ps）させた状況下において，He-Cd レーザー光を照射したスペクトルを図5(b)の曲線 $NF_{オン}$ に示す．この結果，He-Cd レーザー単独励起では観測されなかった $E_{A1}$（$\lambda$=361 nm）に相当する発光ピーク（出力光）が観測された（図1(a)の“オン”状態に対応）．以上の結果は，前述した近接場エネルギー移動制御によるナノフォトニックスイッチの基本的動作原理を実証するものである．

## 5. むすび

本稿では，ZnO 量子構造を用いたナノフォトニックデバイスへの応用について解説した．本稿で述べたデバイスの特長は，半導体量子構造による「量的」に変革された微小なデバイスということだけではなく，伝搬光を用いたのでは駆動することのできない機能をもつ「質的」に変革されたデバイスということである[1]．今回は2端子による単純な構造でのエネルギー移動の観測および制御を行ったが，本構造は，結晶性・寸法の制御性にも非常に優れており，ナノフォトニックスイッチに限らず，さらに複雑で高機能なナノフォトニック機能デバイス（集光器[14]やパルス発生器[15]など）の実現に理想的な系であると考えられる．

**謝　辞**

本稿をまとめるにあたり，有益な議論をいただいた川添忠氏（科学技術振興機構 SORST），試料を提供いただいた李奎哲教授（韓国 浦項工科大学）に感謝します．

## 文　献

1) 大津元一，小林潔：ナノフォトニクスの基礎(オーム社，2006)．
2) M. Ohtsu, K. Kobayashi, T. Kawazoe, S. Sangu and T. Yatsui: IEEE J. Sel. Top. Quant. Electr. **8**, 839 (2002).
3) T. Kawazoe, K. Kobayashi, S. Sangu and M. Ohtsu: Appl. Phys. Lett. **82**, 2957 (2003).
4) T. Kawazoe, K. Kobayashi, K. Akahane, M. Naruse, N. Yamamoto and M. Ohtsu: Applied Physics B: Lasers and Optics **84**, 243 (2006).
5) W. I. Park, J. S. Kim, G.-C. Yi and H.-J. Lee: Adv. Mater. **17**, 1393 (2005).
6) H. D. Sun, T. Makino, Y. Segawa, M. Kawasaki, A. Ohtomo, K. Tamura and H. Koinuma: J. Appl. Phys. **91**, 1993 (2002).
7) D. C. Reynolds, D. C. Look, B. Jogai, C. W. Litton, G. Cantwell and W. C. Harsch: Phys. Rev. **B 60**, 2340 (1999).
8) W. I. Park, D. H. Kim, S.-W. Jung and G.-C. Yi: Appl. Phys. Lett. **80**, 4232 (2002).
9) W. I. Park, G.-C. Yi, M. Y. Kim and S. J. Pennycook: Adv. Mater. **15**, 526 (2003).
10) M. H. Huang, S. Mao, H. Feick, H. Yan, Y. Wu, H. Kind, E. Weber, R. Russo and P. Yang: Science **292**, 1897 (2001).
11) W. I. Park, S. J. An, J. Long, G.-C. Yi, S. Hong, T. Joo and M. Y. Kim: J. Phys. Chem. **B 108**, 15457 (2004).
12) T. Yatsui, M. Ohtsu, S. J. An, J. Yoo and G.-C. Yi: Appl. Phys. Lett. **87**, 033101 (2005).
13) S. Sangu, K. Kobayashi, A. Shojiguchi and M. Ohtsu: Phys. Rev. **B 69**, 115334 (2004).
14) T. Kawazoe, K. Kobayashi and M. Ohtsu: Appl. Phys. Lett. **86**, 103102 (2005).
15) A. Shojiguchi, K. Kobayashi, S. Sangu, K. Kitahara and M. Ohtsu: J. Phys. Soc. Jpn. **72**, 2984 (2003).

(2006年9月15日　受理)

**八井　崇**（やつい　たかし）

2000年東京工業大学総合理工学研究科博士課程修了．工学博士．00年より科学技術振興事業団 ERATO 大津局在フォトンプロジェクト研究員，03年より科学技術振興機構 SORST ナノフォトニクスチーム研究員．近接場光を用いたデバイスの開発に従事．

**三宮　俊**（さんぐう　すぐる）

1999年北海道大学大学院工学研究科博士課程修了．工学博士．99年より科学技術振興事業団 ERATO 大津局在フォトンプロジェクト研究員，03年より(株)リコー研究開発本部先端技術研究所フォトニクス研究室研究員．ナノフォトニクスの産業応用に関する研究に従事．

**大津　元一**（おおつ　もといち）

1978年東京工業大学大学院理工学研究科電子物理工学専攻博士後期課程修了．工学博士．東京工業大学大学院総合理工学研究科教授を経て，04年より東京大学大学院工学系研究科電子工学専攻教授．04年紫綬褒章受章．ナノフォトニクスを世界に先駆けて93年に提唱．以後，理論・デバイス・加工・システムなどの発展に従事．

新春特集 ★化学の夢・未来

# 私のチャレンジしたい化学の未解決問題

好きな研究をまったく自由に進めてよい――．資金・設備・時間のすべてが無制限という自由な環境（もちろん成果も問われません）を得ることができたら，貴方はどんなテーマに挑戦したいですか？ここでは，各分野で活躍する研究者に，夢に描くチャレンジングな研究テーマを語っていただきました．


**大津元一**
東京大学大学院工学系研究科教授

**三木邦夫**
京都大学大学院理学研究科教授

**遠藤 斗志也**
名古屋大学大学院理学研究科教授

**今坂 藤太郎**
九州大学大学院工学研究院教授

**加藤隆史**
東京大学大学院工学系研究科教授

**真嶋哲朗**
大阪大学産業科学研究所教授

**山下正廣**
東北大学大学院理学研究科教授・CREST

**杉山 弘**
京都大学大学院理学研究科教授

**深瀬浩一**
大阪大学大学院理学研究科教授


私のチャレンジしたい 化学の未解決問題①

## 光と物質の融合した科学技術を完成させたい


大津元一（おおつ もといち）
東京大学大学院工学系研究科


### 革新技術を生みだした近接場光

私は電子工学と応用物理学の研究に従事しており化学は専門外であるが，本誌の読者諸兄のために私と化学との接点において夢を語りたい．私は1993年に「ナノフォトニクス」という光のナノテクノロジーを提案し，以来この研究を推進してきた．これには私が「近接場光」と命名した，ナノ寸法物質の表面に発生する光の小さな膜（光の小さな粒）を使う．これにより分光分析，大容量光ストレージ，微細加工，ナノ寸法の光デバイスなどの革新技術が実現した．

### 分子の不思議な振る舞い

この技術と化学との接点の例として，近接場光を分子に当てると分子は不思議な振る舞いをすることが私の研究グループにより発見された．普通，分子を分解するには紫外線を当てる．これは紫外線により分子のなかの電子が反応するから

である．これらはフランクコンドン原理，ボルンオッペンハイマー近似など，著名な科学者の名前の付いた理論で説明されており，従来はそれに学び，関連する科学技術が進展してきた．しかし近接場光の場合，可視光でも分子は分解してしまう．さらに，光には反応しない分子も近接場光には反応し分解するのである．

従来は紫外線が必要であったが，紫外線を発生する光源，とくにレーザーは大型・高価格であることが問題であった．しかし近接場光では日常使われている小型・安価な可視光源が使えるので，この技術的問題が解決された．

## 新現象を説明しうる学問をつくる！

ここで重要かつ本質的なことはこのような問題が解決することではなく，近接場光を使うと上記の理論，近似に従わない現象が起こることである．私は日本で発見されたこのような新現象を十分説明する学問体系をつくりたい．すなわち，欧米の研究者から学ぶ科学技術ではなく，日本でつくられた科学技術を完成させたい．これは電子工学，応用物理，バイオテクノロジーなどの広範な分野へ波及すると期待されているが，さらに化学にも貢献できれば幸いである．

なぜこのような新現象が生じたのだろうか？　従来使われている光は自由空間を飛んでいくので，光と物質を分けて考えることができた．ところが，近接場光は必ず物質の表面に発生するので，もはや光と物質とを分けて考えることができない．これが原因である．

すなわち，光と物質の融合した新しい科学技術が生まれている．私の夢は，これを完成させることである．

大津元一（おおつ もといち）
＜所属＞東京大学教授（大学院工学系研究科）
＜出身大学＞東京工業大学大学院博士課程（1978 年修了）
＜研究テーマ＞ナノフォトニクス
＜趣味＞筋力トレーニング，乱読書

The International Society for Optical Engineering

SPIE Newsroom

10.1117/2.1200610.0427

# Nanodot couplers provide efficient near-field energy transfer

**Takashi Yatsui, Wataru Nomura, and Motoichi Ohtsu**

*Nanodots self-assemble along a groove in a substrate to create a far/near-field converter for nanometer-scale photonic integrated circuits.*

Nanometer-scale photonic integrated circuits are one way to create the optical devices required by future systems.[1] These integrated circuits consist of nanometer-scale dots. An optical near field, the thin film of light on the surface of a nanometric material, is used as the signal carrier. Since an optical near field is free from the diffraction of light due to its size-dependent localization and resonance features, nanophotonics enables the fabrication, operation, and integration of nanometric devices.

Driving such a device requires an external, conventional, diffraction-limited photonic mechanism with a far/near-field converter. A potential converter is a plasmon waveguide. A plasmon is a quasiparticle made of electron plasma and a photon. The waveguide employs a metallized silicon wedge structure to convert far-field light into an optical near field via a one-dimensional plasmon mode.[2] Compared with a metallic core waveguide, or wire, a chain of closely spaced metallic nanoparticles should reduce energy loss[3] because of the lower metal content and plasmon resonance in the metallic nanoparticles. Energy transfer in the nanodot coupler relies on near-field coupling between the plasmon-polariton modes of neighboring particles.

We compared the spatial distribution of the optical near-field intensity in a linear nanodot coupler and a metallic core waveguide. To create the nanodot coupler, carbon hemispheres were deposited and coated with a 100-nm-thick gold film: see Figure 1(a). The same process was applied to carbon wire to make the metallic core waveguide: see Figure 1(c). In the nanodot coupler we found plasmon-polariton transfer as long as 4$\mu$m. Furthermore, the propagation loss was 10 times lower than that of the metallic core waveguide: see Figure 1(b), (d), and (g). Similar energy transfer was observed in a zigzag-shaped nanodot coupler with low energy loss at the corners: see Figure 1(f) and (h).[4] Such high flexibility in the arrangement of nanoparticles is an outstanding advantage of optical far/near-field conversion for driving nanophotonic devices.

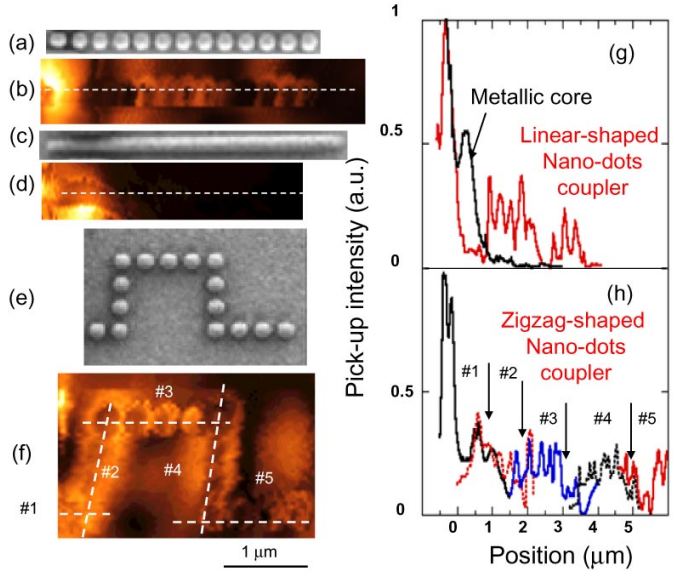


***Figure 1.*** *(a) A scanning electron microscopy (SEM) image and (b) a near-field optical microscopy (NOM) image show a linearly chained nanodot coupler. (c) SEM and (d) NOM images show a metallic core waveguide. (e) SEM and (f) NOM images show a zigzag-shaped nanodot coupler. (g) The solid and dashed curves correspond to the cross-sectional profiles along the dashed white lines in (b) and (d),respectively. (h) The cross-sectional profile follows the dashed white lines in (f).*

We fabricated nanodot couplers at all scales with a self-assembling method that builds nanodot chains by controlling desorption with an optical near field.[5,6] A nanodot chain of

*Continued on next page*

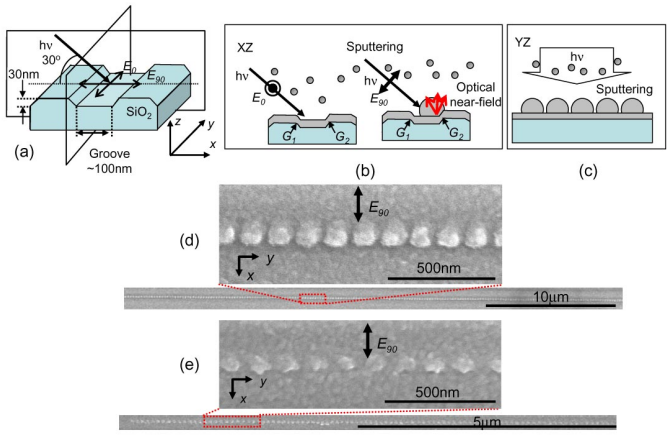


***Figure 2.*** *(a) Size- and position-controlled ultra-long nanodot chain formation occurs along a groove paralleling the y-axis. $E_{90}$ is perpendicular to the y-axis, and $E_0$ parallel to it. (b and c) These cross-sections illustrate planes XZ and YZ. (d and e) These SEM images show deposited aluminum with perpendicular polarization $E_{90}$ ($h\lambda$ = 2.33 and 2.62eV, respectively).*

metallic nanoparticles was created using radio frequency sputtering under illumination on a glass substrate with a simple groove 100nm wide and 30nm deep. During deposition of the metal, linearly polarized light illuminating the groove ($E_{90}$) excites a strong optical near field at the edge of the groove—see Figure 2(b)—which induces desorption of the deposited metallic nanoparticles.[5] A metallic dot has strong optical absorption due to plasmon resonance. This can induce desorption of a deposited metallic nanodot when it reaches the resonant diameter.[5] As the deposition of metallic dots proceeds, growth is governed by a trade-off between deposition and desorption. This plus the photon energy of the incident light determines dot size. Consequently, the metallic nanoparticles should align along the groove.

Illumination with 2.33 and 2.62eV light during aluminum deposition caused the formation of chains of 99.6nm-diameter nanodots with 27.9nm separation, and chains of 84.2nm-diameter nanodots with 48.6nm separation, respectively: see Figure 2(d) and (e). This occurred along a 100-$\mu$m-long groove in a highly size- and position-controlled manner. The dot size decreased in proportion to the increase in photon energy: $99.6\text{nm} \times (2.33/2.62) = 88.5 \sim 84.2\text{nm}$. This indicates that photon energy determines size and that the size-controlled dot-chain formation occurs due to photodesorption of the deposited metallic nanoparticles. The ratios of the center-center distance *(d)* and radius *(a)* of the nanodots—$d/a = 2.56(2.33\text{eV})$ and 3.15 (2.62eV)—are similar to the optimum value (2.4–3.0) for the efficient transmission of optical energy along a nanodot coupler as calculated using Mie's theory.[7] Our results thus imply that *d* was set at the optimum distance for efficient energy transfer of the optical near field, since a field of that strength can induce desorption of the deposited metallic nanoparticles and result in position-controlled dot-chain formation.

In summary: Our deposition method is based on a photodesorption reaction. As such, illumination at multiple photon energies using a simple lithographically patterned substrate could enable the simultaneous fabrication of size- and position-controlled nanoscale structures with different particle sizes as well as with other metals or semiconductors. This combination of features has the potential to dramatically increase the production throughput of the nanoscale structures that future systems will require.

## Author Information

**Takashi Yatsui and Motoichi Ohtsu**
Solution Oriented Research for Science and Technology
Japan Science and Technology Agency
Tokyo, Japan
http://www.nanophotonics.info/
School of Engineering
University of Tokyo
Tokyo, Japan

**Wataru Nomura**
School of Engineering
University of Tokyo
Tokyo, Japan

### References

1. M. Ohtsu, K. Kobayashi, T. Kawazoe, S. Sangu, and T. Yatsui, *Nanophotonics: design, fabrication, and operation of nanometric devices using optical near fields*, **IEEE J. Select. Top. Quant. Elect. 8** (4), pp. 839–862, 2002.
2. T. Yatsui, M. Kourogi, and M. Ohtsu, *Plasmon waveguide for optical far/near-field conversion*, **Appl. Phys. Lett. 27** (27), pp. 4583–4585, 2001.
3. M. L. Brongersma, J. W. Hartmanm, and H. A. Atwater, *Electromagnetic energy transfer and switching in nanoparticle chain arrays below the diffraction limit*, **Phys. Rev. B 62** (24), p. R16356, 2000.
4. W. Nomura, M. Ohtsu, and T. Yatsui, *A nanodot coupler with a surface plasmon polariton condenser for optical far/near-field conversion*, **Appl. Phys. Lett. 86** (18), p. 181108, 2005.
5. T. Yatsui, S. Takubo, J. Lim, W. Nomura, M. Kourogi, and M. Ohtsu, *Regulating the size and position of deposited Zn nanoparticles by optical near-field desorption using size-dependent resonance*, **Appl. Phys. Lett. 83** (9), pp. 1716–1718, 2003.
6. T. Yatsui, W. Nomura, and M. Ohtsu, *Self-assembly of size- and position-controlled ultralong nanodot chains using near-field optical desorption*, **Nano Lett. 5** (12), pp. 2548–2551, 2005.
7. M. Quinten, A. Leitner, J. R. Krenn, and F. R. Aussenegg, *Electromagnetic energy transport via linear chains of silver nanoparticles*, **Opt. Lett. 23** (17), pp. 1331–1333, 1998.

《よくわかる》

# ナノフォトニクスという変革

## 光技術に質的変革をもたらした新概念の歩みと将来

大津元一（東京大学大学院工学系研究科電子工学専攻，ナノフォトニクス）
おおつ　もといち
ohtsu@ee.t.u-tokyo.ac.jp　URL: http://uuu.t.u-tokyo.ac.jp

### 筆者からのメッセージ

1960年にレーザーが発明され，それを用いて1980年代には新しい光技術が急成長しました．それは光通信，光ディスクメモリ，光加工，医療などです．これらの技術をさらに発展させるために光の性能はますます向上し，すでにレーザーを用いて高パワー化，短波長化，短パルス化などが極限的な段階まで追求されています．

一方，光の微小化は可能でしょうか？　光の性能向上を先導してきた欧米の研究開発の状況を調べても，この問題は扱っていないようです．光は広がろうとする性質（回折）のために，凸レンズで集めても光の波長程度の寸法のピントのぼけがあり，これが光の寸法の最小値の限界を決めています．これは回折限界とよばれています．「回折限界を超えて光を微小化（ナノ寸法化）したい．」という私の素朴なウォンツ（wants）が1980年代初頭から始まったナノフォトニクスの研究のきっかけです．当時は奇異な目で見られながら始まった光の微小化は，光の「伝幡」対「非伝幡」，「自由空間」対「微小物質」，「実光子」対「仮想光子」といった対立する基本概念に関する科学的議論を生み，さらに基礎実験の成功は新しい光デバイス，光加工などの技術的革新を生みました．

本稿では日本発の革新技術であるナノフォトニクスの基礎とその成果，将来について紹介します．とくに従来の伝幡光では到底不可能であった，まったく新しい機能や現象を引き出して使うという質的変革が実現したことを示します．

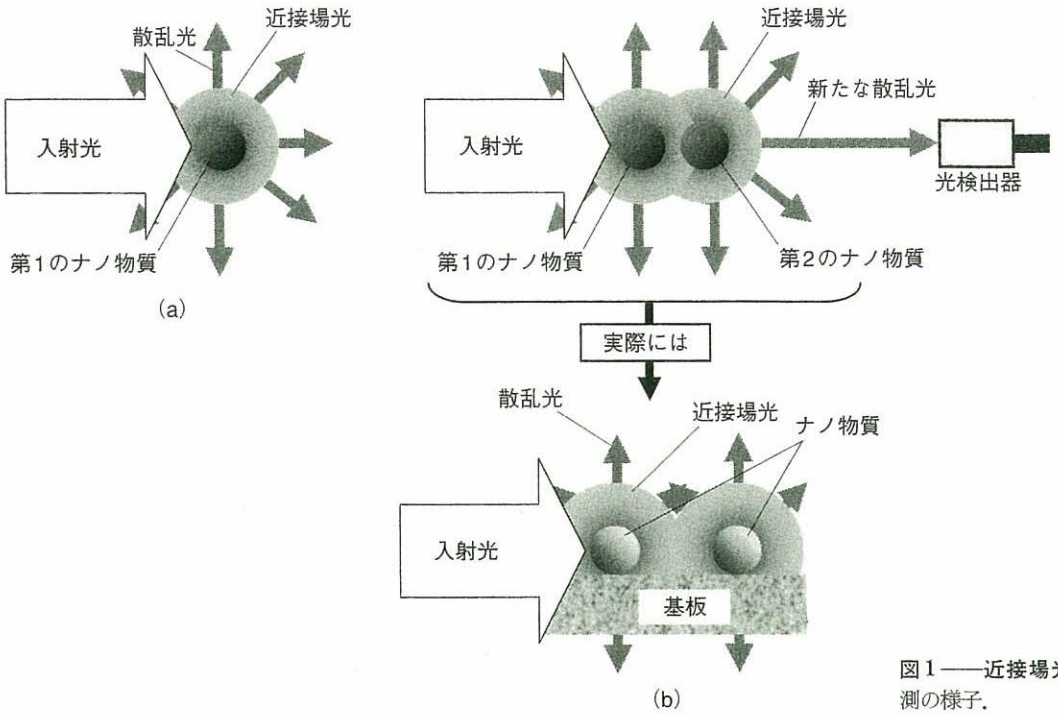


**図1——近接場光.** (a)発生の様子. (b)観測の様子.

## 光の小さな粒

物質に光を当てると散乱することはよく知られています. しかしこのとき, 同物質の表面を覆う膜のような光も発生することはあまり知られていません. この光は「近接場光」とよばれています(図1(a)). この光の膜の厚みは物質の寸法などによって決まった値を取ります[1]. ここで興味のあるのは物質寸法が数ナノメートルから数十ナノメートルと光の波長よりずっと小さい場合で, そのナノ物質および表面に発生した近接場光の組み合わせは光の小さな粒と考えられます. またその場合, この光の膜のエネルギー密度は高くなります. ただし近接場光は物質表面のみに発生し, 自由空間には存在しません. このことは遠くに光検出器を置いてもそこまでは近接場光は伝幡せず, そのエネルギーを測定できないこと, すなわち近接場光は観測できないことを意味しています. 主に欧米で開発された従来の光学は, 自由空間または光の波長よりずっと大きな寸法をもつ巨視的物質中を伝幡する光についての理論でした. したがって近接場光の性質をわかりやすく記述するには従来の光学とは矛盾しないもののまったく異なる機軸の理論, すなわちナノ寸法領域に局在する非伝幡の光についての光学が必要となります.

その機軸は「近接場光の観測」という切り口に立ちます. すべての物理量はその発生だけではなく, 観測が重要であることは現代物理学の本質です. 近接場光は直接観測できませんから,「近接場光の観測」は近接場光の観測可能な量への変換を意味します. 具体的には図1(b)のように近接場光が発生している第1のナノ物質に第2のナノ物質を接近させ, それにより近接場光の場を乱します. そのとき近接場光の一部は2つのナノ物質の両方を覆う膜となり, 残りは散乱光となります. 散乱光は伝幡する光なのでそのエネルギーは遠くの光検出器まで到達しますからこれを測定でき, したがって近接場光が観測されるのです. ここで, 第2のナノ物質は近接場光エネルギーを取り込み自らに移動させ, 観測可能な量に変換する重要な役割をします.

ただし2つのナノ物質と近接場光からなる「ナノ系」はナノ物質を乗せている基板(巨視的寸法をもつ物質), 入射光(さらには散乱光も)のような電磁場(これも巨視的寸法をもちます)からなる「巨視系」に囲まれているので, その理論的取り扱いが複雑になります. ここではナノ系のみを考えたいので巨視系の振る舞いを詳細に議論する必要はありません. そこで, 多体問題でよく知られた「繰り込み」の考え方を使います[2]. すな

わち入射光と巨視的な物質を励起子ポラリトン(コラムI参照)からなるものと考え，この巨視的な系の影響を2つのナノ物質間の電磁的相互作用の大きさの中に取り込みます．

## ナノ系の雲としての近接場光

前節最後に記した「繰り込み」の考え方を使うと，ナノ系は周囲の巨視系とは孤立しているように単純化して考えられるという利点があります．ここで，2つのナノ物質の相互作用の前の状態(始状態)として第1のナノ物質中の電子は高いエネルギー状態(励起状態とよばれています)にあり，第2のナノ物質中の電子は低いエネルギー状態(基底状態とよばれています)にあるものとします．相互作用後の状態(終状態)は第1のナノ物質が基底状態，第2のナノ物質が励起状態です．このとき励起子ポラリトンの授受により相互作用が始まると，図2に示すように始状態から終状態に至る経路として，巨視系のいろいろなエネルギー状態(中間状態とよばれます)へ仮想遷移し，そこから終状態へとさらに仮想遷移する可能性があります．仮想遷移というのは実際のエネルギー移動のともなわない量子力学的遷移，いいかえると仮想励起子ポラリトンを媒介とする遷移です．

現代物理では始状態と終状態が確定(観測)可能な状態であれば，その中間は仮想遷移が許され，始状態から終状態へと変化する確率は仮想遷移を含むすべての遷移経路(始状態から終状態に至る)を通る確率の合計となります．その結果，上記の始状態から終状態に導く源となる2つのナノ物質の電磁的相互作用の大きさ $V$ は

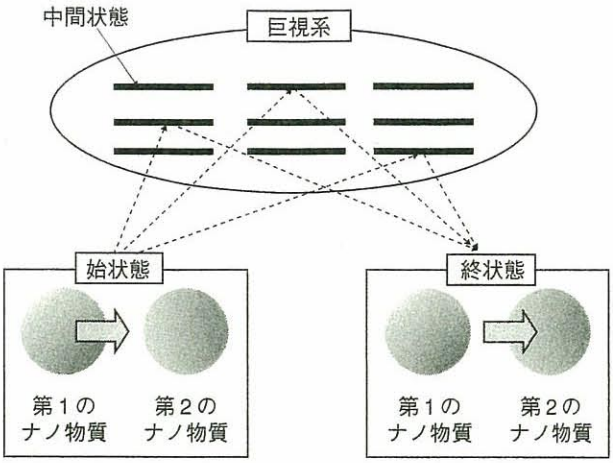


図2——始状態から終状態へ至る経路．

$$V \propto \frac{\exp\left(-\frac{ir}{a}\right)}{r} + \frac{\exp\left(-\frac{r}{a}\right)}{r}$$

という簡単な式で表されます[3]．ここで $i$ は虚数単位，$r$ はナノ物質表面からの距離，$a$ はナノ物質の寸法です．第1項は球面波に相当しますが，これは図1(b)のナノ物質を中心とする散乱光を表しています．第2項は湯川関数とよばれています．その値は $r$ の増加とともに急激に減少します．指数関数の中が $-\frac{r}{a}$ となっていることから，関数の値は距離 $r$ が $a$ 程度になるとほぼ0になることがわかります．すなわちナノ物質の寸法と同程度の空間分布をもつ光が存在することを意味しています．これが近接場光に相当し，あたかもナノ物質を核とした「雲」のようにナノ物質の周りに局在した光が存在すると考えられます．

**コラムI　励起子および励起子ポラリトンとは**

物質中の1つの原子の中の電子が励起され，その電子が原子核の周りをあたかも水素原子中の電子と同じような軌道を回っている状態は励起子とよばれています．また，半導体を例にとると，価電子帯の正孔と伝導帯の電子との間にはクーロン力が働いているので，このクーロン力によって正孔と電子は互いに結びついた1つの粒子のように振る舞います．この正孔と電子の対を1つの粒子のように見なしたものは励起子とよばれています．

光子が物質中に入射すると，物質に吸収され励起子が作られます．その次にはこの励起子が消えてまた光子が作られ，この繰り返しが物質中を伝幡します．すなわち，光子と励起子との間に次々に生成，消滅の変換が生じていますが，この状態つまり両者の混合状態が励起子ポラリトンとよばれています．

さて，図2の巨視系のあらゆる中間状態を考慮すると，それらへの仮想遷移の経路によっては2つのナノ物質間での励起子ポラリトンのエネルギーのやりとりに多様性が生まれます．1つはよく知られたエネルギー保存則を満たす相互作用です．これは共鳴相互過程とよばれ，第1項に相当します．一方，別の経路ではエネルギー保存則を満たさない非共鳴過程も可能で，これは第2項によって表されます(コラムII参照)．ただしいずれの場合も仮想励起子ポラリトンを媒介とする仮想遷移であり，エネルギーの移動は確定していないことに注意して下さい．なぜなら，このような仮想遷移は量子力学特有の現象であり，エネルギー$\Delta E$と時間$\Delta t$との間の不確定性原理$\Delta E \Delta t \geqq \frac{\hbar}{2}$を満たすような短い時間$\Delta t$においてのみ可能になるからです(ここで$\hbar$はプランクの定数$h$を$2\pi$で割った値です)．そして，この仮想遷移を含めることにより局所的な場，すなわち近接場光が自動的に導出されるのです．

## 技術のシーズと社会のニーズ

前節の議論からナノ物質の間を移動し相互作用を媒介する仮想励起子ポラリトンが近接場光であると考えることができます．これはあたかも原子核の中の陽子と中性子とを結びつける中間子と類似の描像です．このように考えると，近接場光によって，一方のナノ物質中の1つのエネルギー準位にある電子のエネルギーを他方のナノ物質中のエネルギー準位へ移動させることができることに気がつきます．その際，非共鳴過程がおこりえるので両準位は必ずしも互いに共鳴しなくてもよさそうです．このことは近接場光を用いて信号や情報をナノ物質間で伝送できること，つまり新しい機能をもつ光デバイスが原理的に可能なことを示唆しています．さらに移動するエネルギーが大きくなると，ナノ物質の構造や形までが変わること，すなわち新しい種類の光加工が可能なことを示唆しています．これらを実現する技術はナノフォトニクスとよばれ，私が1993年に提案したものです[4]．

前節の式の第2項をみると，ナノ物質間の相互作用を媒介する仮想励起子ポラリトンは空間を伝幡する波としての性質をもっていませんので光の回折とは無縁です．したがって光の波長以下の寸法のナノ物質を用いた光デバイスや光加工は回折限界を超えることができます．しかしここまで考えると，近接場光を応用するナノフォトニクスにおいて重要なことは単に回折限界を超えるという変革(これは大寸法から小寸法への改良なので「量的変革」といえます)ではなく，伝幡光では到底不可能であった非共鳴過程を利用して，まったく新しい機能や現象を引き出して使うという変革(これは無から有を生むので「質的変革」といえます)を実現することであることに気づきます．

つまり，本稿冒頭に述べた「光の微小化のウォ

**コラムII　エネルギーの保存について**

「エネルギーの保存則を満たさない」のならば，余分なエネルギーはどこから来，不足のエネルギーはどこへ消えたのでしょうか．この疑問に関しては，ここではナノ系のエネルギーの保存について議論していることに注意して下さい．すなわち，ナノ系は巨視系とは孤立しているように単純化して考えているので，上記のエネルギーの過不足分は実際には巨視的系から補充されているのです．つまりナノ系と巨視系とを合わせた全体の系ではエネルギー保存則は成り立っているので何の不思議もないのですが，ナノ系のみを考えるとエネルギー保存則を満たさないような現象がおこっています．ナノフォトニクスはこのような特殊な現象を引き起こすので，ナノ系と巨視系との境界線をどこに引くかということが重要になります．たとえば図1(b)下部の2つのナノ物質の寸法を基板に対してどのくらい小さくするか，また基板のどの位置に乗せるか，といった微細加工技術が必要であることを意味します．後段の「光加工の質的変革」の項に記す微細加工はそのような目的のためにも開発がすすんでいるのです．

ンツ」が，技術の質的変革をもたらすシーズ(seeds)になったのです．いいかえると光の微小化がもたらす量的変革よりも(この変革を利用したいという社会のニーズ(needs)ももちろんありますが)，上記の質的変革こそが本質的であることが明らかになってきました．

具体例を紹介しましょう．近接場光を発生させるためにガラスファイバの先端を尖らせてナノ寸法の針を作る技術が世界に先駆けて日本で確立し，これを用いてDNAなどの数ナノメートルの物質の形やその構造を調べることができる分析装置が実用化されました．これは従来の光を使った計測装置の分解能の回折限界を超える精密な装置であり，量的変革を実現したものです．また，この針をレコード針として使って1平方インチあたり1テラビット(1兆個のビット)の情報を記録再生する高密度・大容量装置(CD, DVDさらにはHDDなどの装置の記録再生限界を超えるもの)を実用化する技術開発も国を挙げて進んでいます[5]．これも量的変革の例ですが，社会のニーズに十分に，否それ以上に応えた例です．以下では肝心の質的変革を実現した例を示しましょう．

## 光デバイスの質的変革

質的変革を実現した代表例として光デバイスがあります．たとえば図3は異なる寸法の立方体状の半導体でできた量子ドット(コラムIII参照)とよばれるナノ物質3つからなる光スイッチです．外から光が入ると入力端子の量子ドットに近接場光が発生し，となりの量子ドットと相互作用が始まります．このとき3つの量子ドットの大きさの比を調整して作製しておくことにより，その中の電子と正孔の対からなる励起子(コラムI参照)のエネルギー準位をあらかじめ調整しておき，先述の非共鳴過程を利用してエネルギーをとなりの量子ドットに移動させます．ただし，エネルギーが逆戻りしないように移動後は熱的な緩和などを利用して低いエネルギー準位に移動させます．これらの過程を利用して，出力端子の量子ドットに近接場光を発生させたり，しなかったりさせるスイッチ機能を実現します．これは制御端子とよばれる量子ドットに制御用の第2の光を外から入れるか否かによって制御できます．なお，伝幡光を使っていたのでは非共鳴過程はおこりませんので，これは光デバイスの質的変革の代表例です．図3の下部には出力端子の量子ドットから発生する近接場光のエネルギーの空間分布を測定した結果を示していますが，これからもわかるように副次的な効果としてこの光デバイスの1辺の寸法は20ナノメートル程度です．これは光波長の20分の1以下，半導体レーザーなどの寸法の50分の1以下で，量的変革も実現しています．同様の原理で光スイッチ以外にも多様な光デバイスが提案されており，また実用的なデバイスの開発が進み，さらには新しい情報伝送，情報処理などのシステムへの応用が検討されています．

**コラムIII　量子ドットとは**

巨視的寸法をもつ物質中の電子のとりうるエネルギーの値はほぼ連続的です．しかし，物質の寸法が小さくなると，その中に閉じ込められた電子は飛び飛びの値のエネルギーしかとれなくなります．すなわち電子のエネルギー準位が離散化されるという，いわゆる量子効果が現れます．このような量子効果を示す微小な微粒子は量子ドットとよばれています．

## 光加工の質的変革

一方，光加工における質的変革の例として，物質を削る技術の1つである光リソグラフィがあります．光リソグラフィでは削りたい物質の表面にフォトレジストとよばれる高分子膜を塗っておきます．この高分子は光に反応して化学変化をおこしますので，これに光をあてるとフォトレジストが削られます．この後に他の方法でフォトレジストの下の物質を削るのですが，ここではフォトレジストを削ることだけを採り上げます．

従来は伝幡光を使っていたので，削ることのできる最小寸法は回折限界によって制限されていました．波長の短い紫外線を使うとこの回折限界の値が小さくなるので，最近では紫外線，さらには

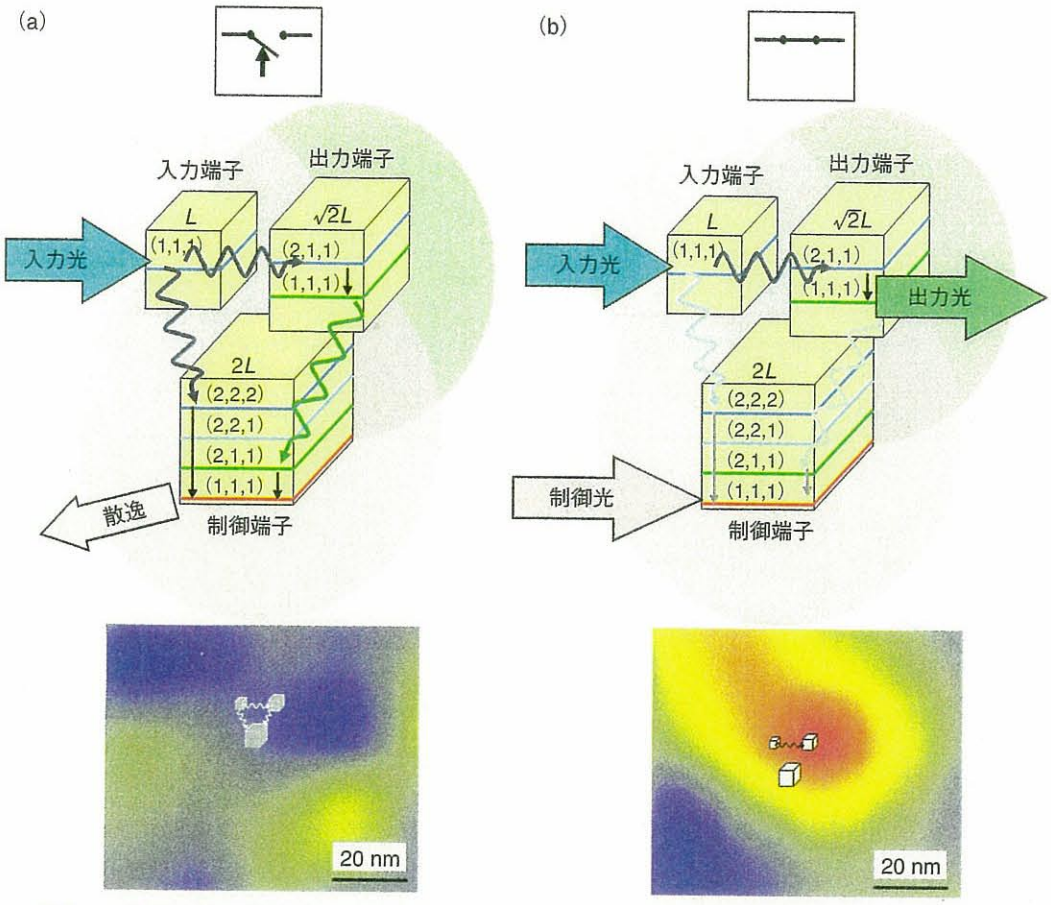


**図3——光スイッチ.** (a)スイッチが開いた状態. (b)スイッチが閉じた状態. 両図とも3つの立方体は量子ドット. その1辺の寸法比は$1:\sqrt{2}:2$. 立方体中の横線は励起子のエネルギー準位. (1,1,1)などの数字はエネルギー準位を表す量子数. 波形矢印はエネルギー移動の方向. 下向きの矢印は緩和の方向. 立方体の周囲の円は発生する近接場光. 図の下部は塩化銅の3つの量子ドット(1辺の寸法が各々4ナノメートル, 6ナノメートル, 8ナノメートル)を用いた光スイッチの出力端子から発生する近接場光のエネルギーの空間分布の測定結果.

超短波長の光(極端紫外光, シンクロトロン放射光など)を光源とする技術開発が進んでいますが, これらの光源は大型・高価なので実用的ではなく, 光リソグラフィは限界を迎えています. この限界を超えるために伝幡光の代わりに近接場光を使います. すると削る寸法は回折限界とは無縁となり, この限界を超えて微小化されます. この方法によって図4(a)に示すように幅20ナノメートルの細線状の周期的パターンが作られています. これはフォトマスク(写真のネガフィルムのようなもの)をフォトレジストの上におき, フォトマスクに描かれた細線の隙間から近接場光を発生させて加工したもので, 量的変革の例ですが, 社会のニーズに十分に応えています.

しかしここで肝心なことは質的変革が実現しているということです. 近接場光は回折限界とは無縁なので, どのような波長の光源を使っても構いません. 加工寸法は上記のフォトマスク面の隙間の寸法によって決まるからです. ただし通常は紫外線の光源を使います. なぜなら現在入手できるフォトレジストのほとんどは紫外線にしか反応しないからです. しかしこれは共鳴過程による反応であることに注意しましょう. 近接場光の場合には非共鳴過程が可能なので, 紫外線ではなく赤や青の光をフォトマスクにあてて近接場光を発生させると, フォトレジストは反応して削られ, 図4(b)のように微小なパターンができてしまいます. すなわち非共鳴過程によりエネルギーを移送させることができ, 紫外線でなくとも赤, 青などの光でも近接場光から反応をおこさせることができるのです. このことは大型で高価な短波長光源はもはや不要になったこと, 通常の伝幡光には反応しない高分子もフォトレジストとして使えること, 伝幡光による光リソグラフィでは難しい複雑なパ

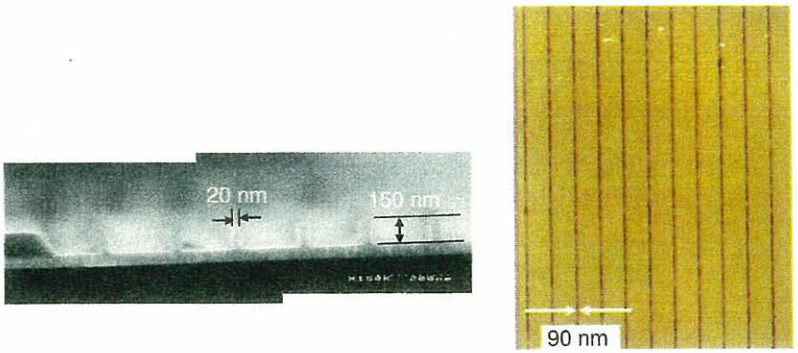


(a) (b)

**図4——光リソグラフィにより作られたフォトレジスト上のパターン.** (a)幅20ナノメートル，深さ150ナノメートルの細線状の周期パターンの断面図((株)キヤノン，黒田亨氏のご厚意による)．(b)非共鳴過程により作られた細線状の周期パターン(上から見た図)．

ターンも加工できることなどの質的変革を生みました．もはや光リソグラフィとよぶべきでない，新しい加工法と考えられます．このように新しい加工法が実現し，その実用的な装置の開発も進んでいます．

## 将来へむけて

これまでの光科学と技術では，光のエネルギーの流れは光源から光検出器へと向かっており，また光により物質を励起するとき，それは光波長以上の寸法にわたる巨視的なものでした．そのため，光と物質は明確に分けて考えることができました．ところがナノフォトニクスにおいては光のエネルギーの流れは2つの物質の間で双方向的であり，また光による物質励起も微視的です．このことは光と物質とを融合した考え方，すなわち「光・物質融合科学技術」が必要となることを示唆しています．

今後はナノメートル領域における光と物質の相互作用の素過程，エネルギー移動などの特徴を一層たくみに制御して使うことにより，さらに新しい情報伝送，情報処理，微細加工が実現すると期待されます．すでに前節で概説した質的変革が発展していますし，さらに前節の光スイッチなどを利用した新しい情報セキュリティのシステムなどが提案されています．

**付記** ナノフォトニクスは仮想励起子ポラリトンが媒介するナノ物質間の局所的電磁相互作用を利用し，その結果を外部に取り出す技術であり，多くの可能性をもつためにここ数年，国際会議などでも研究発表の件数が急増しています．ところが完全に伝幡光を使う技術をも「ナノフォトニクス」とよんでしまう例が近年散見されます．情報理論の黎明期において，創始者シャノンは情報理論という名称が単なるbandwagon(パレードを先導する楽隊車)としてむやみに利用されることに強く警鐘を鳴らしましたが，われわれはそれを思い出すべきでしょう[6]．すなわち上記の局所的電磁相互作用にもとづいていない研究が多く，伝幡光利用技術をもってナノフォトニクスと称する紛らわしい主張がみられます．ナノフォトニクスを真に展開する場合，ナノ寸法領域における光と物質の相互作用に対する深い物理的洞察が必要であり，光と物質が融合した科学技術の深化にこそ意義があるのです．単に研究費を獲得するためのキーワードに使うのは危険でしょう．

**謝辞** 本稿をまとめるにあたり，その内容を吟味くださった東京工業大学教授小林潔氏，科学技術振興機構研究員川添忠氏，東京大学客員助教授成瀬誠氏に感謝致します．

## 文献

(1) 大津元一: in '光の小さな粒', 裳華房(2001)pp. 18～29
(2) K. Kobayashi et al.: in 'Progress in Nano-Electro-Optics I', M. Ohtsu ed., Springer-Verlag (2003)pp. 119～157
(3) 大津元一・小林潔: in '近接場光の基礎', オーム社(2003)pp. 138～141
(4) 大津元一・小林潔: in 'ナノフォトニクスの基礎', オーム社(2006)pp. 15～16
(5) T. Matsumoto: in 'Progress in Nano-Electro-Optics III', M. Ohtsu ed., Springer-Verlag (2005)pp. 93～126
(6) C. Shannon: IEEE Trans. Information Theory, 2, 3(1956)

特集：科学研究費補助金の現状

# 工学系の科研費審査に携わって

大　津　元　一

私は以前よりいくつかの種目の科学研究費補助金（科研費と略称）の審査，他省庁・他機関の競争的研究資金の審査，更には研究実施の評価などに携わってきたが，ここ数年は科研費の特別推進研究（特別推進と略称），特定領域研究（特定領域と略称）を審査する機会を頂いた．本稿では毎年同時期に行われた特別推進，特定領域の両審査について，工学系研究者としての立場から思い起こすことを述べさせて頂きたい．

両審査は数物系科学，化学，工学の3分野の審査員が各々10名程度で，かつほぼ合同で書類審査をへて面接審査を行う．学術全般から見るとこの3分野は互いに類似の分野と思われるかもしれないが，厳密に審査しようとするとやはり3分野の専門性，文化の違いがでてくる．もちろん申請課題の独創性，先駆性が重要であるが，前2者は理学系であり現象の発見，説明などに主眼がおかれ，後1者は工学系なのでものづくり，システムの形成，そのための細部改良などを行う．従って理学系からみてやや独創性に欠ける内容でも工学系としては非常に重要な課題である場合が多い．これらを3分野合同で審査するので，審査員の目から鱗が落ちて高く評価される場合と，相互理解不足のままに終わる場合とがある．

さらに，同じ工学系の内部でも文化の違いはある．申請者の研究実績は発表論文の質と量によって判断されるが，最近の工学系のいくつかの分野では原著論文よりも国際会議での発表の方が重要とされる場合があり，さらには特許申請なども重要視されるようになっている．また，工学系のカバーする範囲は電気，機械，材料など広範であり，電気関連の研究に従事する私にとっても材料，化学工学に関する申請内容を十分に理解するのは容易ではない．このように考えると，工学系といえども文化に違いがでてきた現在，合同で審査する分野の見直しなども必要と考えられる．

特別推進，特定領域の申請書類は膨大であり，書く方も読む方も大きな労力を費やしている．採択後の中間評価，終了評価などに関しても同様である．他省庁・他機関では特別推進，特定領域の研究費を遙かに上回る額の競争的資金もあるが，必ずしも申請書類の分量はそれほど膨大でない場合がある．これらについては学術的独創性，先駆性だけではない多様な要因を含むからという理由も考えられるが，それらと比較すると特別推進，特定領域の審査は極めて学術的に厳密である．科学技術に関わる知的原動力としての優れた研究を支援する科研費審査として，この厳密性がこれからも維持されることを希望している．ただし，実際面では申請者，審査員ともに多忙を極めることは否めない．審査員は特別推進，特定領域のみでなくその他の複数の競争的研究資金の審査にもかり出される傾向

がある．また，一方の資金に関して審査する者が，他の資金に申請して審査を受ける場合も少なくない．審査の中立性を保つために「競争的研究資金の審査」の専門職の確立を期待する．

工学系の研究には基礎から実用化に至る研究の段階が複数あることが多い．従って1人の研究者が各段階で異なる競争的研究資金を申請する場合がある．これらは共通する概念による研究ではあるが，工学系の研究としては異なる種目と判断せざるを得ない場合がある．特に実用化の段階では産学連携の場合が多く，申請代表者は産学間の調整のみを行うが，研究費は配分されないこともある．しかしこのような場合でも，複数の研究資金申請と見なされることもあり，慎重な判断が必要となる．

特別推進，特定領域の研究は独創性，先駆性にあふれた内容を数年間にわたり推進するものであるが，あくまでもそれは優れた研究を加速する初期段階であり，本格的研究はこれらの期間が終了するころからいよいよ始まると考えられる．その意味で必要なのは研究期間終了後のケアである．すでに研究の継続に対して資金を与える制度は作られていると理解しているが，往々にして継続資金は小規模であり，発展のためには十分とは言いがたい．細心の審査の上，思い切った取捨選択を行って発展に十分な規模の研究費の配分ができればありがたい．

最近の多くの競争的研究資金は，研究成果の出口（実用化など）を求めているようである．工学系研究では出口の必要性は他分野よりも高いと思われるが，やはり研究と出口とは別物である．出口は他省庁・他機関で追求することが適切な場合が多く，特別推進，特定領域ではやはり科学の wants をかなえ，技術の seeds を生み，科学技術の突破口を作る研究課題を応援していただきたい．そのためには言い古されているようであるが，only one の研究を見出す名伯楽としての審査が必要である．

私が特別推進，特定領域の審査を拝命している間にも，これらの募集要領，審査方法などが毎年のように見直され，社会の要求に合うように絶えず改良されてきた．その意味でこれらの制度は常に進化している．私が審査員の役職を退いてからすでに2年以上経過しているので，本稿で指摘した問題点はすでに解決しているかも知れない．とすればそれは私の不勉強の限りである．また，これらを問題点として指摘したことは審査員としての私の能力不足に起因する可能性があるが，その場合にはご叱責頂ければ幸いである．

**大津　元一**（おおつ・もといち）
東京大学大学院工学系研究科 教授，東京工業大学名誉教授

# [Ⅳ] PUBLISHED BOOKS

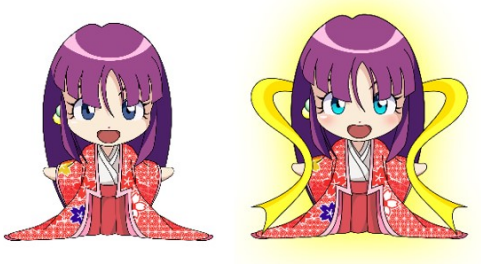

# 15. Nanooptics

Nanooptics deals with optical near fields, the electromagnetic fields that mediate the interaction between nanometric particles located in close proximity to each other. The projection-operator method is a theoretical description of how a virtual exciton–polariton is exchanged between these particles, corresponding to the nonresonant interaction. The optical near field mediates this interaction, and is represented by a Yukawa function, which means that the optical near-field energy is localized around the nanometric particles like an electron cloud around an atomic nucleus. Its decay length is proportional to the particle size. This chapter is primarily a review of nanophotonics, a leading branch of nanooptics, which is the technology utilizing the optical near field. The true nature of nanophotonics is to realize qualitative innovation in photonic devices, fabrication, and systems by utilizing novel functions and phenomena caused by optical near-field interactions, which are impossible as long as conventional propagating light is used. As evidence of such qualitative innovation, this chapter describes novel nanophotonic devices, nanophotonic fabrication, nanophotonic systems, and extensions related to science.





## 15.1 Basics

Nanooptics deals with the light generated in or on nanometer-sized particles. It has been applied to open an innovative field of technology, i. e., *nanophotonics*, in order to develop novel photonic devices, fabrications, and systems, as proposed by *Ohtsu* [15.1]. Nanophotonics is a means, for example, to reduce the size of photonic devices, improve the resolution of optical fabrications, and increase the storage density of optical disk memories.

Considering photonic devices, the technologies listed below, which bear some relation to nanophotonics, have recently been developed. Nevertheless, they cannot reduce the size of these devices beyond the diffraction limit of light.

1. **Photonic crystal** [15.2] This is a filter device used to control optical interference and light scattering by installing a subwavelength-sized periodic structure in the device material, as is the case for a diffraction grating. Constructive interference between the scattered light takes place at the center of the material, concentrating the optical energy. In contrast, at the edge of the material, the scattered light interferes destructively. In order to maintain the destructive interference, the rim must be sufficiently larger than the wavelength of light; otherwise the constructive interference is not maintained, and light concentrated at the center leaks to the rim. This means that a photonic crystal involves conventional wave-optical technology and the minimum size of the device is limited by diffraction.
2. **Plasmonics** [15.3] This technology utilizes the resonant enhancement of the light in a metal by exciting free electrons. The optical energy can be concentrated as a plasmon on the metal surface as a result

of the strong interaction with free electrons. However, this technology is based on wave optics in the metal, and so is again limited by diffraction. Related technologies, such as metaoptics [15.4] and optics in materials with a negative refractive index [15.5], are also limited by diffraction.

3. **Silicon photonics** [15.6] This technology involves developing narrow-striped optical waveguides using high-refractive-index silicon crystals to confine the light effectively. This is also an application of wave optics in silicon, and is limited by diffraction.
4. **Quantum-dot laser** [15.7] This is a laser device that uses nanometer-sized semiconductor quantum dots as the gain media. Since the quantum dots are much smaller than the wavelength of light, the light cannot be confined in an individual quantum dot efficiently due to scattering and diffraction. To solve this problem, a large number of quantum dots are installed in a conventional laser cavity, which means that the device size is limited by diffraction.

Although the four examples listed above have been popular subjects of study in recent years, they are all based on diffraction-limited wave optics. Even if novel or nanometer-sized materials are used in the future, the size of a photonic device cannot be reduced beyond the diffraction limit as long as propagating light is used for its operation. This also applies to improvements in the resolution of optical fabrication and for increasing the storage density of optical disk memories. To go beyond the diffraction limit, one needs non-propagating nanometer-sized light to induce primary excitation in a nanometer-sized material in such a manner that the spatial phase of the excitation is independent of that of the incident light.



## 15.2 Nanophotonics Principles

The use of optical near fields has been proposed as a way to transcend the diffraction limit imposed on optical science and technology [15.8]. This proposal holds that an optical near field can be generated on a subwavelength-sized aperture by irradiating the propagating light. It also holds that the size of the spatial distribution of the optical near-field energy depends not on the wavelength of the incident light, but on the aperture size. Although these claims are no more than those in the framework of primitive wave optics, optical near fields have been applied to realize diffraction-free, high-resolution optical microscopy (i. e., optical near-field microscopy), which achieved rapid progress after high-resolution, high-throughput fiber probes were invented and fabricated in a reproducible manner [15.9, 10]. However, in the early stage of these studies, the concept of optical near fields was not clearly discriminated from that of an evanescent wave on a planar material surface (i. e., a two-dimensional topographical material) or that of a guided wave in a subwavelength-sized cross-sectional waveguide (i. e., a one-dimensional topographical material).

In order to distinguish these clearly, note that an evanescent wave is generated by the primary excitations, i. e., electric dipoles, induced near the two-dimensional material surface, which align periodically depending on the spatial phase of the incident light. In contrast, the guided wave in a subwavelength-sized cross-sectional waveguide is generated by the electronic dipoles induced along the one-dimensional waveguide material. They align periodically depending on the spatial phase of the incident light. Examples are the silicon and metallic waveguides used for silicon photonics and plasmonics, respectively. The two-dimensional evanescent wave and one-dimensional guided wave are both light waves, which are generated by periodic alignment of electric dipoles depending on the spatial phase of the incident light.

Unlike these waves, an optical near field is generated by the electronic dipoles induced in a nanometric particle (i. e., a subwavelength-sized zero-dimensional topographical material). Their alignment is independent of the spatial phase of the incident light because the particles are much smaller than the wavelength of the incident light. Instead, it depends on the size, conformation, and structure of the particles. Due to this independence and dependence, optical science and technology beyond the diffraction limit can be realized only by an optical near field, not by an evanescent wave or a guided wave.

Classical electromagnetics explains the mechanisms of optical near-field generation described above (Fig. 15.1): electric dipoles are induced by irradiating a nanometric particle with the incident light. Among the electric lines of forces originating from these electric dipoles, the optical near field is represented by those that originate from the positive charge of the electric dipole

and terminate on the negative charge. This does not propagate to the far field. Since the particle is much smaller than the wavelength of the incident light, the alignment of the electric dipoles is determined independently of the spatial phase of the incident light. Therefore, the spatial distribution and decay length of the optical near-field energy depend not on the wavelength of the light, but on the size, conformation, and structure of the particle. Moreover, the scattered light is represented by the closed loop of the electric line of forces, and propagates to the far field.

Methods such as Green's function, numerical calculation using the finite-difference time domain (FDTD) method, have been developed for semiquantitative description of the optical near field based on conventional optical theories (i. e., the theories discussed in other chapters of this handbook) [15.11]. However, conventional optics theories do not provide any physically intuitive pictures of non-propagating nanometric optical near fields because these theories have been developed to describe light waves propagating through macroscopic space or materials. For nanooptics and nanophotonics, a novel theory has been developed based on a framework that is completely different from those of the conventional theories.

This novel theory is based on how one observes an optical near field, i. e., the interaction and energy transfer between nanometric particles via an optical near field. This perspective is essential because the interaction and energy transfer are indispensable for nanophotonic devices and nanophotonic fabrications. That is, in order to observe a non-propagating optical near field, a second particle is inserted to generate observable scattered light by disturbing the optical near field (Fig. 15.2). However, the real system is more complicated than that shown in Fig. 15.2 because the nanometric subsystem (the two particles and the optical near field) is buried in the macroscopic subsystem consisting of the macroscopic substrate material and the macroscopic electromagnetic fields of the incident and scattered light (Fig. 15.3).

The premise behind the novel theory is to avoid the complexity of describing all of the behaviors of nanometric and macroscopic subsystems rigorously, since we are interested only in the behavior of the nanometric subsystem. The macroscopic subsystem is expressed as an exciton–polariton, which is a mixed state of material excitation and electromagnetic fields. Since the nanometric subsystem is excited by an electromagnetic interaction with the macroscopic subsystem, the projection-operator method is effective for describing the quantum-mechanical states of these systems [15.12].

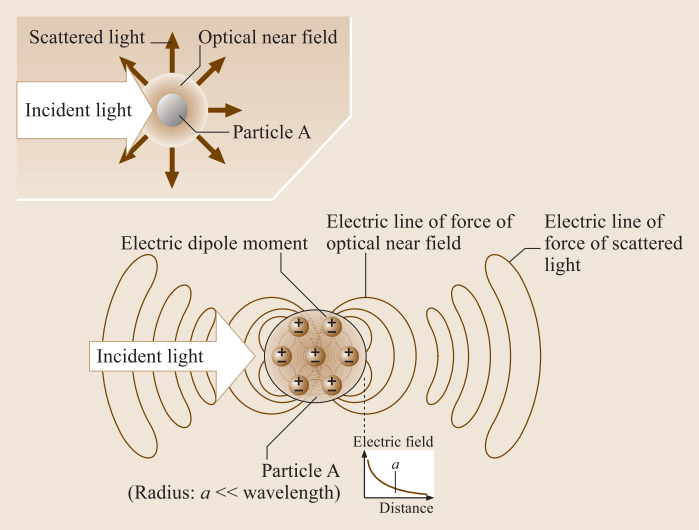


**Fig. 15.1** The generation of optical near fields

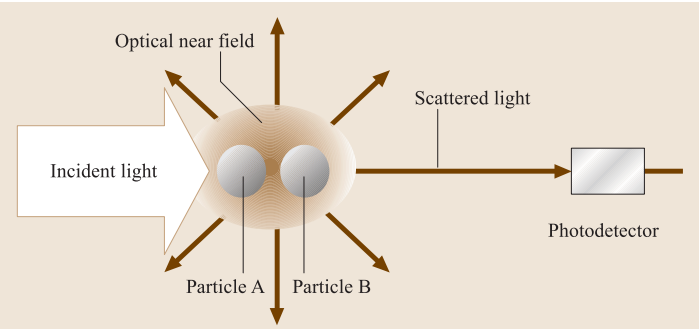


**Fig. 15.2** The observation of optical near fields

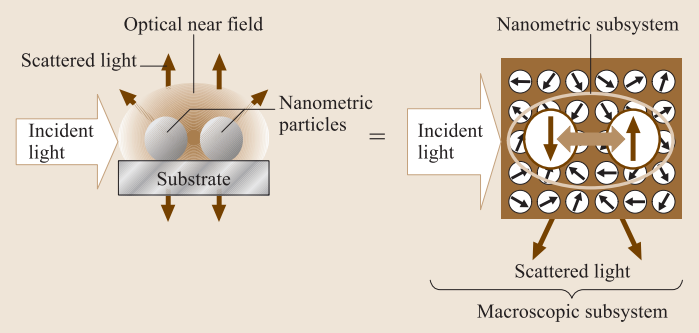


**Fig. 15.3** A nanometric subsystem composed of two particles and an optical near field, buried in a macroscopic subsystem

Under this treatment, the nanometric subsystem is regarded as being isolated from the macroscopic subsystem, while the functional form and magnitude of the effective interactions between the elements of the nanometric subsystem are influenced by the macroscopic

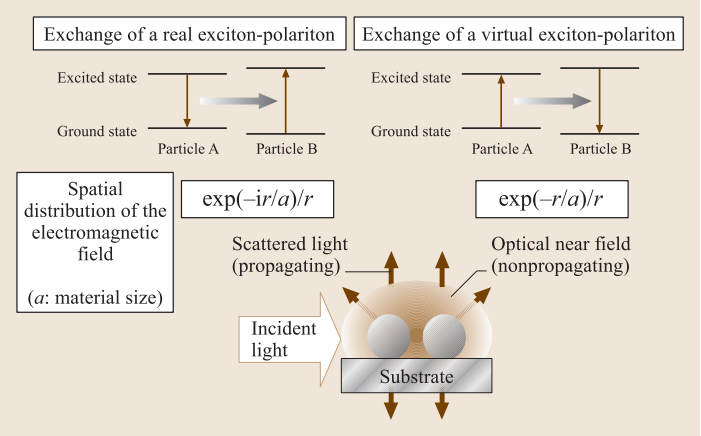


**Fig. 15.4** The exchange of a real exciton–polariton and a virtual exciton–polariton

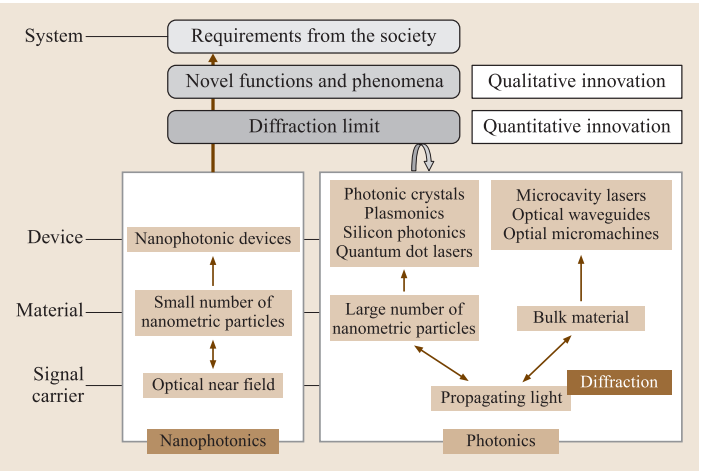


**Fig. 15.5** Nanophotonics for realizing qualitative innovation

subsystem. That is, the two nanometric particles can be considered as being isolated from the surrounding macroscopic systems and as interacting by exchanging the exciton–polariton energies.

Since the time required for this local electromagnetic interaction is very short, the uncertainty principle allows the exchange of a virtual exciton–polariton between the two nanometric particles, as well as that of a real exciton–polariton (Fig. 15.4). The former exchange corresponds to the nonresonant interaction between the two particles. The optical near field mediates this interaction, which is represented by a Yukawa function. The Yukawa function represents the localization of the optical near-field energy around the nanometric particles like an electron cloud around an atomic nucleus whose decay length is equivalent to the material size [15.12]. The latter corresponds to the resonant interaction mediated by the conventional propagating scattered light, which is represented by a conventional spherical wave function.

As described, the optical near field is an electromagnetic field that mediates the interaction between nanometric particles located in close proximity to each other. Nanooptics deals with this field. Nanophotonics is the technology that utilizes this field to realize novel device, fabrications, and systems. That is, a photonic device with a novel function can be operated by transferring the optical near-field energy between nanometric particles. In such a device, the optical near field transfers a signal and carries the information. Novel photonic systems become possible by using these novel photonic devices. Furthermore, if the magnitude of the transferred optical near-field energy is sufficiently large, structures or conformations of nanometric particles can be modified, which suggests the feasibility of novel photonic fabrication.

Note that the true nature of nanophotonics is to realize qualitative innovation in photonic devices, fabrications, and systems by utilizing novel functions and phenomena caused by optical near-field interactions, which are impossible as long as conventional propagating light is used (Fig. 15.5). On reading this note, one may understand that the advantage of going beyond the diffraction limit, i. e., quantitative innovation, is no longer essential, and is only a secondary nature of nanophotonics. In this sense, one should also note that optical near-field microscopy, i. e., the methodology used for image acquisition and interpretation in a nondestructive manner, is not an appropriate application of nanooptics and nanophotonics because the magnitude of the optical near-field energy transferred between the probe and sample must be extrapolated to zero.

Although few examples of qualitative innovations in nanooptics exist, nanophotonics has already realized this innovation by correctly utilizing the true nature of the optical near-field interaction, which is reviewed in the following sections.

## 15.3 Nanophotonic Devices

For the operation of nanophotonic devices, it is essential to transfer the signal and fix the transferred signal magnitude at the output terminal, which can be achieved by transferring and dissipating the optical near-field en-

ergy, respectively [15.13]. Several research groups have recently begun similar discussions on this operation (for example, refer to [15.14]). A pair of two closely spaced equivalent quantum dots is used as the input terminal of the nanophotonic device (Fig. 15.6). As a result of the optical near-field interaction between the two quantum dots driven by the input optical signal, the quantized energy levels of the exciton in the quantum dots are split into two. One corresponds to the symmetric state of the exciton, and the other is the antisymmetric state. They represent the respective parallel and antiparallel electric dipole moments induced in the two quantum dots.

The third, larger quantum dot, installed proximal to the input terminal (Fig. 15.7), is used as the output terminal of the device. The higher energy level of the exciton in this quantum dot is tuned to that of the symmetric state of the input terminal, which is made possible by adjusting the size of the third quantum dot. As a result of this tuning, optical near-field energy can be transferred from the input to the output terminal, allowing signal transfer. The excitation transferred to the output terminal is relaxed immediately to the lower energy level in the third quantum dot by coupling with phonons, which fixes the magnitude of the transferred signal.

A device utilizing the symmetric state of the input terminal in the manner shown in Fig. 15.7 is called a *phonon-coupled device*. Examples of phonon-coupled devices include nanophotonic switches, logic gates, such as AND and NOT gates [15.15], content-addressable memory [15.16], and digital-to-analog

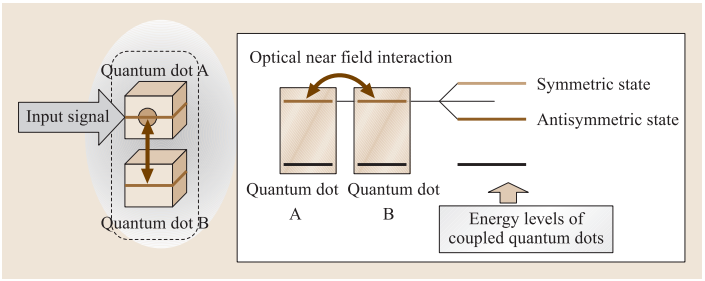


**Fig. 15.6** Two closely spaced quantum dots to be used as the input terminal of a nanophotonic device

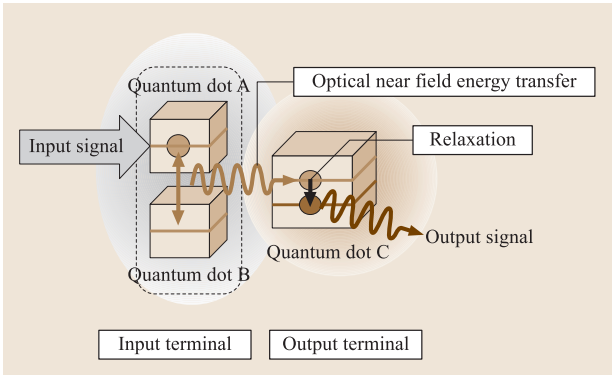


**Fig. 15.7** Optical near-field energy transfer from the input to the output terminal and successive fast relaxation

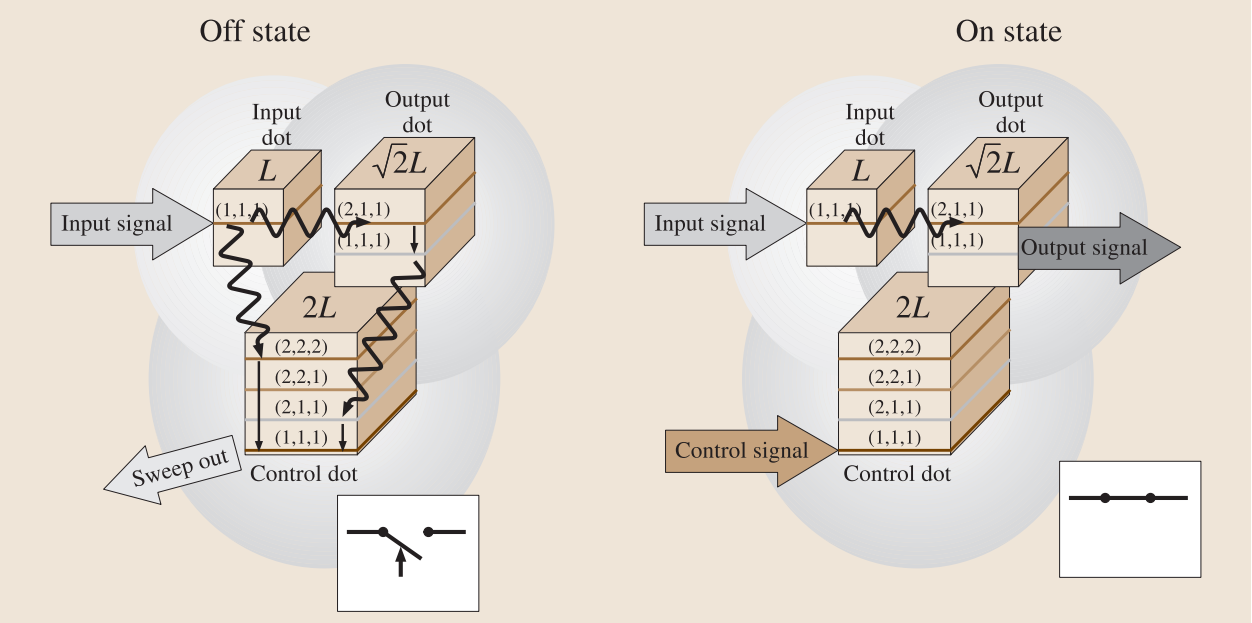


**Fig. 15.8** The structure of a nanophotonic switch. $L$ is the size of the quantum dot used as the input terminal

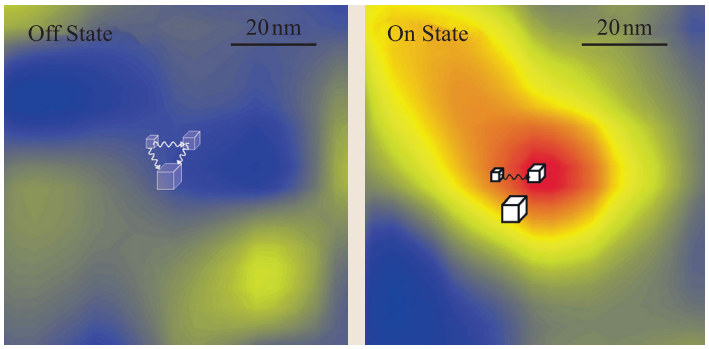


**Fig. 15.9** The spatial distribution of the output signal energy at the output terminal of the nanophotonic switch. This switch used three cubic CuCl quantum dots with sizes of 4, 6, and 8 nm, separated by a fixed distance of 3 nm

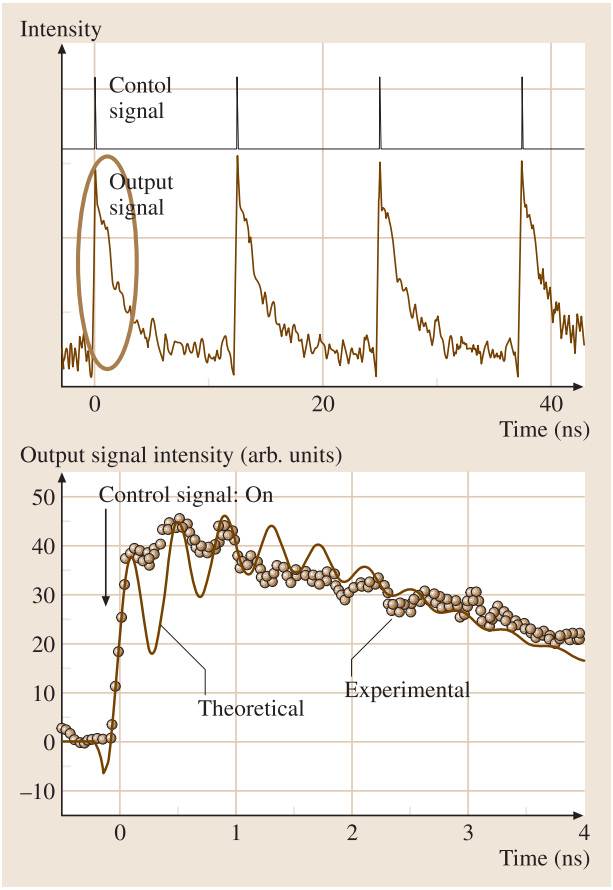


**Fig. 15.10** Dynamic behavior of the output signal of a nanophotonic switch. The figure on the *bottom* shows the experimental and theoretical curves of the part of the output signal identified by the ellipse in the figure on the *top*

converters [15.17]. Conversely, a device utilizing the antisymmetric state is called a *propagating light-coupled device*; for example, optical buffer memory and superradiant-type optical pulse generators [15.18].

As an example of a phonon-coupled device, Fig. 15.8 shows a nanophotonic switch whose operation has been modified slightly from that shown in Fig. 15.7 [15.19]. Three cubic quantum dots with a size ratio of $1 : \sqrt{2} : 2$ are used as the input, output, and control terminals, respectively. This device utilizes the optical near-field energy transfer between the resonant energy levels of the exciton and successive fast relaxation. Note that the conventional optical transition between two resonant exciton levels in the adjacent quantum dots, e.g., the (1,1,1) and (2,1,1) energy levels of the input and output terminals, is forbidden. That is, no energies are transferred as long as the propagating light mediates the interaction between the quantum dots. In contrast, when using an optical near field, this transition is allowed due to the exchange of the virtual exciton–polariton. This is an example of a qualitatively innovative device operation because it is impossible as long as conventional propagating light is used. Figure 15.9 shows the spatial distributions of the output signal energy on the output terminal for the off and on states of the switching operation. The device is as small as 15 nm. Figure 15.10 represents the dynamic behavior of the output signal, which agrees well with the calculated results based on the virtual exciton–polariton model.

A figure of merit has been used as an important parameter for evaluating device performance. In the case of a switch, it is defined as a combination of device volume, switching time, switching energy, the ratio between on- and off-signal magnitudes, etc. The figure of merit for the nanophotonic switch is 10–100 times larger than those of conventional photonic switches operated using propagating light (e.g., devices using optical micromirrors, Mach–Zehnder interferometer-type waveguides, optically nonlinear media, and the quantum sublevels in a quantum dot). Furthermore, the magnitude of the heat dissipated from the nanophotonic switch is estimated to be as low as $10^{-12}$ W in the case of 1 GHz repetitive operation, which is only $10^{-5}$ times that of a conventional semiconductor transistor. Such a large figure of merit and the ultralow heat dissipation suggest a variety of applications to novel computation and information processing systems.

For applications to advanced systems, nanophotonic devices must be connected to conventional macroscopic photonic devices, such as optical fibers or semiconductor lasers. Figure 15.11 shows a novel device developed for this interconnection that concentrates the propagating light energy to a nanometric region [15.20]. It has

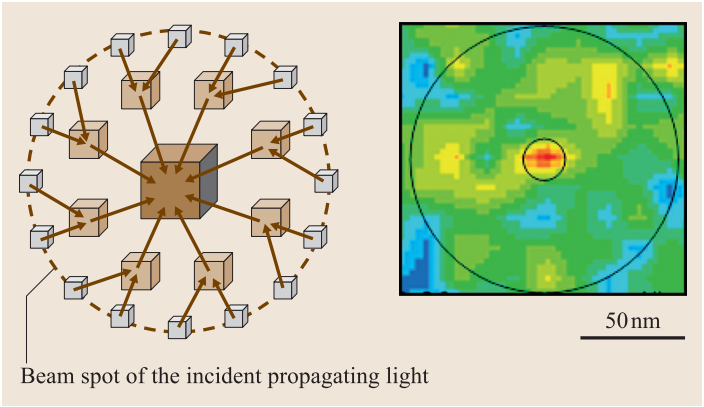


**Fig. 15.11** The structure of an optical nanofountain and the spatial distribution of the optical signal energy, which used CuCl quantum cubes of 2–10 nm

smaller quantum dots on the circular rim, medium-sized quantum dots installed inside, and the largest quantum dot fixed at the center. The propagating light energy incident into this circular device is concentrated to the largest quantum dot at the center due to both successive optical near-field energy transfer from the smaller to the larger quantum dots and fast relaxation, as in the case of the nanophotonic switch. This device has been named an *optical nanofountain* and its equivalent numerical aperture is as high as 40.



## 15.4 Nanophotonic Fabrications

Optical fabrications beyond the diffraction limit are required to produce a variety of conventional devices and to fabricate the nanophotonic devices reviewed in Sect. 15.3. To fabricate nanophotonic devices, several capabilities are required. A variety of materials must be deposited on a substrate and the inaccuracy of their sizes and positions must be as low as 1 nm for efficient, reproducible optical near-field energy transfer. However, conventional fabrication technologies using electron beams, ion beams, and propagating light cannot meet these requirements due to their low resolution, contamination, damage to the substrate, and low throughput.

To meet these requirements, novel technologies must be developed that can be realized by utilizing optical near-field energy transfer. Representative examples of such nanophotonic fabrications are reviewed in this section.

### 15.4.1 Photochemical Vapor Deposition

Photochemical vapor deposition is a way to deposit materials on a substrate using a photochemical reaction that pre-dissociates metalorganic molecules by irradiating gaseous molecules or molecules adsorbed on the substrate with ultraviolet light. Consequently, the electrons in the molecules are excited to a higher energy level following the Franck–Condon principle. This is an adiabatic process because no molecular vibrations or rotations are excited; i. e., the Born–Oppenheimer approximation is valid. After excitation, the electron transits to the dissociative energy level. As a result of this transition, the molecule is dissociated and the atoms composing the molecule are deposited on the substrate. By using an optical near field as the light source for this deposition scheme, nanometric materials can be fabricated whose size and position are accurately controlled by the spatial distribution of the optical near-field energy. Nanometric metallic particles of Zn and Al and light-emitting semiconductor particles (e.g., ZnO and GaN) have been deposited with size and positional accuracies beyond the diffraction limit [15.21–25]. This is an example of a quantitative innovation.

Although an ultraviolet light with high photon energy must be used for the aforementioned adiabatic process, it has been found that an optical near field with a much lower photon energy (i. e., visible light) can dissociate the molecule. This has been explained by a theoretical model of the virtual exciton–polariton exchange between a metalorganic molecule and the fiber probe tip used to generate the optical near field. In other words, this exchange excites not only the electron, but also molecular vibration. This is a nonadiabatic process, which does not follow the Franck–Condon principle, and therefore the Born–Oppenheimer approximation is no longer valid. Several experimental results have been reported, including the nonadiabatic dissociation of diethylzinc (DEZn) molecules by a visible optical near field and the deposition of nanometric Zn particles [15.26]. The virtual exciton–polariton model explains this nonadiabatic process quantitatively by introducing the contribution of a phonon excited in the fiber probe tip [15.27].

The presented nonadiabatic process suggests that the large, expensive ultraviolet light sources that are

indispensable for conventional photochemical vapor deposition are no longer required. It also suggests that the process can even dissociate optically inactive molecules (i. e., inactive to the propagating light), which is advantageous for environment protection because most optically inactive molecules are chemically stable and harmless. For example, optically inactive $Zn(acac)_2$ molecules have been dissociated nonadiabatically using an optical near field to deposit nanometric Zn particles [15.28].

## 15.4.2 Photolithography

Photolithography is a technology used to carve substrate material. After coating the substrate with a thin film of a photoresist, light is irradiated through a photomask to induce a photochemical reaction in the photoresist. When the aperture on the photomask is smaller than the wavelength of the light, the transmission of the propagating light is sufficiently low while an optical near field is generated at the aperture. Using the photochemical reaction between the optical near field and the photoresist, a nanometric pattern beyond the diffraction limit is formed on the photoresist, and a chemical etching process is subsequently used to carve the substrate. Practical nanophotonic technologies, such as using a two-layered photoresist, have been developed to form deep patterns and to realize a quantitative innovation (Fig. 15.12) [15.29].

As long as an adiabatic process is used for photolithography, ultraviolet light with a high photon energy is required to induce the photochemical reaction via the optical near field. However, photolithography using a nonadiabatic process is possible, as was the case

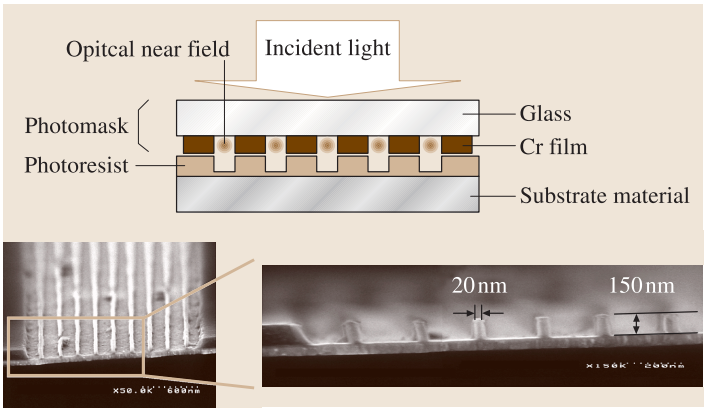


**Fig. 15.12** The structure of the photolithography system and the cross-sectional profile of the photoresist after development. The photographs were supplied courtesy of R. Kuroda, Canon Corp

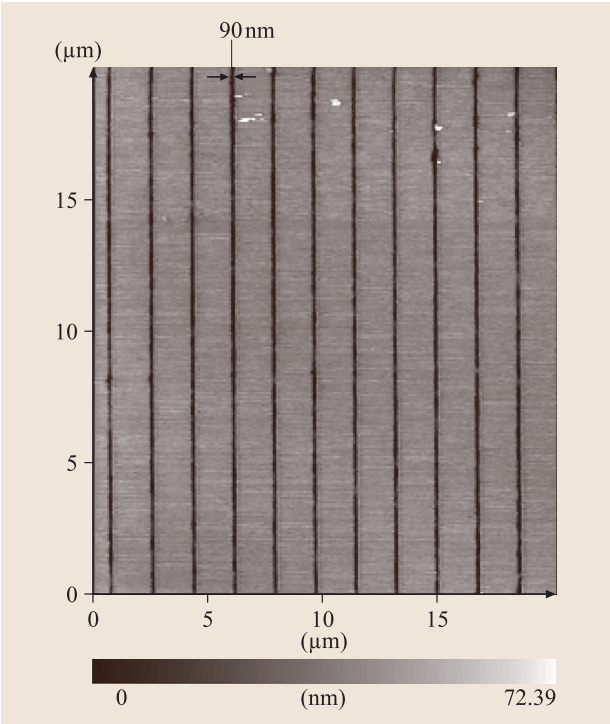


**Fig. 15.13** Top view of a photoresist with a corrugated pattern that was fabricated nonadiabatically using optical near fields

in Sect. 15.4.1; i. e., a photochemical reaction can even be induced using visible light with a very low photon energy. Figure 15.13 shows a narrow corrugated pattern fabricated using nonadiabatic photolithography [15.30], which has been analyzed theoretically based on a virtual exciton–polariton model by introducing the contribution of phonons. This result represents a qualitative innovation in photolithography, suggesting that large, expensive ultraviolet light sources are no longer required, and that harmless, chemically stable molecules can be used as the photoresist, even if they are optically inactive. As an example, an optically inactive resist film has been used for electron-beam lithography. Although this film is optically inactive, a photochemical reaction is induced and fine patterns can be fabricated by using a photomask consisting of a two-dimensional array of circular disks (Fig. 15.14) [15.30].

Fabrication using the adiabatic process suffers from the contribution of the small amount of propagating light transmitted through the aperture on the photomask and the plasmon generated on the photomask. This limits the resolution of fabrication and the pattern contrast. In contrast, since the nonadiabatic process is free from these contributions, greater resolution, higher contrast,

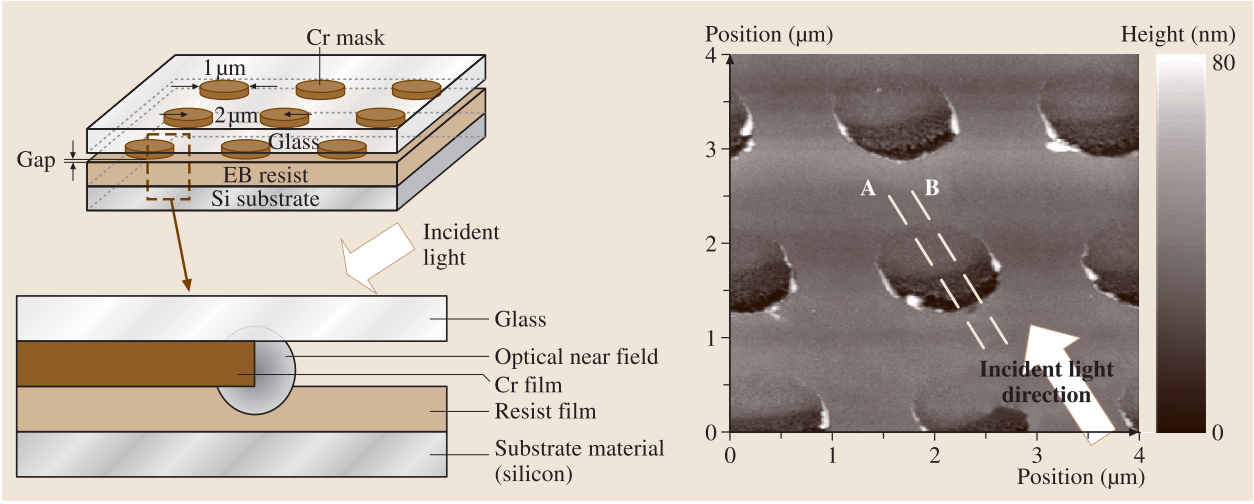


**Fig. 15.14** Bird's-eye view of the optically inactive resist film used for electron-beam lithography, fabricated nonadiabatically using optical near fields

and a variety of patterns (e.g., Ts, Ls, and rings) have been realized [15.30].

### 15.4.3 Self-Organized Deposition and Nanoimprinting

Self-organized deposition is a way to deposit nanometer-sized particles, as discussed in Sect. 15.4.1. In this case, however, a fine structure, e.g., a narrow groove, is first patterned on the substrate instead of using a fiber probe or photomask (Fig. 15.15) [15.31]. While sputtering metallic particles on this patterned substrate, irradiation with propagating light is used to desorb the deposited particles. This irradiation generates an optical near field in the groove, which excites free electron oscillations in the deposited metallic particles. The size of the deposited metallic particles increases with continued sputtering. As a result, the center frequency of the electron oscillation spectrum shifts and its spectral linewidth increases due to the finite path length of the free electrons and resultant damping of the resonant oscillation. The magnitudes of the center frequency shift and linewidth increase are nearly proportional to the particle size if it is sufficiently small [15.32].

When the shifted center frequency is tuned to the optical near-field frequency (i. e., the particle grows to a specific size), the magnitude of the optical near-field energy absorbed by the particle is maximal at this size-dependent optical absorption resonance. Moreover, the desorption rate is maximal under this resonant condition, so a further increase in particle size is prohibited by the balance between the magnitudes of sputtering and desorption [15.33, 34]. Since the size of a deposited particles depends on the photon energy of the optical

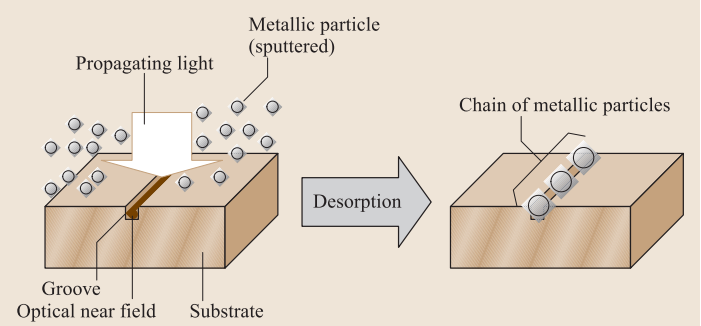


**Fig. 15.15** The principle of self-organized deposition

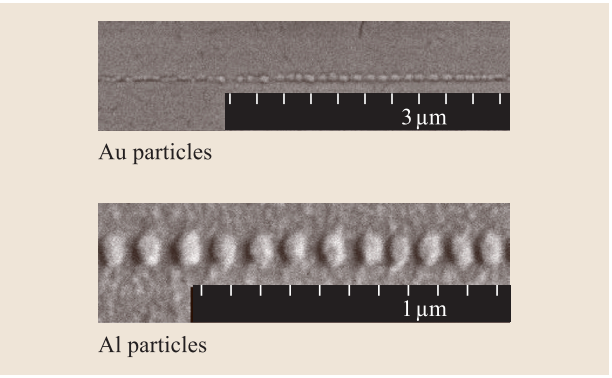


**Fig. 15.16** Chains of gold and aluminum particles fabricated via self-organized deposition using red (wavelength = 633 nm) and green (wavelength = 532 nm) light. Their diameters are 100 nm and 70 nm, respectively

near field as the result of this balance, the size can be controlled accurately.

This accurate size-control method forms the first particle, on which a new optical near field is subsequently generated because the propagating light is still being irradiated. As a result of this secondary optical near field, a second particle forms next to the first one, and the size of the second particle is equivalent to that of the first because of size-dependent resonant optical absorption [15.33]. Because this formation process occurs successively, a chain of the metallic particles is formed along the groove within the area irradiated by the propagating light (Fig. 15.16). Note that this chain is formed in a self-organized manner, and neither a fiber probe nor a photomask is used. The sizes and separations of these particles are determined accurately by the photon energy of the optical near field.

As a recently developed fabrication technology, light-assisted nanoimprinting has enabled the formation of nanometric structures, without the requirement for a development process [15.35]. By using optical near fields, the adiabatic process forms a pattern that is even smaller than that of the mold [15.36]. Further progress is expected if a nonadiabatic process can also be utilized.



## 15.5 Extension to Related Science and Technology

Nanophotonics has led nanooptics and realized qualitative innovation. As examples of its extension to related science and technology, this section reviews applications to novel photonic systems and atom photonics.

Nanophotonic systems utilize nanophotonic devices. For example, novel architectures have been proposed for optical signal transmission systems and their performance has been confirmed experimentally. They include interconnections and summation involving an optical nanofountain [15.16], computing using nanophotonic switches and an optical nanofountain [15.17], and broadcasting using multiple nanophotonic switches [15.37]. They have realized quantitative innovations by decreasing the device size and power consumption beyond the diffraction limit. More importantly, qualitative innovation has been realized as a consequence of the novel functions of nanophotonic devices, which are impossible with conventional photonic devices.

An optical/magnetic hybrid disk storage system with a storage density of $1\,\mathrm{Tb/in^2}$ has been developed. Quantitative innovation has already been realized by transcending the diffraction limit of optical storage density [15.38]. Qualitative innovation in optical storage and readout has been also proposed by applying the hierarchy in optical near fields to memory retrieval [15.39].

An example of an extension to related science is atom photonics, which controls the thermal motion of neutral atoms in a vacuum using optical near fields [15.40]. Theoretical studies have examined single-atom manipulation based on the virtual exciton–polariton model [15.41]. Recent experimental studies have examined atom guidance through a hollow optical fiber [15.42], atom-detecting devices [15.43], atom deflectors [15.44], and an atomic funnel [15.45]. Atom photonics will open a new field of science that examines the interaction between virtual exciton–polaritons and a single atom. Furthermore, it can be applied to novel technologies for atomic-level material fabrication.

## 15.6 Summary

As a result of the development of nanophotonics, which utilizes the local electromagnetic interactions between nanometric particles mediated by optical near fields, nanooptics now exists as a novel field of optics in nanometric space. However, the name nanophotonics is occasionally used for photonic crystals, plasmonics, silicon photonics, and quantum-dot lasers using conventional propagating lights. Here, one should consider a stern warning by C. Shannon on the casual use of the term information theory, which was a trend in its study during the 1950s [15.46]. The term nanophotonics has been used in a similar way, although some work in nanophotonics is not based on optical near-field interactions. For the true development of nanophotonics, one needs deep physical insights into the virtual exciton–polariton and the nanometric subsystem composed of electrons and photons. It is both unethical and misleading to use the name nanophotonics in a casual manner, for example, to obtain a research grant. Since nanooptics should be defined as a field of optical science and technology including nanophotonics, Shannon's warning should be extended to the term nanooptics.

## References


15.1 M. Ohtsu: *Progress in Nano-Electro-Optics V*, ed. by M. Ohtsu (Spinger, Berlin, Heidelberg 2006) Preface to Volume V: Based on "nanophotonics" proposed by Ohtsu in 1993, OITDA (Optical Industry Technology Development Association, Japan) organized the nanophotonics technical group in 1994, and discussions on the future direction of nanophotonics were started in collaboration with academia and industry

15.2 E.Yablonovitch: Inhibited spontaneous emission in solid-state physics and electronics, Phys. Rev. Lett. **58**, 2059 (1987)

15.3 V. A. Podolskiy, A. K. Sarychev, V. M. Shalaev: Plasmon modes and negative refraction in metal nanowire composites, Opt. Exp. **11**, 735 (2003)

15.4 R. A. Shelby, D. R. Smith, S. Schultz: Experimental verification of a negative index of refraction, Science **292**, 77 (2001)

15.5 J. B. Pendry: Negative refraction makes a perfect lens, Phys. Rev. Lett. **85**, 3966 (2000)

15.6 H. Rong, A. Liu, R. Nicolaescu, M. Paniccia: Raman gain and nonlinear optical absorption measurements in a low-loss silicon awveguide, Appl. Phys. Lett. **85**, 2196 (2004)

15.7 Y. Arakawa, H. Sakaki: Multidimensional quantum well laser and temperature dependence of its threshold current, Appl. Phys. Lett. **40**, 939 (1982)

15.8 E. A. Synge: A suggested method for extending microscopic resolution into the ultra-microscopic region, Philos. Mag. **6**, 356 (1928)

15.9 M. Ohtsu: *Near-Field Nano/Atom Optics and Technology* (Spinger, Berlin, Heidelberg 1998) pp. 31–69

15.10 M. Ohtsu, H. Hori: *Near-Field Nano-Optics* (Kluwer Academic Plenum, New York 1999) pp. 113–142

15.11 M. Ohtsu, K. Kobayashi: *Optical Near Fields* (Springer, Berlin, Heidelberg 2004) pp. 88–108

15.12 M. Ohtsu, K. Kobayashi: *Optical Near Fields* (Springer, Berlin, Heidelberg 2004) pp. 109–120

15.13 S. Sangu, K. Kobayashi, A. Shojiguchi, M. Ohtsu: Logic and functional operations using a near-field optically coupled quantum-dot system, Phys. Rev. B **69**, 115334 (2004)

15.14 M. Achermann, M. A. Petruska, S. Kos, D. L. Smith, D. D. Koleske, V. I. Klimov: Energy-transfer pumping of semiconductor nanocrystals using an epitaxial quantum well, Nature **429**, 642 (2004)

15.15 T. Kawazoe, K. Kobayashi, K. Akahane, M. Naruse, N. Yamamoto, M. Ohtsu: Demonstration of nanophotonic NOT gate using near-field optically coupled quantum dots, Appl. Phys. B **84**, 243 (2006)

15.16 M. Naruse, T. Miyazaki, F. Kubota, T. Kawazoe, K. Kobayashi, S. Sangu, M. Ohtsu: Nanometric summation architecture based on optical near-field interaction between quantum dots, Opt. Lett. **30**, 201 (2005)

15.17 M. Naruse, T. Miyazaki, T. Kawazoe, K. Kobayashi, S. Sangu, F. Kubota, M. Ohtsu: Nanophotnic computing based on optical near-field interactions between quantum dots, IEICE Trans. Electron. **E88-C**, 1817 (2005)

15.18 A. Shojiguchi, S. Sangu, K. Kitahara, M. Ohtsu: Superradiance and dipole ordering of an n two-level system interacting with optical near fields, J. Phys. Soc. Jpn. **72**, 2984 (2003)

15.19 T. Kawazoe, K. Kobayashi, S. Sangu, M. Ohtsu: Demonstration of a nanophotonic switching operation by optical near-field energy transfer, Appl. Phys. Lett. **82**, 2957 (2003)

15.20 T. Kawazoe, K. Kobayashi, M. Ohtsu: Optical nanofountain: A biomimetic device that concentrates optical energy in a nanometric region, Appl. Phys. Lett. **86**, 103102 (2005)

15.21 V. V. Polonski, Y. Yamamoto, M. Kourogi, H. Fukuda, M. Ohtsu: Nanometric patterning of zinc by optical near-field photochemical vapour deposition, J. Microsc. **194**, 545 (1999)

15.22 Y. Yamamoto, M. Kourogi, M. Ohtsu, V. Polonski, G. H. Lee: Fabrication of nanometric zinc pattern with photodissociated gas-phase diethylzinc by optical near field, Appl. Phys. Lett. **76**, 2173 (2000)

15.23 T. Yatsui, T. Kawazoe, M. Ueda, Y. Yamamoto, M. Kourogi, M. Ohtsu: Fabrication of nanometric single zinc and zinc oxide dots by the selective photodissociation of adsorption-phase diethylzinc using a nonresonant optical field, Appl. Phys. Lett. **81**, 3651 (2002)

15.24 J. Lim, T. Yatsui, M. Ohtsu: Observation of size-dependent resonance of near-field coupling between a deposited Zn dot and the probe apex during near-field optical chemical vapor deposition, IEICE Trans. Electron. **E 88-C**, 1832 (2005)

15.25 Y. Yamamoto, M. Kourogi, M. Ohtsu, G. H. Lee, T. Kawazoe: Lateral integration of Zn and Al dots with nanometer-scale precision by near field optical chemical vapor deposition using a sharpened optical fiber probe, IEICE Trans. Electron. **E85-C**, 2081 (2002)

15.26 T. Kawazoe, Y. Yamamoto, M. Ohtsu: Fabrication of a nanometric Zn dot by nonresonant near-field optical chemical-vapor deposition, Appl. Phys. Lett. **79**, 1184 (2001)

15.27 T. Kawazoe, K. Kobayashi, S. Takubo, M. Ohtsu: Nonadiabatic photodissociation process using an optical near field, J. Chem. Phys. **122**, 024715 (2005)

15.28 T. Kawazoe, K. Kobayashi, M. Ohtsu: Near-field optical chemical vapor deposition using $Zn(acac)_2$ with a non-adiabatic photochemical process, Appl. Phys. B **84**, 247 (2006)

15.29 M. Naya, I. Tsurusawa, T. Tani, A. Mukai, S. Sakaguchi, S. Yasutani: Near-field optical pho-

tolithography for high-aspect-ratio patterning using bilayer resist, Appl. Phys. Lett. **86**, 201113 (2005)
15.30 T. Kawazoe, K. Kobayashi, S. Sangu, M. Ohtsu, A. Neogi: Unique Properties of Optical Near Field and their Applications to Nanophotonics. In: *Progress in Nano-Electro-Optics V*, ed. by M. Ohtsu (Springer, Berlin, Heidelberg 2006) pp. 109–162
15.31 T. Yatsui, W. Nomura, M. Ohtsu: Self-assembly of size- and position-controlled ultralong nanodot chains using near-field optical desorption, Nano Lett. **5**, 2548 (2005)
15.32 C. Sönnichsen, T. Franzl, T. Wilk, G. von Plessen, J. Feldmann: Drastic reduction of plasmon damping in gold nanorods, Phys. Rev. Lett. **88**, 077402 (2002)
15.33 K. F. MacDonald, V. A. Fedotov, S. Pochon, K. J. Ross, G. C. Stevens, N. I. Zheludev, W. S. Brocklesby, V. I. Emel'yanov: Optical control of gallium nanoparticle growth, Appl. Phys. Lett. **80**, 1643 (2002)
15.34 T. Yatsui, S. Takubo, J. Lim, W. Nomura, M. Kourogi, M. Ohtsu: Regulating the size and position of deposited Zn nanoparticles by optical near-field desorption using size-dependent resonance, Appl. Phys. Lett. **83**, 1716 (2003)
15.35 M. D. Austin, H. Ge, W. Wu, M. Li, Z. Yu, D. Wasserman, S. A. Lyon, S. Y. Chou: Fabrication of 5 nm linewidth and 14 nm pitch features by nanoimprint lithography, Appl. Phys. Lett. **84**, 5299 (2004)
15.36 T. Yatsui, Y. Nakajima, W. Nomura, M. Ohtsu: High-resolution capability of optical near-field imprint lithography, Appl. Phys. B **84**, 265 (2006)
15.37 M. Naruse, T. Kawazoe, S. Sangu, K. Kobayashi, M. Ohtsu: Optical interconnects based on optical far- and near-field interactions for high-density data broadcasting, Opt. Exp. **14**, 306 (2006)
15.38 T. Matsumoto, Y. Anzai, T. Shintani, K. Nakamura, T. Nishida: Writing 40 nm marks by using a beaked metallic plate near-field optical probe, Opt. Lett. **31**, 259 (2006)
15.39 M. Naruse, T. Yatsui, W. Nomura, N. Hirose, M. Ohtsu: Hierarchy in optical near-fields and its application to memory retrieval, Opt. Exp. **13**, 9265 (2005)
15.40 M. Ohtsu: *Near-Field Nano/Atom Optics and Technology* (Spinger, Berlin, Heidelberg 1998) pp. 218–293
15.41 K. Kobayashi, S. Sangu, H. Ito, M. Ohtsu: Near-field optical potential for a neutral atom, Phys. Rev. A **63**, 013806 (2001)
15.42 H. Ito, T. Nakata, K. Sakaki, M. Ohtsu, K. I. Lee, W. Jhe: Laser Spectroscopy of Atoms Guided by Evanescent Waves in Micron-Sized Hollow Optical Fibers, Phys. Rev. Lett. **76**, 4500 (1996)
15.43 K. Totsuka, H. Ito, T. Kawamura, M. Ohtsu: High spatial resolution atom detector with two-color optical near fields, Jpn. J. Appl. Phys. **41**, 1566 (2002)
15.44 K. Totsuka, H. Ito, K. Suzuki, K. Yamamoto, M. Ohtsu, T. Yatsui: A slit-type atom deflector with near-field light, Appl. Phys. Lett. **82**, 1616 (2003)
15.45 A. Takamizawa, H. Ito, S. Yamada, M. Ohtsu: Observation of cold atom output from an evanescent-light funnel, Appl. Phys. Lett. **85**, 1790 (2004)
15.46 C. E. Shannon: The bandwagon, IRE Trans. Inform. Theory **2**, 3 (1956)

# ナノフォトニクスの展開

ナノフォトニクス工学推進機構 編
大津元一 監修

橋本正洋
大津元一
成田貴人
黒田　亮
西田哲也
川添　忠
八井　崇
成瀬　誠

米田出版

# 目次